RECOGNITION OF NUCLEOTIDES AND PEPTIDES USING DESIGNED BETA-HAIRPIN PEPTIDES AND DYNAMIC COMBINATORIAL CHEMISTRY

Matthew E. Cuellar

A dissertation submitted to the faculty of the University of North Carolina at Chapel Hill in partial fulfillment of the requirements for the degree of Doctor of Philosophy in the Department of Chemistry.

Chapel Hill
2008

Approved by:

Marcey L. Waters

Valerie Sheares Ashby

Michael T. Crimmins

Jeffrey S. Johnson

Joseph L. Templeton

ABSTRACT

MATTHEW E. CUELLAR: Recognition of Nucleotides and Peptides Using Designed Beta-Hairpin Peptides and Dynamic Combinatorial Chemistry
(Under the direction of Marcey L. Waters)

Non-covalent interactions contribute to the stability and formation of biomolecules, e.g. proteins, DNA, and RNA. More relevant to this dissertation, they also contribute to the interaction between these biomolecules, e.g. protein-protein, protein-RNA, and protein-DNA interactions. This work describes the use of model systems (peptide and small molecule) to mimic protein-RNA and protein-protein interactions.

This dissertation is divided into three parts. The first part describes the attempted use of designed beta-hairpin peptides to selectively bind 7mGTP. Despite attempts using different binding techniques (fluorescence titration, microcalorimetry, and NMR titration), the binding of 7mGTP by the beta-hairpin peptides could not be quantified. The second part describes the use of designed beta-hairpin peptides for recognition of polyproline (PPII) helices in a model system. This work demonstrates the use of disulfide exchange to investigate non-covalent interactions in a peptide model system. The third part describes the development and the use of dynamic combinatorial chemistry (DCC) mediated by disulfide exchange. The development of analytical methodology using ultra performance liquid chromatography coupled with mass spectrometry analysis (UPLC/MS) is described. DCC was used to synthesize and identify receptors for both nucleotides and peptides containing a lysine residue with different methylation states.

ACKNOWLEDGEMENTS

I would like to thank my advisor Marcey Waters for giving me the opportunity to perform research in her lab and work on such challenging projects. I will always be grateful for her advice and mentorship these past five years. In addition, I would like to thank the faculty of the chemistry department for serving on my committee and teaching me valuable lessons both inside and outside the classroom.

My newfound knowledge and appreciation for mass spectrometry would not be possible without the help of Dr. Matthew Crowe, Miss Christine Hebling, and Dr. Curt Heine. I thank Matt for taking the time to teach me and answer my questions about mass spectrometry. I thank Christine for keeping the UPLC/MS running and helping me troubleshoot problems encountered in my research. I thank Curt for teaching me how to use the UPLC/MS and for helping me develop the mass spectrometry analysis needed for the DCC project.

I thank all Waters group members (past & present) for providing a fun and enjoyable workplace during my time at UNC. I have learned much from all of you and hope that I have taught you some things as well. I am especially grateful to the current group members who have respected my personal space as I wrote this dissertation. I thank all my friends at UNC who helped me get through the rough times of graduate school.

I thank my family for their love, support, and prayers during these last five years. You have always believed in me, especially when I did not believe in myself. None of my success would have been possible without you.

Last, and certainly not least, I thank my wonderful wife, Becca. You have seen me at my worst and continued to love and believe in me, even when I did not believe in myself. We started on this journey individually but completed this first part together.

TABLE OF CONTENTS

LIST OF TABLES

Table

LIST OF FIGURES

Figure

LIST OF SCHEMES

LIST OF ABBREVIATIONS

4-DMAP	4-(*N*,*N*-dimethylamino)-phthalimide
7mGTP	7-methyl guanosine triphosphate
Å	angstrom
A	alanine
Ac	acetate
Ala	alanine
aq.	aqueous
Arg	arginine
Asn	asparagine
Asp	aspartic acid
ATP	adenosine triphosphate
C	cysteine
CMP	cytosine monophosphate
CTP	cytosine triphosphate
Cys	cysteine
Asp	aspartic acid
DAPA	4-DMAP amino acid derivative
D_2O	deuterium oxide
DCC	dynamic combinatorial chemistry
DCM	dichloromethane
DMF	*N*,*N*-dimethylformamide
DMSO	dimethylsulfoxide

DNA	deoxyribose nucleic acid
E	glutamic acid
eIF4E	eukaryotic initiation factor, subunit 4E
ε value	molar extinction coefficient
eq.	equation
equiv.	equivalents
ESI	electrospray ionization
ESI-MS	electrospray ionization-mass spectrometry
Et_3N	triethylamine
EtOAc	ethyl acetate
EVH1	ena-vasp homology 1
F	phenylalanine
Fm	fluorenylmethyl
FMN	flavin mononucleotide
G	glycine
Gly	glycine
Gln	glutamine
Glu	glutamic acid
GMP	guanosine monophosphate
GTP	guanosine triphosphate
ΔG	gibbs' free energy
H	histidine
h	hours

His	histidine
^{1}H NMR	proton nuclear magnetic resonance spectroscopy
HPLC	high performance liquid chromatography
I	isoleucine
Ile	isoleucine
ITC	isothermal titration calorimetry
K	lysine
K	degrees kelvin
L	leucine
Leu	leucine
Lys	lysine
M	methionine
M	molar
m7G	7-methyl guanosine
m7GppN	7-methyl guanosine triphosphate nucleotide
mRNA	messenger RNA
mM	milimolar
μM	micromolar
MeCN	acetonitrile
MeOH	methanol
Met	methionine
min	minutes
N	asparagine

n/a	not available
nc	not calculated
nm	nanometer
ND	not determined
[O]	oxidation
P	proline
PPII	polyproline (type II)
Phe	phenylalanine
Pro	proline
PTM	post-translational modification
pyr	pyridine
Q	glutamine
R	arginine
REDOX	Reduction and Oxidation
rt	room temperature
RNA	ribose nucleic acid
S	serine
Ser	serine
T	threonine
t	time
TFA	trifluoroacetic acid
Thr	threonine
Trp	tryptophan

Tyr	tyrosine
UPLC	ultra high performance liquid chromatography
UV	ultraviolet
V	valine
Val	valine
W	tryptophan
Y	tyrosine

Chapter 1

Efforts to Bind Mutated Nucleotides with Designed Beta Hairpin Peptides

I. Background and Introduction

A. mRNA cap recognition

Nascent pre-mRNAs are "capped" at their 5' termini by nuclear guanylyl- and methyl transferases. The structure formed is 7-methyl-GpppN (Figure 1.1), where G is the guanine nucleobase, N is any nucleotide, and ppp is the triphosphate linkage.[1]

Figure 1.1: Structure of mRNA cap: m7GpppN

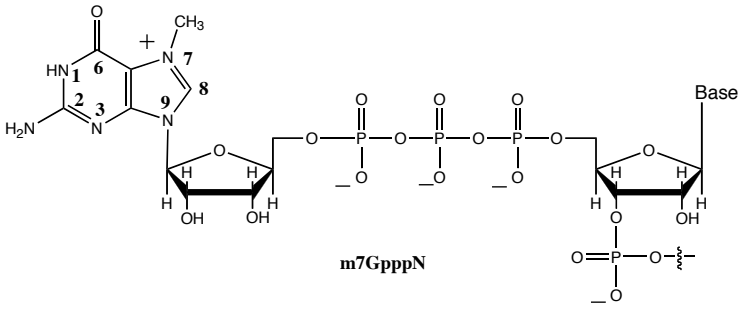

Capping of mRNA is involved in many roles of the mRNA life cycle. Some of these include: (1) acting as a stabilizing element,[2] (2) aiding in pre-mRNA splicing,[3] (3) playing a role in

[1] Shuman, S. *Prog. Nucl. Acid Res. Mol. Biol.* **1995**, *50*, 101-129.

[2] (a) Green, M. R.; Maniatis, T.; Melton, D. A. *Cell* **1983**, *32*, 681-694. (b) Furuichi, Y.; LaFiandra, A.; Shatkin, A. J. *Nature* **1977**, *266*, 235-239.

[3] (a) Izaurralde, E.; Lewis, J.; Gamberi, C.; Jarmolowski, A.; McGuigan, C.; Mattaj, I. W. *Nature* **1995**, *376*, 709-712. (b) Lewis, J. D.; Izaurralde, E.; Jarmolowski, A.; McGuigan, C.; Mattaj, I. W. *Genes Dev.* **1996**, *10*, 1683-1698.

nucleo-cytoplasmic transport of mRNAs,[4] and (4) playing a role in protein synthesis.[5] The cap is recognized by eukaryotic initiation factor 4E (eIF4E). The recognition event recruits the translational machinery to the 5' end of mRNAs.

eIF4E is a component of the trimeric eIF4F complex which also contains eIF4A and eIF4G. eIF4G is a bridge linking eIF4E and eIF4A. eIF4A is an RNA helicase that unwinds the secondary structure in the 5' untranslated region of mRNA, with the assistance of cofactor eIF4B. As a result, the ribosome is able to access the initiation codon. eIF4G interacts with eIF3 to recruit the 40S ribosomal subunit.[6]

eIF4E is the least abundant of the general translation initiation factors and is considered the limiting reagent in the formation of eIF4F. This also makes it the limiting factor in recruitment of the ribosome. Therefore, eIF4E is a target for regulation of mRNA translation. eIF4Es are regulated through phosphorylation and the interaction with 4E-binding proteins (4E-BPs). When eIF4E forms a complex with the 4E-BPs, the binding of eIF4G is reduced. As a result, the eIF4F complex does not form and translation does not occur. Upon phosphorylation, 4E-BPs dissociate from eIF4E, allowing eIF4G to bind and eIF4F to form.[5,7]

Three-dimensional structures of the murine[8] (Figure 1.2) and yeast[9] eIF4E, both bound to m7GDP, were solved by X-ray crystallography and solution NMR, respectively.

---

[4] Izaurralde, E.; Mattaj, I. W. *Cell* **1995**, *81*, 153-159.

[5] Raught, B.; Gingras, A.-C. *Int. J. Biochem. Cell Biol.* **1999**, *31*, 43-57.

[6] Merrick, W. C.; Hershey, J. W. B. *In Translational Control*, Cold Spring Harbor Press, Cold Spring Harbor, NY, **1996**, pp. 31-69.

[7] Svitkin, Y. V.; Ovchinnikov, L. P.; Dreyfuss, G.; Sonenberg, N. *EMBO J.* **1996**, *15*, 7147-7155.

[8] Marcotrigiano, J.; Gingras, A.-C.; Sonenberg, N.; Burley, S. K. *Cell* **1997**, *89*, 951-961.

These structures have provided insight into the mechanism of interaction between eIF4E and m7GpppN. The cap is bound between two Trp residues (Figure 1.3) via π-π stacking interactions. In the murine protein, mutation of Trp to the non-aromatic Leu residue results in loss of cap binding.[10] But mutation of Trp to the aromatic Phe only reduces cap binding.[11] These studies suggest that π-π stacking and/or cation-π interaction is the dominant non-covalent interaction present.

Figure 1.2: Crystal structure of eIF4E (murine) showing recognition of m7G via π-π stacking between Trp56 and Trp102. Also, hydrogen bonding by Glu103 and Trp102 is observed.

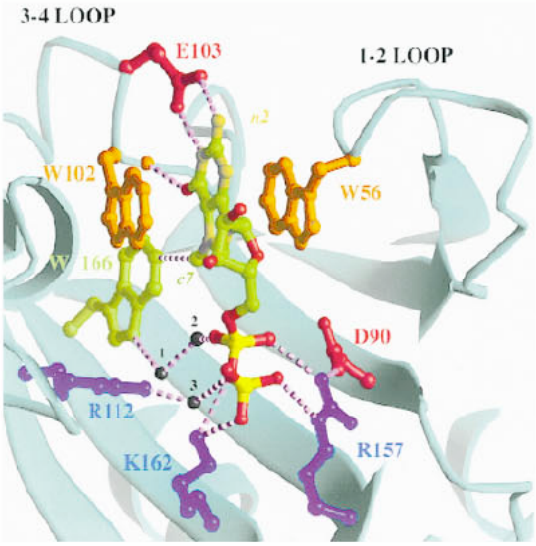

Binding is strengthened by hydrogen bonds. The carboxylate in a Glu residue hydrogen bonds with N1 and N2 of the cap. One of the Trp residues involved in π-π stacking also contributes through hydrogen bonding (via its backbone NH) to the carbonyl oxygen

[9] Matsuo, H.; Li, H.; McGuire, A. M.; Fletcher, C. M.; Gingras, A.-C.; Sonenberg, N.; Wagner, G. *Nature Struct. Biol.* **1997**, *4*, 350-354.

[10] (a) Morino, S.; Hazama, H.; Ozaki, M.; Teraoka, Y.; Shibata, S.; Doi, M.; Ueda, H.; Ishida, T.; Uesugi, S. *Eur. J. Biochem.* **1996**, *239*, 597-601. (b) Ueda, H.; iyo, H.; Doi, M.; Inoue, M.; Ishida, T.; Morioda, H.; Tanaka, T.; Hishikawa, S.; Uesugi, S. *FEBS Lett.* **1991**, *280*, 207-210.

[11] Altmann, M.; Edery, I.; Trachsel, H.; Sonenberg, N. *J. Biol. Chem.* **1988**, *263*, 17229-17232.

found at position 6 of the guanine. Thus, all the hydrogen bonding requirements for Watson-Crick base pairing are satisfied by eIF4E. Other non-covalent interactions assist in cap recognition and the reader is referred to the primary literature[8,9] for further details.

Figure 1.3: Structures and abbreviations of commonly used amino acids.

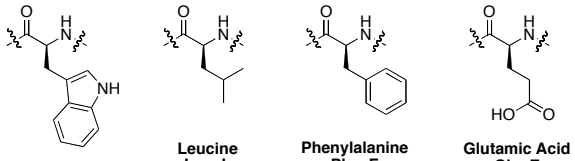

Overexpression of eIF4E causes accelerated cell division, malignant transformation, and inhibition of apoptosis.[12] In breast, head-and-neck, and lung cancers, eIF4E overexpression occurs up to 30-fold.[13] In addition to these deleterious effects caused by eIF4E overexpression, a viral protein (VP39) exists that binds m7Gppp cap between two aromatic residues.[14] The recognition of the mRNA cap by VP39 provides a path for viral infection. The development and synthesis of highly specific, synthetic cap analogues may neutralize these consequences. Lastly, methylation of G in DNA is a common source of DNA damage. Proteins in the base-excision repair pathway bind to 7mG via an aromatic cleft very similar to that of eIF4E.[15]

B. Cation-π Interaction

The cation-π interaction can be defined as an electrostatic attraction between a positive charge and the quadrupole moment of a π system, typically aromatic.[16] Aromatic

---

[12] Gingras, A. C.; Raught, B.; Sonenberg, N. *Annu. Rev. Biochem.* **1999**, *68*, 913-963.

[13] Hershey, J. W.; Miyamoto, S. *Translational Control*, Cold Spring Harbor Press, Cold Spring Harbor, NY, **2000**, pp. 637-654.

[14] Quiocho, F. A.; Hu, G.; Gershon, P. D. *Curr. Opin. Struct. Biol.* **2000**, *10*, 78-86.

[15] Schärer, O. D. *Angew. Chem. Int. Ed.* **2003**, *42*, 2946-2974.

molecules can be thought of as both polar and hydrophobic molecules. Consider benzene as an example; it is a hydrocarbon and does not have a dipole moment. However, it has a quadrupole moment that results in a permanent, non-spherical charge distribution. An ion can be attracted to the favorable region of this quadrupole. This interaction cannot be modeled as an ion-quadrupole interaction, quantitatively. Ion-quadrupole interactions are expected to show a $1/r^3$ distance dependence for the stabilization energy but the distance dependence observed in a cation-π interaction is typically $1/r^n$ with $n < 2$, resembling a Coulombic (1/r) interaction.[16a] Thus, the quadrupole moment provides a way to visualize the distribution of charge in aromatics. This charge distribution leads to the expectation of significant electrostatic interactions. The electrostatic component of binding is suggested from a theoretical study of alkali metals binding to benzene. The affinity observed ($Li^+ > Na^+ > K^+ > Rb^+$) follows the trend predicted by electrostatics. However, the electrostatic interaction is not the only contributor. Therefore, the electrostatic model helps predict trends and rationalize the interaction. Polarizability of the aromatic group is important to the interaction but not the defining feature, either.

Cation-π interactions have been proposed for many interactions in biology.[17] In the case of mRNA cap recognition, the interaction is between a protein (eIF4E) and an RNA strand (mRNA cap). The alkylation of the guanine base results in quaternary nitrogen, which is positively charged. Rather than interact with an anionic group, the positively charged guanine is sandwiched between two aromatic (Trp) groups. It has been suggested that this interaction is driven by a cation-π interaction.[14]

---

[16] (a) Dougherty, D. A. *Science* **1996**, *271*, 163-168. (b) Ma, J. C.; Dougherty, D. A. *Chem. Rev.* **1997**, *97*, 1303-1324.

[17](a) Gallivan, J. P.; Dougherty, D. A. *Proc. Natl. Acad. Sci. USA* **1999**, *96*, 9459-9464. (b) Crowley, P. B.; Golovin, A. *Proteins* **2005**, *59*, 231-239.

C. Beta-hairpin Peptides to Mimic Trp-Base-Trp Interaction

Previous work in the Waters group led to the development of a β-hairpin receptor (Figure 1.4) composed of all natural amino acids that binds to nucleotides. Its K_a for ATP was 5815 M^{-1} (K_d = 170 μM) in buffer solution[18]. The recognition elements are aromatic and electrostatic interactions. Two tryptophans stack with the nucleobase (contributing -1.8 kcal/mol to binding) while two lysines interact with the phosphate tail (-3 kcal/mol). This particular receptor is unique because the folding of the peptide defines the binding pocket; therefore the receptor is a true bio-mimetic species. In a follow up investigation[19], WKWK was shown by NMR titration in 10mM NaCl to bind more strongly to GTP (2200 M^{-1}) than ATP (700 M^{-1}). The selectivity of this β-hairpin for the guanine base makes it a good starting point for the optimization of both 7mGTP binding affinity and specificity.

Figure 1.4: ATP-binding β-hairpin (WKWK)

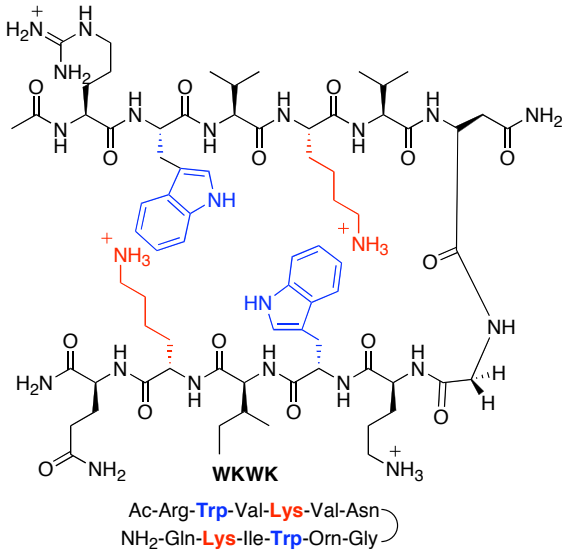

[18] Butterfield, S. M.; Waters, M. L. *J. Am. Chem. Soc.* **2003**, *125*, 9580-9581.

[19] Butterfield, S. M. Sweeney, M. M.; Waters, M. L. *J. Org. Chem.* **2005**, *70*, 1105-1114.

The goal of this project is to design a beta-hairpin peptide that models eIF4E's Trp sandwich region that selectively binds the mRNA cap. The stacking interaction observed upon binding of ATP by WKWK provides a good starting point for peptide design. In addition, the selectivity for the guanine base should facilitate the binding of G-based nucleotides. The hypothesis is that the cation-π interaction will help make the peptide receptor selective for 7mGTP over GTP. This peptide will be used to quantify the binding of both 7mGTP and GTP.

II. Experiment Design

A. Design of Peptide Model System

Using WKWK as a starting point, some modifications were made to develop a receptor for 7mGTP. The lysines in the binding pocket were relocated to the N or C terminus to avoid charge-charge repulsion in the binding site. These were replaced with either threonine or glutamine. Threonines were used because they are polar and have a high β-sheet propensity. Glutamines were used because they are polar and similar in length to lysine. The peptides incorporating these design elements (Figure 1.5) were KKG-WTWT, WTWT-K, and WQWQ-K. An additional peptide WTWK was included because it is well folded and known to interact with purine bases.[2] In WKWK, the overall charge of the peptide is +4 to maximize solubility and prevent aggregation. KKG-WTWT (+4), WTWT-K (+3), and WQWQ-K (+3) possess Lys residues near the C and N terminus to incorporate this design strategy. WTWK (+3) still has one Lys in the proposed binding site.

Figure 1.5: Peptides for 7mGTP recognition: KKG-WTWT, WTWK, WTWT-K, WQWQ-K.

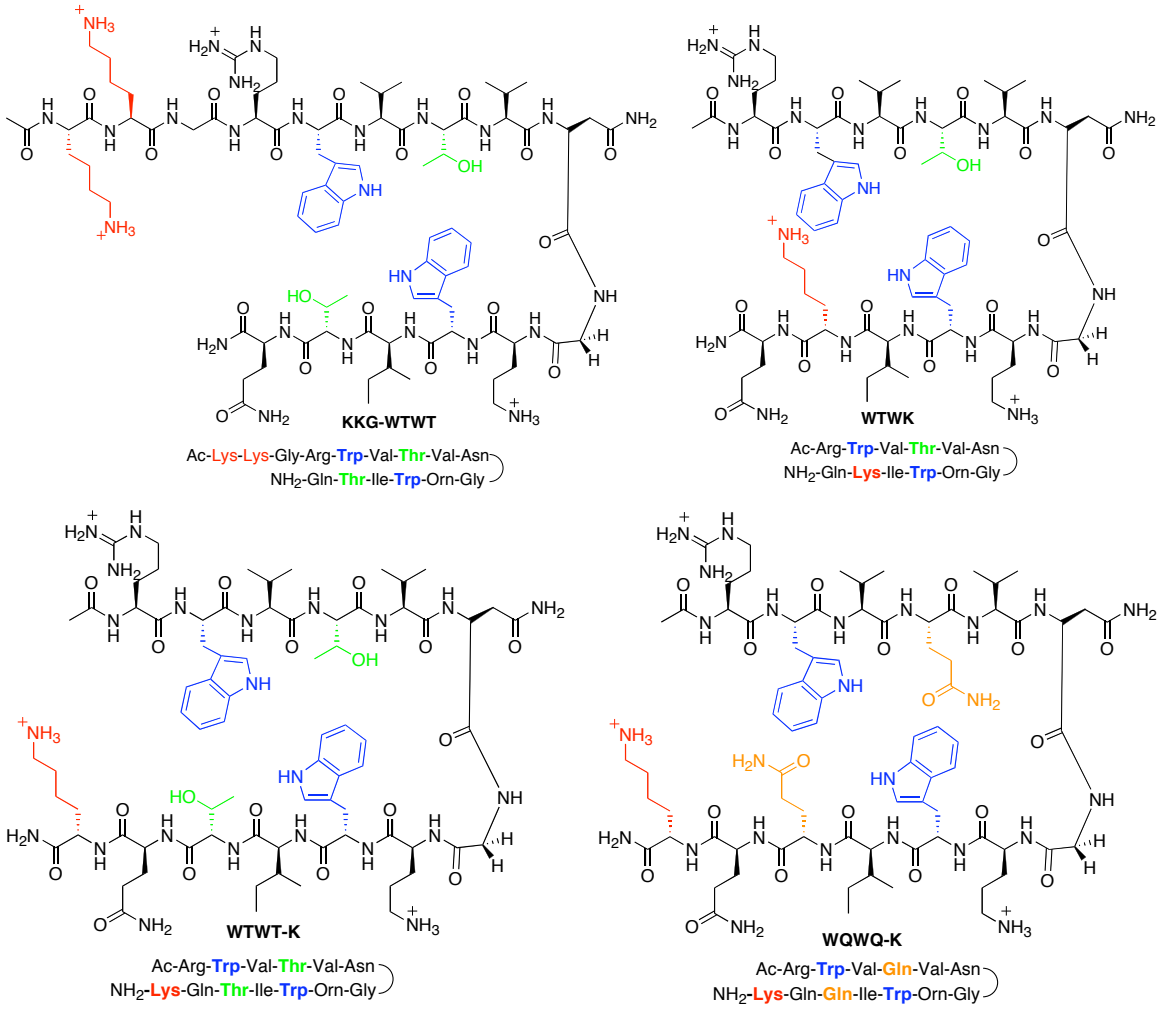

B. Quenching of Tryptophan Fluorescence

The binding constant between WKWK and ATP was measured by fluorescence quenching of Trp with ATP. In order to use the same technique to measure the binding of 7mGTP, two problems need to be addressed. The first is overlapping fluorescence. 7mGTP is a fluorescent molecule and its excitation wavelength and fluorescence emission overlap with those of Trp. (Figure 1.6) The other problem is an absorbance issue and it is defined as the

inner filter effect.[20] In order to fluoresce, a molecule must be excited by absorbing light at a specific wavelength. In the case of the inner filter effect, a portion of this light is absorbed by another molecule or species in solution. As a result, the light intended for fluorescence is filtered out by another source and a false decrease in fluorescence is observed. 7mGTP exhibits an inner filter effect on Trp by absorbing strongly in the excitation range of Trp: 280-300 nm. (Figure 1.7) Despite these problems, Stolarski has used fluorescence quenching of Trp to quantify the binding of 7mGTP by eIF4E. He corrects for both the inner filter effect[21] and overlapping fluorescence. [22]

Figure 1.6: Fluorescence Emission of 7mGTP and KKG-WTWT. Excitation at 280 nm.

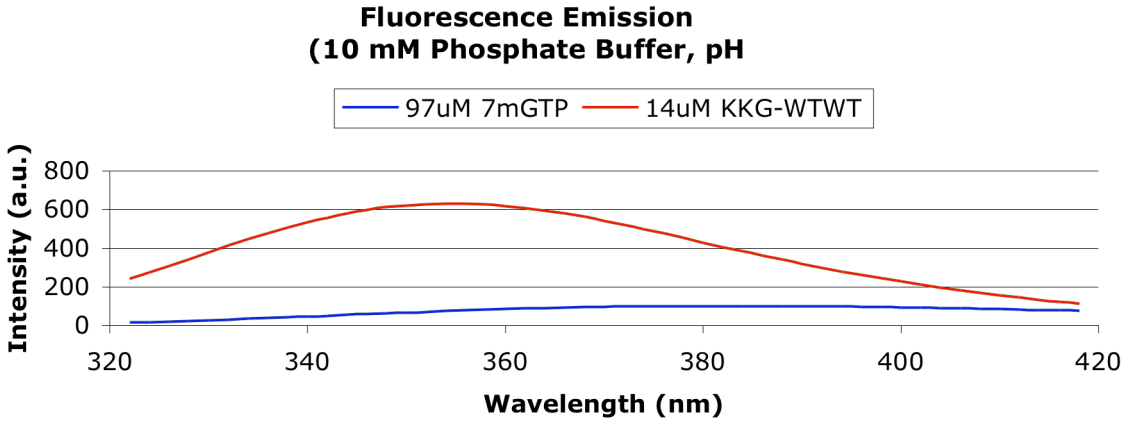

Figure 1.7: UV absorbance of 7mGTP and KKG-WTWT

[20] Parker, C. A. *Photoluminescence of Solutions*, Elsevier Publishing Company, Amsterdam, **1968**, p. 220-234.

[21] Niedzwiecka, A. *Personal Communication* **2005**.

[22] Niedzwiecka, A.; Darzynkiewicz, E.; Stolarski, R. *Biochemistry* **2004**, *43*, 13305-13317.

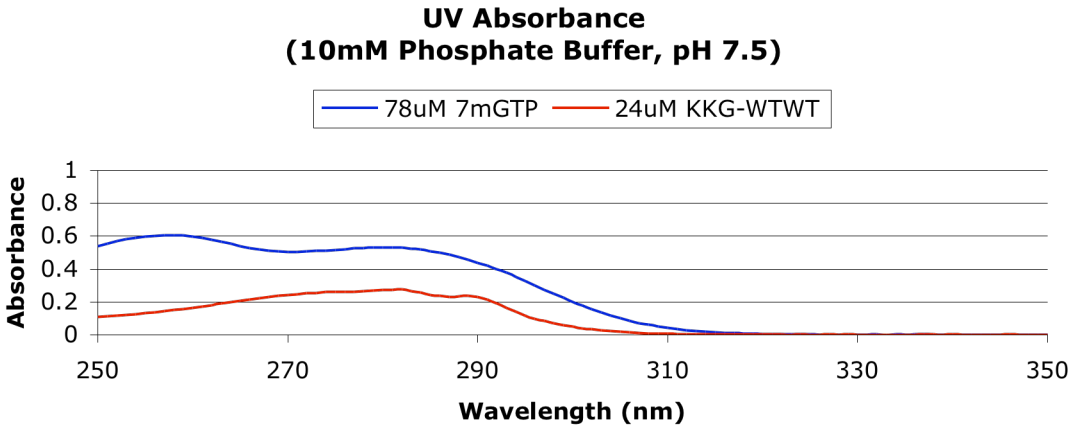

A calibration curve was used to correct the inner filter effect. This equation determined the effect of 7mGTP absorbance on Trp fluorescence. This calibration curve required a substitute substrate that satisfied three criteria. First, the substrate must absorb in a manner similar to both 7mGTP and GTP. Second, the peptide's affinity at low μM for the substrate should be weak. Lastly, the substrate cannot be fluorescent. Since the peptide's affinity for the substrate is weak, the decreasing fluorescence is solely due to the inner filter effect. GMP met all of these criteria and was tested as a potential substrate.

Using this calibration, the fluorescence of each titration point (peptide + nucleotide) was corrected. First, a Beer's law plot was created to confirm the linear relationship between absorbance and concentration of the peptide•nucleotide mixture. This was particularly useful for samples containing high amounts of nucleotide because the acquired absorbance was greater than 1. Second, the absorbance of each sample point was corrected using the Beer's Law plot. The corrected absorbance value was inserted into the calibration curve equation to determine the decrease in fluorescence as a result of the inner filter effect. Third, the raw fluorescence value was corrected by adding the artificial decrease in fluorescence to this raw

value. The corrected fluorescence values were fit to the binding equation reported by Stolarski.[22]

C. Competitive Binding Assay

As an alternative to Trp fluorescence quenching, a competitive binding assay using a fluorescent dye was developed. This approach is similar to the indicator displacement assays developed by Anslyn.[23] Using the fluorescent dye as the indicator (I), the peptide as the host (H), and 7mGTP as the guest (G), the following interactions were hypothesized:

$$I + H \overset{K_i}{\rightleftharpoons} [I\text{-}H] + G \overset{K_d}{\rightleftharpoons} I + [H\text{-}G] \quad (\mathbf{1.1})$$

First, an indicator must be selected which can interact with the host to form a reversible indicator•host complex through non-covalent interactions. Upon formation of the complex, a spectroscopic property (absorbance, fluorescence) of the indicator changes. After addition of a guest, the indicator•host complex dissociates to form a host•guest complex. The indicator's spectroscopic property that changed reverts back to its state at the beginning of the assay.

The dye functions as the signal for this binding study, rather than the Trp. Since the dye's absorbance and fluorescence wavelengths are different than those for Trp, the inner filter effect and overlapping fluorescence are not significant. First, a binding constant (K_i) would be determined for the peptide and the dye. If there is an interaction between the peptide and the dye, then quenching of the dye's fluorescence should be observed as peptide concentration increased. After determining K_i, the nucleotide would be titrated into the mixture and the dye would be displaced by the nucleotide as a result of the peptide and nucleotide associating. The peptide•nucleotide association would return the dye back to its starting state. In the case of fluorescence, unquenching would occur. A variety of

[23] Wiskur, S. L.; Ait-Haddou, H.; Lavigne, J. J.; Anslyn, E. V. *Acc. Chem. Res.* **2001**, *34*, 963-972.

commercially available dyes were investigated (Figure 1.8). Each contained a large, planar, aromatic group that suggested it might bind well to the β-hairpin.

Figure 1.8: Fluorescent Dyes used in Competitive Binding Studies

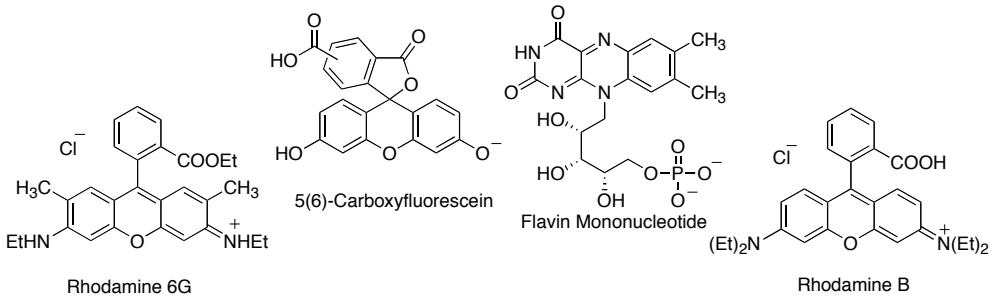

D. Isothermal Titration Calorimetry

As an alternative to spectroscopic techniques, calorimetry was used to investigate the binding process. Recent technological and methodological advances in the field of calorimetry make it possible to measure the small amount of heat associated with the non-covalent interactions between the components in a binding process.[24] These advances resulted in the development of isothermal titration calorimetry (ITC). ITC provides a direct route to the complete thermodynamic characterization of bimolecular equilibrium interactions. One experiment can determine the binding constant (K_a or K_d), binding enthalpy (ΔH), and stoichiometry (N).[25] This is an advantage over spectroscopic techniques, which only provide a binding constant. In order to determine the binding enthalpy, a van't Hoff analysis is needed but this can lead to values with large errors and, in some systems, may not

[24] Wiseman, T.; Williston, S.; Brandts, J. F.; Lin, L. N. *Anal. Biochem.* **1989**, *179*, 131-137.

[25] (a) Fisher, H. F.; Singh, N. *Methods Enzymol.* **1995**, *259*, 194-221. (b) Ladbury, J. E.; Chowdhry, B. Z. *Chem. Biol.* **1996**, *3*, 791-801. (c) Jelesarov, I.; Bosshard, H. R. *J. Mol. Recognit.* **1999**, *12*, 3-18. (d) Campoy, A. V.; Freire, E. *Biophys. Chemist.* **2005**, *115*, 115-124.

even be possible.[26] Another advantage of ITC is the avoidance of reporter labels (isotopes, fluorophores, chromophores, etc.) to monitor the reaction. Incorporation of reporter labels may require significant cost and/or time. Since ITC uses the change in heat as a signal, the natural host and guest can be used to conduct the experiment. The main drawback of the ITC experiment is that the ΔH measured is a global value. As a result, only non-mechanistic information about the binding process is acquired. Strong ($K_a > 10^8$ M^{-1}) and weak ($K_a < 10^4$ M^{-1}) binding constants can be difficult to determine by ITC but all those in between are considered measurable. Like any other technique, ITC has its disadvantages but its advantages make it worth investigating.[26]

In an ITC experiment,[26] there are two cells: a sample cell and a reference cell (Figure 1.9). The reference cell contains the buffer or solvent that is used for the experiment. The sample cell contains one part of the titration experiment, typically the receptor or host. The ligand or guest is typically added to the sample cell via a syringe located above the sample cell. There's a connection between the two cells to measure the temperature difference (ΔT) between them. Upon titration, an enthalpic change results in the sample cell. The instrument compensates for this enthalpic change by adding or removing heat from the sample cell to maintain $\Delta T = 0$. If the change is exothermic, less heat per unit time is needed for the sample cell to maintain $\Delta T = 0$. If the change is endothermic, the opposite effect will be observed.

Figure 1.9: Diagram of the ITC instrument[25b]

[26] Naghibi, H.; Tamura, A.; Sturtevant, J. M. *Proc. Natl. Acad. Sci. USA* **1995**, *92*, 5597-5599.

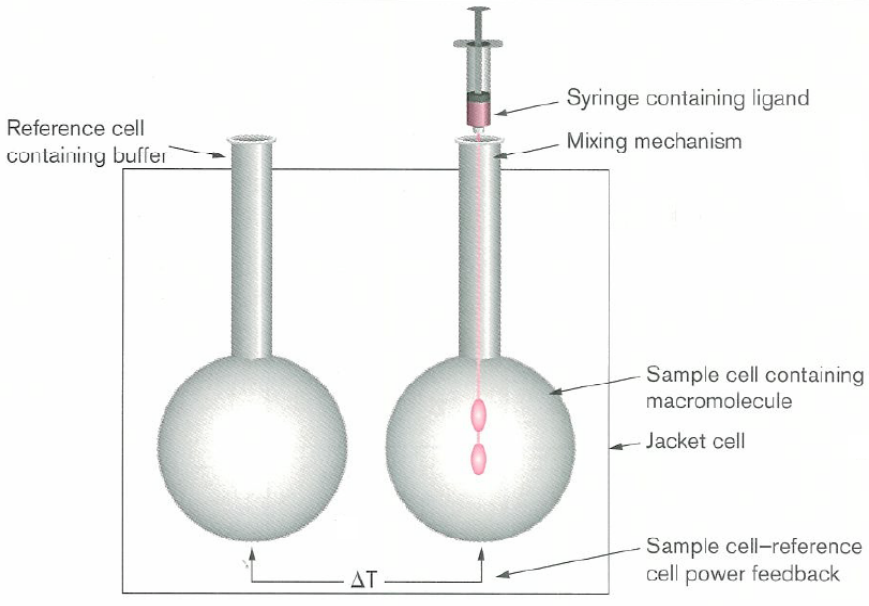

Calorimetry is an intriguing technique because it is capable of simultaneously measuring the binding constant (K_a) and enthalpy of binding (ΔH). K_a can be determined because the amount of ligand and host used for the experiment is known. Using the equation, $\Delta G = -RT\ln K_a$, the binding constant can be converted to a ΔG value. Since both the ΔG and ΔH are determined experimentally, the ΔS value can be directly determined using the equation, $\Delta G = \Delta H - T\Delta S$. Therefore, a full thermodynamic profile can be acquired in one experiment.

A couple of notes should be remembered regarding an ITC experiment. First, heat changes can be a result of dilution (host or guest) so appropriate control experiments need to be done to correct for this. Second, the binding sites of the host should be fully saturated. If this is achieved then the heat changes observed at the end of the experiment are solely due to dilution. Lastly, binding studies are concentration dependent so the ITC experiment needs to be conducted at the appropriate concentrations. To accommodate this requirement, a unitless value, c, is used. c is the product of the binding constant and the concentration of ITC cell

component, $c = K_a$ x [Cell]. For a simple experiment, this value should be greater than 10 but less than 100.

E. NMR Titration Binding Studies

As an alternative to both fluorescence and calorimetry based binding studies, ^{1}H NMR titration was considered as well. This experiment relies on the aromatic chemical shifts of tryptophan to monitor the binding event. For this experiment, the guest is titrated into a solution containing the host and the binding is monitored by the change in chemical shift of the Trp residues. Since the binding is hypothesized to occur between the Trp residues, their chemical shifts should change as a function of guest concentration. At saturation, the Trp chemical shift should stop changing. The overall change in chemical shift can be plotted versus the concentration of guest in order to get a binding constant.

F. Trp Analog Synthesis

Imperiali[27] recently reported the synthesis of a fluorescent amino acid, DAPA, similar in size to Trp (Figure 1.10) but exhibiting different fluorescence properties (Table 1.1). Synthesis of this non-natural amino acid and incorporation into a β-hairpin by solid phase peptide synthesis (SPPS) will provide a peptide that is similar to the Trp containing peptides. Measurement of binding by fluorescence quenching of DAPA by 7mGTP could serve as an alternative way to determine a binding constant.

Figure 1.10: Size comparison of Trp and DAPA

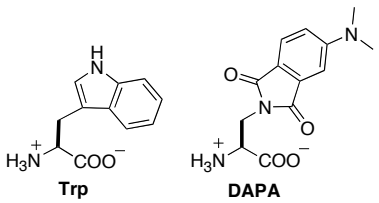

[27] Vazquez, M. E.; Rothman, D. M.; Imperiali, B. *Org. Biomol. Chem.* **2004**, *2*, 1965-1966.

Table 1.1: UV and Fluorescence Properties of Trp and DAPA in pH 7.5 Phosphate Buffer

Amino Acid	Absorbance λ_{max}	Excitation λ	Emission λ
Trp	280 nm	280 nm	354 nm
DAPA	421 nm	395 nm	536 nm

III. Results

A. Quenching of Trp Fluorescence

A calibration curve was acquired for both WTWT-K and WQWQ-K with GMP. The absorbance was recorded at 297 nm (WTWT-K and WQWQ-K) and the fluorescence was recorded at either 356 nm (WTWT-K) or 350 nm (WQWQ-K). The calibration curves were very similar to each other (see experimental). Using the same peptides, a binding study was conducted by titrating the nucleotide (GTP or 7mGTP) into a fixed amount of peptide. For these samples, the Beer's law plot was created to acquire the true absorbance value for the calibration curve. Using the corrected absorbance values, the calibration curve reported the decrease in fluorescence as a result of the inner filter effect. In the case of GTP, the calibration curve worked for some of the titration points but then broke down as the concentration of nucleotide increased (see experimental). Binding constants were acquired with the corrected data but, in the case of WTWT-K, large error was observed (Table 1.2). In the case of 7mGTP, the calibration curve never worked and increasing Trp fluorescence was observed from the start.

Table 1.2: Binding constants using calibration curve (10mM Phosphate Buffer, pH 7.5)[a]

Peptide	K_d(GTP) in μM[b]	K_d(7mGTP) in μM
WTWT-K	199 ± 110	n/a
WQWQ-K	113 ± 20	n/a

a. Each point measured in triplicate; b. Error based on fitting

Since the calibration curve approach was unsuccessful, another approach to measure binding was attempted. In this approach, 7mGTP was used to quench Trp fluorescence but only the overlapping fluorescence was corrected. Even thought the inner filter effect contributes to the quenching observed, this experiment was performed to estimate the binding constant. The initial results (Table 1.3) indicated that WTWT-K bound 7mGTP just as well as KKG-WTWT and that in both cases, K_d values are in the high micromolar range.

Table 1.3: Binding Constants from 7mGTP Titration (10mM Phosphate Buffer, pH 7.5) uncorrected for Inner Filter Effect[a]

Peptide	K_d (μM)	K_a (M^{-1})[b]
KKG-WTWT	158 ± 5	6330 ± 220
WTWT-K	144 ± 8	6920 ± 370

a. Each point measured in triplicate; b. Error based on fitting

B. Competitive Binding Assay

For the competitive binding assay, fluorescence was used as the signal since the excitation and emission wavelengths of 5(6)-carboxyfluorescein do not overlap with those of Trp or 7mGTP. A K_i was determined for 5(6)-carboxyfluorescein and the peptide by measuring the change in 5(6)-carboxyfluorescein fluorescence as peptide concentration was increased. A strong interaction was observed between 5(6)-carboxyfluorescein and each of the peptides: $K_i < 6$ μM (Table 1.4). However, as the concentration of 5(6)-carboxyfluorescein was decreased to optimize K_i, the overall change in fluorescence intensity ($\Delta F = F_o - F_\infty$; F_o is initial fluorescence and F_∞ is saturation fluorescence) decreases and the error range of each point exceeds the fluorescence change. All attempts to improve the binding of the dye by the peptide were unsuccessful. As a result, no reliable, reproducible data could be acquired for 5(6)-carboxyfluorescein and the peptide at the measured concentrations.

Table 1.4: K_i at 0.5 μM 5(6)-Carboxyfluorescein (10mM Phosphate Buffer, pH 7.5)[a]

Peptide	K_i (μM)[b]	ΔF (a.u.)
KKG-WTWT	2.2 ± 0.8	90
WTWT-K	4.1 ± 0.9	40
WTWK	5.3 ± 0.8	35

a. Each point measured in triplicate b. Error based on fitting

A new dye was sought for the competitive binding assay. Rhodamine B and 6G, commercially available dyes, were chosen because they each possess large, planar, aromatic groups like 5(6)-carboxyfluorescein. The electron poor face of each rhodamine suggested it might interact favorably with the electron rich Trp. Fluorescence studies were attempted to measure binding but the fluorescence was not quenched, it was enhanced. As a result, the interaction could not be quantified.

An indicator that would exhibit larger fluorescence changes upon interacting with the peptide was needed for the competitive binding assay. WKWK was shown to bind flavin mononucleotide (FMN) in water (K_d = 450 μM) using fluorescence spectroscopy.[28] The affinity was shown to be a combination of aromatic and electrostatic interactions between FMN's aromatic face with Trp and FMN's phosphate group with the Lys side chains, respectively. Both of these interactions were observed between WKWK and ATP.[19] Most notable about this study was the large change in fluorescence intensity upon titration. The fluorescence intensity decreased 5-fold from F_o to F_∞. (Figure 1.11)

[28] Butterfield, S. M.; Goodman, C. M.; Rotello, V. M.; Waters, M. L. *Angew. Chem. Int. Ed*. **2004**, *43*, 724-727.

Figure 1.11: FMN fluorescence quenching in the presence of increasing concentrations of WKWK. [28]

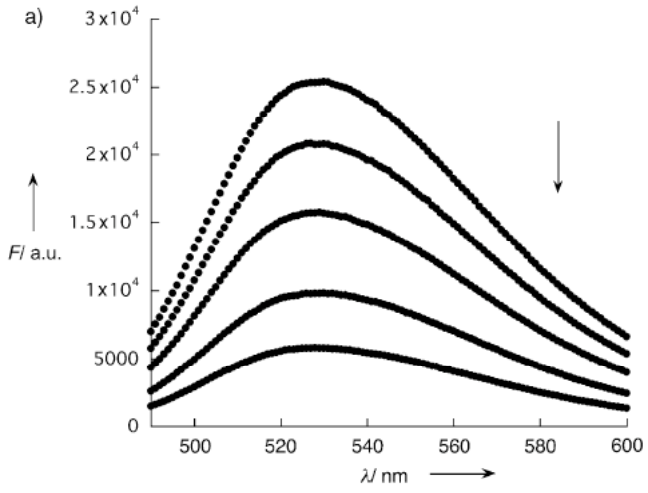

FMN was tested with WTWK because it contained part of WKWK's electrostatic component. As expected, ΔF was large (~500 a.u.) and a reproducible dissociation constant (K_i = 840 μM) was obtained. The binding was not as strong as that for 5(6)-carboxyfluorescein but a weak interaction between I and H was believed to facilitate the interaction between H and G (Equation 1.1). K_d can be obtained by fitting the FMN emission intensities as a function of 7mGTP concentration (see experimental).[29] The following conditions were reported to best fit the fluorescence data to the binding curve (see experimental): I = $10K_i$, H = $20K_i$, and G ranges from 0 to 40 x 10^3 K_i. G will vary from one system to another but the conditions for I and H do not figure to change. These conditions project the following: [FMN] = 8.4 x 10^3 μM, [WTWK] = 16.8 x 10^3 μM, and a potential [7mGTP] = 3.36 x 10^7 μM. Typical concentration ranges for these fluorescence experiments are in the low to mid μM range. Nevertheless, an attempt was made at the following concentrations: 34 μM FMN, 626 μM WTWK, and 0 to 1570 μM 7mGTP. Unquenching was observed but the data could not be fit to the binding curve. No follow up was done because

[29] Wang, Y.; Rando, R. R. *Chem. Biol.* **1995**, *2*, 281-290.

the minimum concentrations seemed too high to be useful and/or practical. In addition the peptide's solubility limit was approached for these studies.

C. Isothermal Titration Calorimetry (ITC)

As an alternative to fluorescence based methods, ITC was attempted. In this experiment, the binding constant was acquired directly from the heat given off (or consumed) while the peptide and NTP associate. This method avoids the use of reporter labels and can measure binding constants in the following range: $10^4 < K_a < 10^8$ M^{-1}or mM < K_d < μM range. The binding constant for initial experiments was estimated based on the K_d (144 μM) of 7mGTP by WTWT-K (Table 1.3).

Dilution studies were performed for both WTWT-K and 7mGTP. In the case of peptide, the heat of dilution was negligible. The heat of dilution for the WQWQ-K peptide was assumed to be negligible too. In the case of 7mGTP, the heat of dilution was very endothermic. Unfortunately the data for the 7mGTP heat of dilution could not be used to correct binding studies with the WTWT-K peptide because the concentrations of 7mGTP used in each experiment were different.

The best data acquired via ITC involved the titration of 7mGTP into the sample cell containing WQWQ-K. This data indicated that the dissociation constant for 7mGTP was 5 mM for WQWQ-K; however, this result was not reproducible. Binding saturation was not observed and that may be a cause for the inconsistent results. GTP was not investigated because no consistent, reproducible data could be acquired for 7mGTP. As a result, another method that could determine weak binding constants was needed. In addition it should be applicable for both GTP & 7mGTP binding studies.

D. NMR Titration Binding Studies

NMR titration was used to measure the binding constant because the binding appeared to be too weak to measure by ITC. The desalted peptide (WQWQ-K or WTWT-K) was titrated with the nucleotide (GTP or 7mGTP) to measure the binding constant in 10 mM Phosphate Buffer, pH 7.5. For the study of WKWK with nucleotides, the experiment was performed by injecting nucleotide (μL quantity) to a sample containing the peptide receptor.[19] The same approach was attempted initially but precipitation was observed during the experiment. To avoid this, multiple samples were made with a fixed peptide concentration and variable nucleotide concentration (see experimental).

For both peptides studied (WQWQ-K and WTWT-K) a higher affinity for GTP was observed relative to 7mGTP (Table 1.5). In the case of WTWT-K, the K_a for GTP is within error of the K_a for 7mGTP. In the case of WQWQ-K, there is at least a two-fold difference between the K_a's for GTP and 7mGTP. In all cases, binding saturation is not observed (see experimental). Unfortunately the binding could not be saturated with the nucleotide because this required stock solutions of nucleotide that were too high in concentration and may result in aggregation. As a result, a different approach was needed to investigate binding.

Table 1.5: Binding constants acquired by NMR titration (10mM Phosphate Buffer, pH 7.5)[a]

	K_a (7mGTP)	**K_a (GTP)**
WQWQ-K	144 M^{-1} ± 9.3	323 M^{-1} ± 20
WTWT-K	272 M^{-1} ± 37	482 M^{-1} ± 111

a. Error based on fitting

E. Trp Analog Synthesis

We next investigated replacing Trp with an unnatural fluorescent amino acid. We chose to use the amino acid reported by Imperiali.[28] The reported procedure (Scheme 1.1) consists of two parts. First is the synthesis of the amino acid side chain via reductive amination of 4-aminophthalic acid followed by sublimation to the desired anhydride **3**. The

second part consists of protection and deprotection strategies to prepare the commercially available amino acid (N-α-Fmoc-N-β-t-Boc-L-diaminopropionc acid) for side chain modification **6**. All of these steps have been performed successfully. The final step, allyl deprotection, has been met with some difficulty during the purification. This research is ongoing.

Scheme 1.1: DAPA synthesis

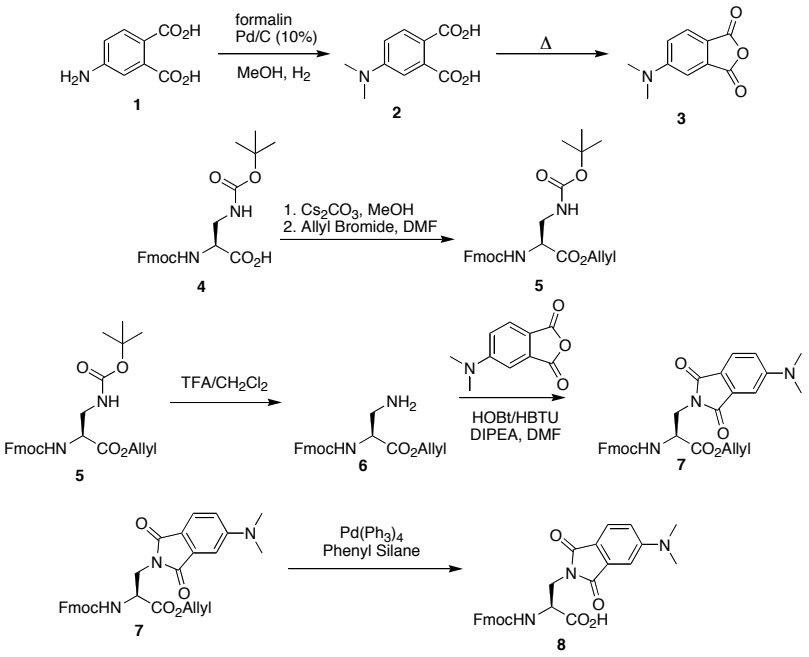

IV. Discussion

A. Quenching of Trp Fluorescence

The calibration curve was insufficient for 7mGTP and GTP because their binding by the peptide was too weak. The calibration curve works well for Niedziecka and Stolarski[23] because their binding constant for 7mGTP is stronger than that for the β-hairpin used in these studies. A calibration curve with higher concentration range was needed for the present binding study. However, that was not possible since the absorbance value for the corresponding GMP points would exceed the range and validity of Beer's law. Since

fluorescence quenching was proving to be difficult, an alternative method to quantify binding was sought. A method that showed no bias for the spectroscopic properties of host or guest would be desirable.

B. Competitive Binding Assay

In the case of 5(6)-carboxyfluorescein, a large ΔF was needed so that when unquenching occurs, the change in fluorescence is outside of the error in the measurement. If not addressed, the unquenching result may not be reproducible. Also, the peptide's affinity for the 5(6)-carboxyfluorescein was strong. As a result, the affinity of 7mGTP would need to be stronger in order to displace the fluorescent dye from the peptide. The dissociation constant for this process would have to be less than 6 μM. Subsequent studies showed that the binding of 7mGTP was not this strong. Even if ΔF was as large as the one for flavin, then unquenching probably would not have been observed.

The fluorescence intensity for both the rhodamine dyes (B and 6G) increases in the presence of increasing peptide concentration. The cause of this result is unknown at this time. One difference between the rhodamine dyes and 5(6)-carboxyfluorescein is the overall charge of the aromatic face. Rhoadamines have cationic aromatic faces while 5(6)-carboxyfluorescein has an anionic face. This difference may be the cause for enhanced fluorescence.

In the case of flavin mononucleotide, the desired result was found but the data could not be fit to the binding curve. If enough 7mGTP had been added to saturate the peptide's binding site, then full unquenching would have been observed and the data could have been fit to the binding curve. In order to acquire that result, 7mGTP was required at ~1 M concentration. Stronger binding between the peptide and flavin mononucleotide would

require less peptide and 7mGTP for the competition assay. However, the peptide•dye interaction cannot be stronger than the peptide•7mGTP interaction or that assay may not proceed correctly.

C. Isothermal Titration Calorimetry

Weak binding was observed in the case of 7mGTP titration into WQWQ-K. The projected binding constant (K_a = 197 M^{-1}, K_d = 5 mM) is within the theoretical detection limit of the instrument. This fact is supported by the c value for this binding study, c = 2.2. Recall, c = K_a x Cell concentration. In summary, the experiment was conducted correctly. Despite the appropriate conditions, binding saturation was not observed at the end of the titration experiment (Figure 1.38). If the K_d is assumed to be in the mid to high μM range, then the concentration of host, for this experiment, is at approximately the K_d. As a result, titration of 7mGTP into the cell should result in saturation of the host's binding sites; however, this is not observed. The lack of binding saturation for the host, in this particular experiment, supports the projected binding constant.

D. NMR Binding Studies

A comparison of the binding constants indicates that both peptides (WQWQ-K and WTWT-K) bind GTP more strongly than 7mGTP. Upon analyzing the plotted data, two things stand out. First, GTP binding studies are closer to saturation than 7mGTP binding studies. So the values for 7mGTP binding are not as accurate as those for GTP binding. Second, a comparison of the GTP and 7mGTP data shows that, at similar nucleotide concentrations, the amount of upfield shifting is different. Consider the WTWT-K binding study at similar concentrations of NTP (Figures 1.41 and 1.42). The Trp chemical shift for 7mGTP titration has moved 0.020 ppm further than that for GTP. If this study was carried

out to saturation then the binding constant for 7mGTP would be different, probably lower than for GTP. A similar trend is observed for WQWQ-K data (Figures 1.39 and 1.40).

E. Trp Analog Synthesis

All synthetic steps were performed analogous to the reported procedure. Difficulties arose in two of the steps. The sublimation step was not as high yielding as the reported procedure. Sublimed product was very pure but starting material always remained. Repeated sublimations increased the overall yield. Difficulty characterized the final step: allyl deprotection. The problem appeared in the purification step. TLC showed that starting material was consumed but product could never be isolated cleanly. Different lots of $Pd(PPh_3)_4$ were tested but the same problems arose. Currently, this synthesis has been performed successfully up to allyl ester containing DAPA side chain.

The cause for the difficulties with allyl deprotection has not been identified. Efforts are underway to complete this synthesis. The lack of success with other binding methods further emphasizes the importance of this synthesis.

V. Conclusions

Several types of binding studies were investigated to quantify the interaction of a designed beta-hairpin peptide with 7mGTP. Fluorescence based binding studies were attempted but were not successful in determining a binding constant. For the case of Trp fluorescence quenching, the binding was too weak to measure with the assistance of a calibration curve. For the case of competitive binding assays, the interaction between the peptide and dye was either too strong (5(6)-Carboxyfluorescein), too weak (Flavin Mononucleotide), or unable to be determined (Rhodamines). ITC binding studies were investigated but the binding was too weak for reproducible measurement. ^{1}H NMR titrations

were investigated but the binding was too strong for measurement. The synthesis of a Trp analogue (DAPA) was initiated but attempts to remove the allyl group were unsuccessful. As a result, this approach was never fully investigated.

The unique absorbance and fluorescence properties of 7mGTP make it a difficult target to bind in aqueous solution. Calorimetry is probably the best approach since it shows no bias to spectroscopic properties but the binding appears too weak to use this method. Alternatively, the use of another electron-rich aromatic side chain could be used to maximize the cation-pi interaction hypothesized for 7mGTP recognition.

VI. Experimental Procedures

A. Peptide Synthesis and Purification

Peptides were synthesized by automated solid phase peptide synthesis on an Applied Biosystems Pioneer Peptide Synthesizer using Fmoc (9-fluorenylmethoxycarbonyl) protected amino acids on a PAL-PEG-PS resin. The amino acids residues were activated for coupling with HBTU (O-benzotriazole-N,N,N',N',-tetramethyluronium hexafluorophosphate) and HOBt (N-hydroxybenzotriazole) in the presence of DIPEA (diisopropylethylamine) in solvent DMF (N,N-dimethylformamide). Deprotections were carried out in 2% DBU (1,8-diazabicyclo[5.4.0]undec-7-ene), 2% piperdine in DMF for approximately 10 minutes. Extended cycles (75 minutes) were used for each amino acid coupling step. The N-terminus was acetylated with 5% acetic anhydride, 6% lutidine in DMF for 30 minutes. Cleavage of the peptide from the resin was performed in 95:2.5:2.5 TFA (trifluoroacetic acid): TIPS (Triisopropylsilane): water for 3-4 hours. TFA was evaporated and ether was used to precipitate the cleavage products. The water soluble peptides were extracted with water and lyophilized. Peptides were purified by reversed phase HPLC, using a Waters Atlantis dC_{18} (5μm, 10 x 100mm) column and a gradient of 1 to 60% B in 50 minutes, where solvent A was 95:5 water:acetonitrile, 0.1 % TFA and solvent B was 95:5 acetonitrile:water, 0.1 % TFA. Once purified, the peptides were lyophilized to powder and the peptide identity was confirmed by ESI (Positive Ion mode) mass spectrometry. Peptides used for binding studies were then desalted by size exclusion chromatography using polyacrylamide column and lyophilized to powder.

B. Fluorescence Quenching of Trp

Peptide samples were prepared in 10 mM phosphate buffer, pH 7.5, and their concentrations were determined in 6 M guanidine hydrochloride using the absorbance of the tryptophan residues at 280 nm ($\varepsilon_{280,\,Trp}$ = 5690 $M^{-1}\bullet cm^{-1}$).[30] Nucleotide stock solutions were prepared in 10 mM phosphate buffer, pH 7.5. Concentrations were determined by UV spectroscopy using the molar extinction coefficient of the nucleotides ($\varepsilon_{253,\,GMP} = \varepsilon_{253,\,GTP}$ = 13700 $M^{-1}\ cm^{-1}$; $\varepsilon_{297,\,7mGTP}$ = 3537 $M^{-1}\ cm^{-1}$).[31]

Calibration Curve

Fluorescence scans were obtained using an excitation wavelength of 297 nm. Absorbance scans were obtained at a wavelength of 297 nm. Both fluorescence and absorbance data were obtained at ambient temperature. The emission intensity of tryptophan as a function of peptide + GMP absorbance was fit to a curve using linear regression analysis on Kaleidegraph. Figures 1.12 and 1.13 are sample calibration curves.

Figure 1.12: Calibration Curve for GMP and WTWT-K (17.5 μM) in 10 mM Phosphate Buffer, pH 7.5 at 298 K.

[30] Edelhoch, H. *Biochemistry* **1967**, *6*, 1948-1954.

[31] *CRC Handbook of Biochemistry and Molecular Biology, 3rd Edition, vol. 1: Nucleic Acids*, CRC Press, **1975**.

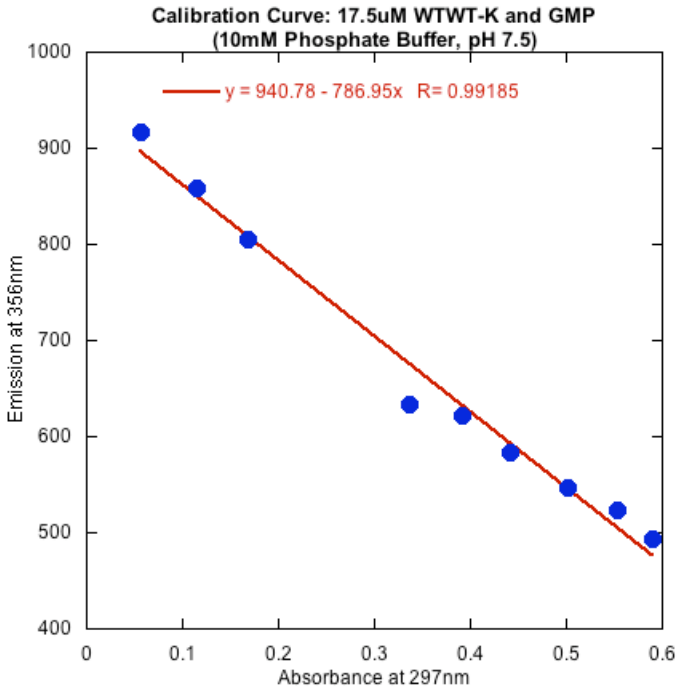

Figure 1.13: Calibration Curve for GMP and WQWQ-K (19.0 μM) in 10 mM Phosphate Buffer, pH 7.5 at 298 K.

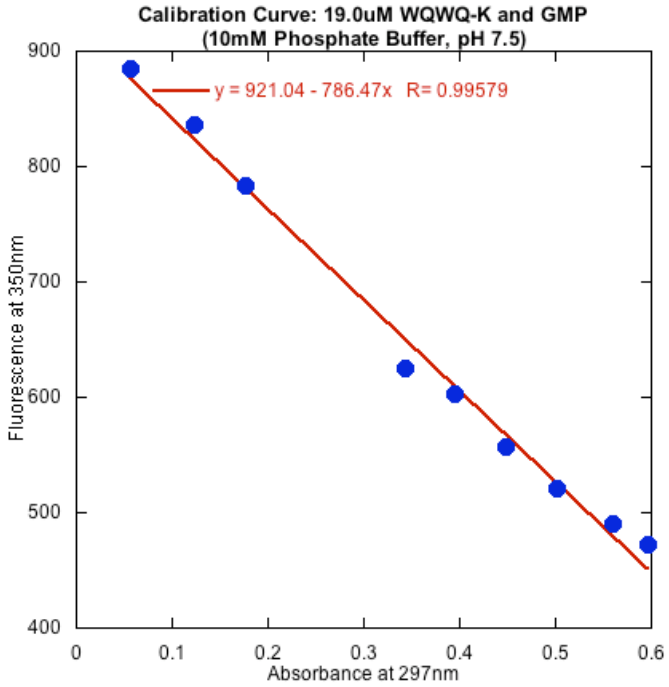

Beer's Law Plot

The absorbance of each sample at 297 nm (peptide + nucleotide) was plotted as a function of nucleotide concentration and fit to a curve using linear regression analysis on Kaleidegraph. Figures 1.14 through 1.19 are sample Beer's law plots.

Figure 1.14: Beer's Law Plot for GMP and WTWT-K (17.5 μM) in 10 mM Phosphate Buffer, pH 7.5 at 298 K.

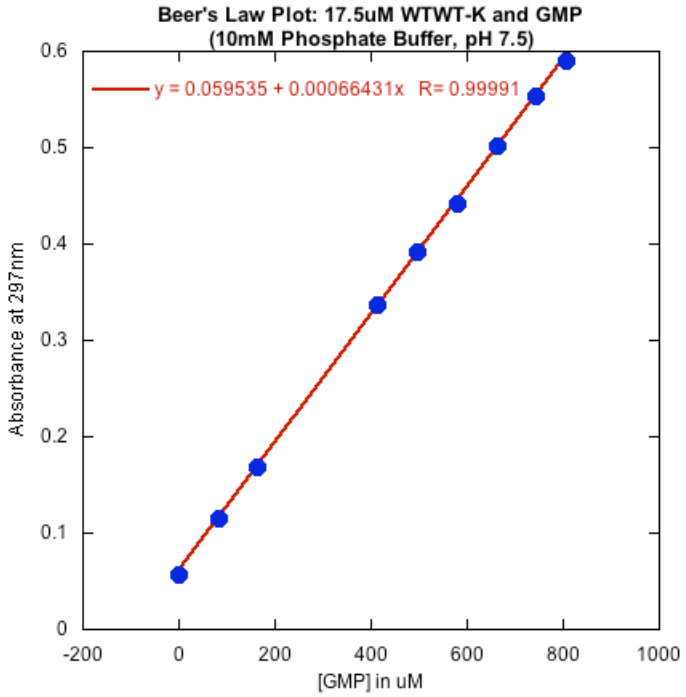

Figure 1.15: Beer's Law Plot for GTP and WTWT-K (17.5 μM) in 10 mM Phosphate Buffer, pH 7.5 at 298 K.

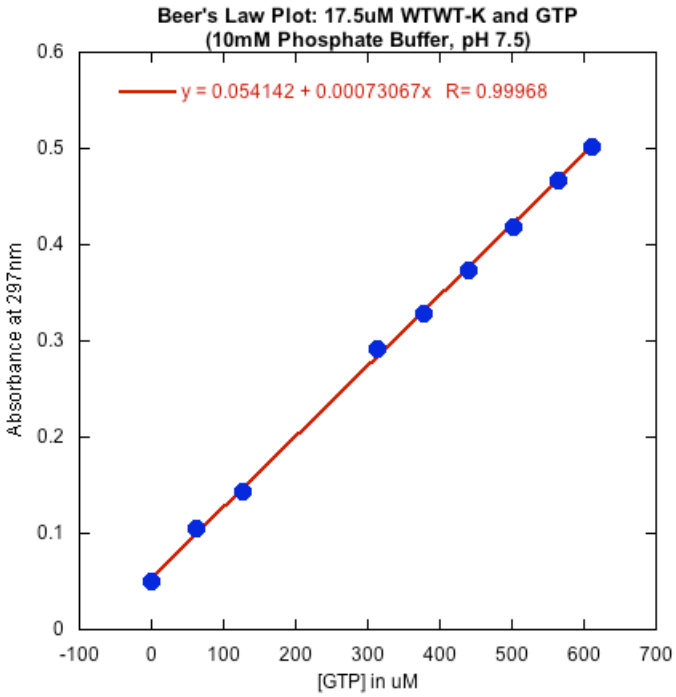

Figure 1.16: Beer's Law Plot for 7mGTP and WTWT-K (17.5 μM) in 10 mM Phosphate Buffer, pH 7.5 at 298 K.

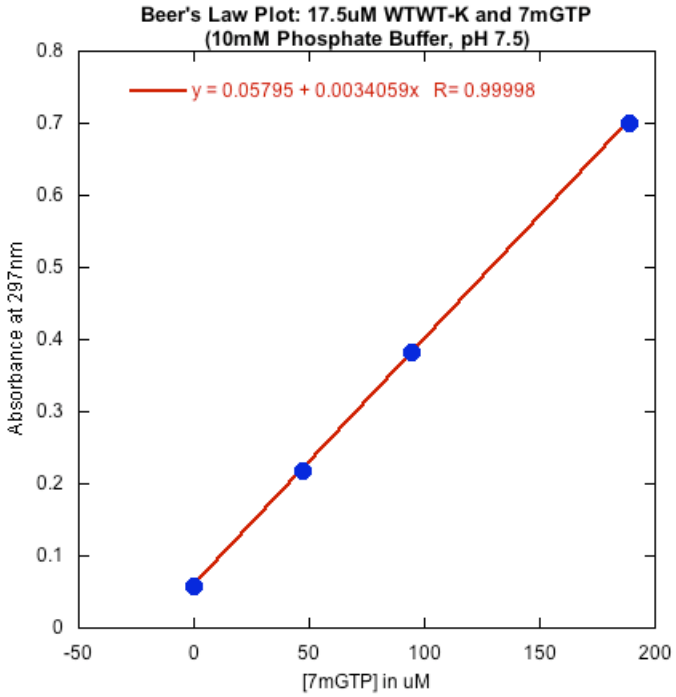

Figure 1.17: Beer's Law Plot for GMP and WQWQ-K (19.0 μM) in 10 mM Phosphate Buffer, pH 7.5 at 298 K.

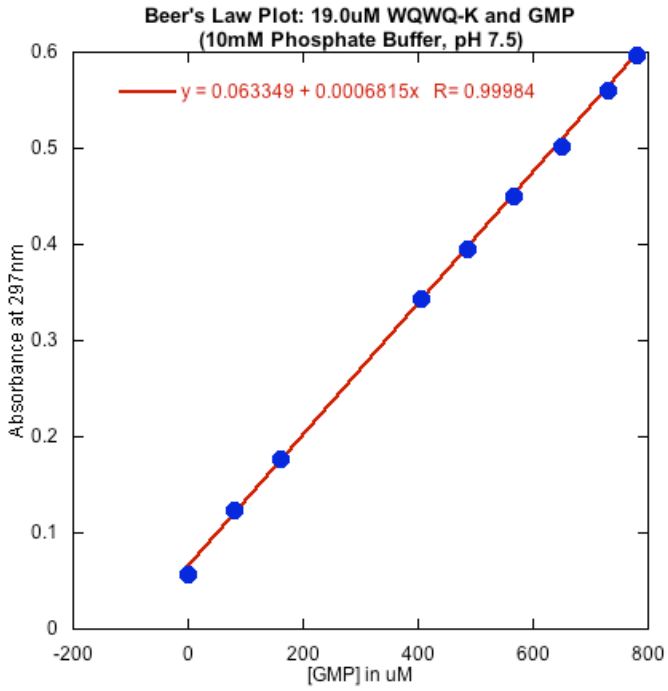

Figure 1.18: Beer's Law Plot for GTP and WQWQ-K (19.0 μM) in 10 mM Phosphate Buffer, pH 7.5 at 298 K.

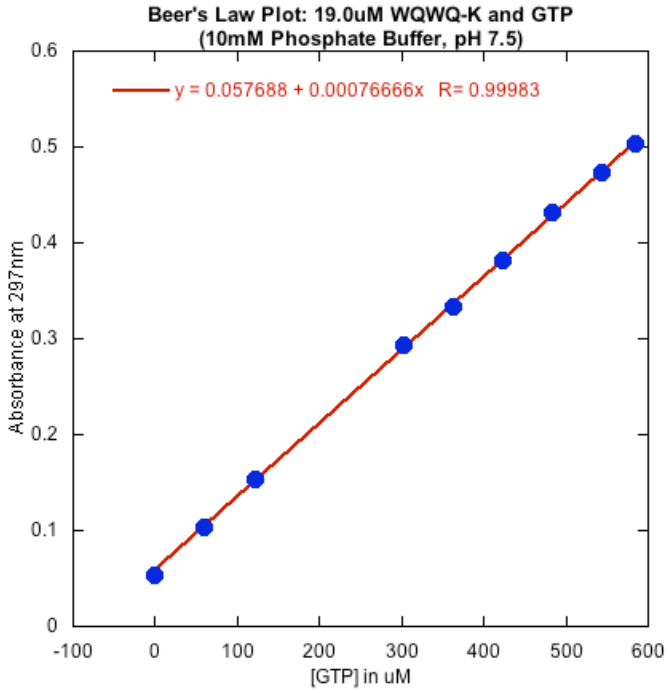

Figure 1.19: Beer's Law Plot for 7mGTP and WQWQ-K (19.0 μM) in 10 mM Phosphate Buffer, pH 7.5 at 298 K.

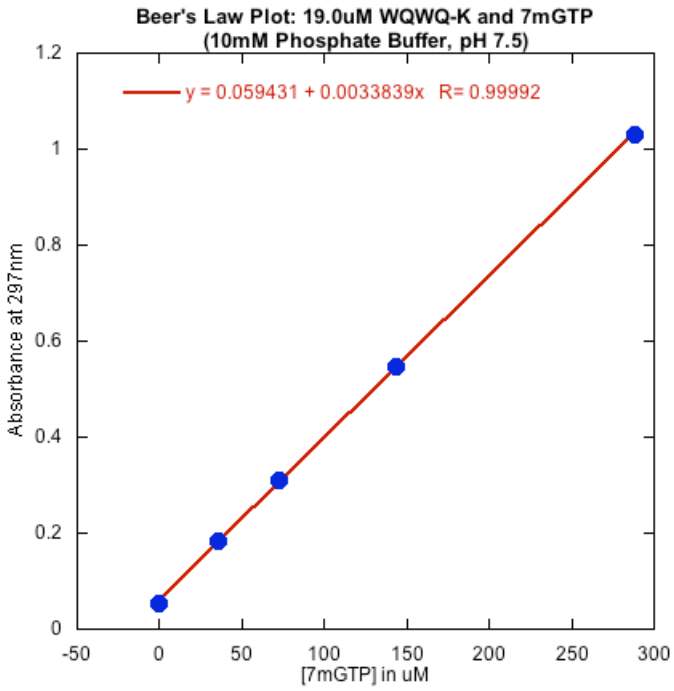

Correcting Data

The theoretical concentration of NTP in each mixture was entered into the Beer's law equation to acquire the theoretical absorbance value for each titration sample (peptide + NTP). This value was designated as the corrected absorbance. The fluorescence value from the calibration curve was obtained by substituting the corrected absorbance (x). The fluorescence value returned (y) is called the corrected fluorescence. The first sample's fluorescence (peptide only) is not altered by the inner filter effect. As a result, this value should be similar to the raw fluorescence value and is sometimes identical. As more NTP is added, the difference between the raw and corrected fluorescence values increases; this is a result of the inner filter effect. To correct for the inner filter effect, one must determine the difference, in corrected fluorescence, between the first sample and the sample of interest. This difference is the amount of fluorescence decrease as a result of the inner filter effect. This difference is added back into the raw fluorescence value in order to correct for the loss.

The resulting values are considered the true fluorescence values for each titration point. The true fluorescence emission for Trp as a function of GTP concentration was fit to the following binding equation on Kaleidegraph.[32]

$$F_c = [F_o + F_\infty (H/K_i)] / [1 + (H/K_i)] \quad \textbf{(1.2)}$$

F_c is the corrected fluorescence intensity, F_o is the initial fluorescence intensity, F_∞ is the fluorescence intensity at binding saturation, H is the concentration of peptide, and K_i is the dissociation constant.

Figure 1.20: Corrected Fluorescence Titration for GTP and WTWT-K (17.5 μM) in 10 mM Phosphate Buffer, pH 7.5 at 298 K.

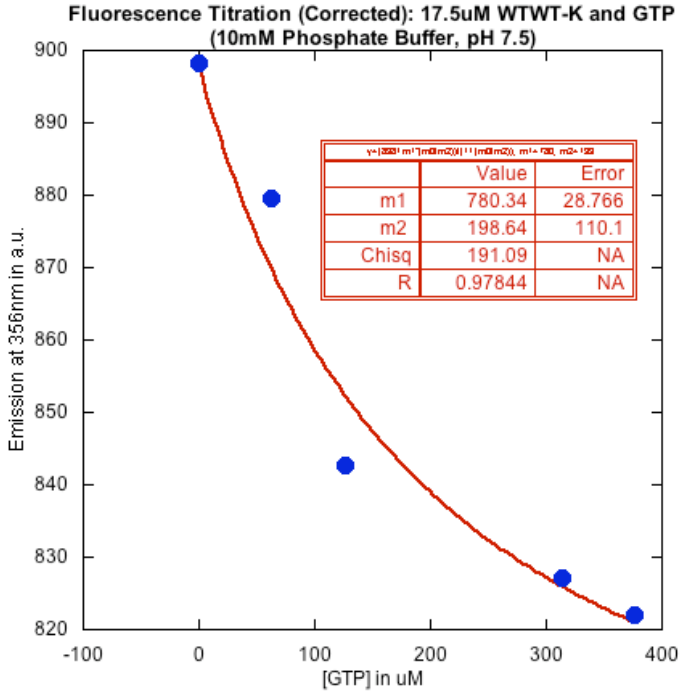

Figure 1.21: Comparison of Corrected and Uncorrected Fluorescence Data for GTP and WTWT-K (17.5 μM) in 10 mM Phosphate Buffer, pH 7.5 at 298 K.

[32] Lim, W. A.; Fox, R. O.; Richards, F. M. *Protein Sci*. **1994**, *3*, 1261-1266.

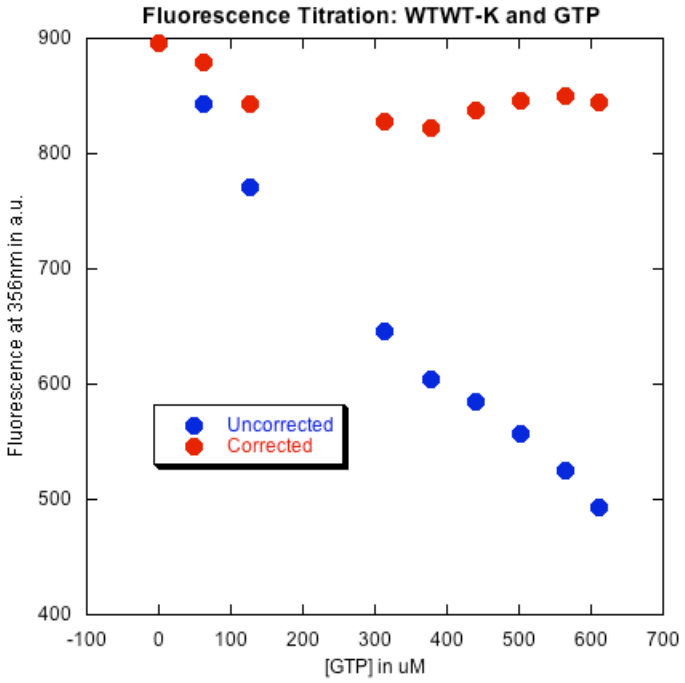

Figure 1.22: Corrected Fluorescence Titration for GTP and WQWQ-K (19.0 μM) in 10 mM Phosphate Buffer, pH 7.5 at 298 K.

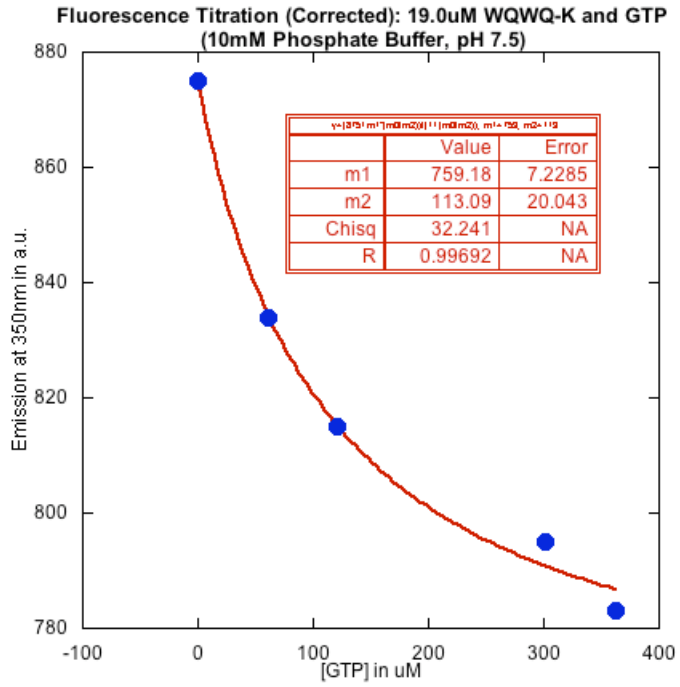

Figure 1.23: Comparison of Corrected and Uncorrected Fluorescence Data for GTP and WQWQ-K (19.0 μM) in 10 mM Phosphate Buffer, pH 7.5 at 298 K.

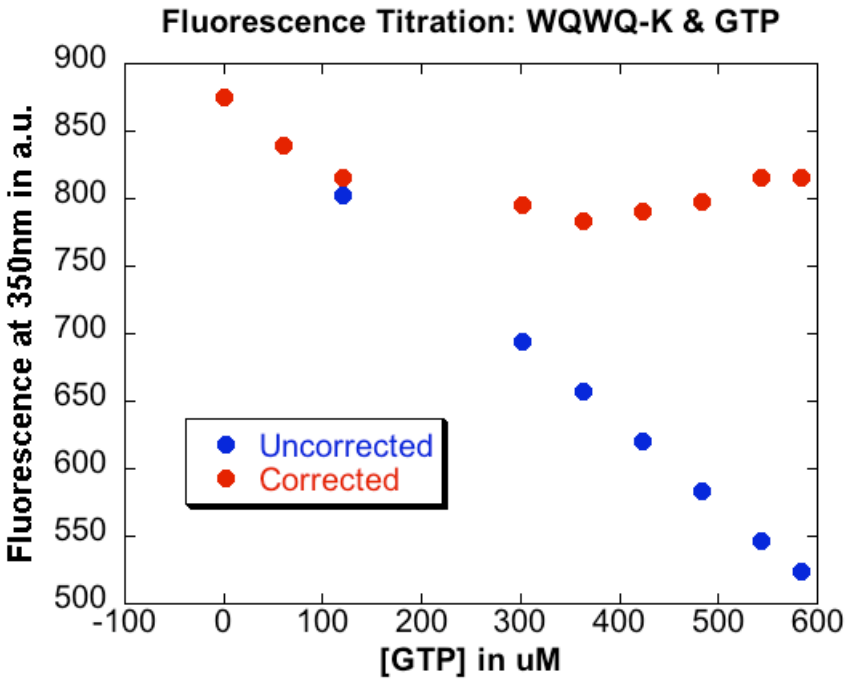

Corrected fluorescence emission for Trp as a function of 7mGTP concentration was (supposed to be) fit to the following binding equation on Kaleidegraph.[22]

$$F = F_o - [cx](\Delta\phi + \phi_{lig\text{-}free}) + G\,\phi_{lig\text{-}free} \quad \textbf{(1.3)}$$

$$\text{where } [cx] = \frac{(G+H)}{2} + \frac{1-\sqrt{(K_a(G-H)+1)^2 + 4K_aH}}{2K_a}$$

This equation corrects for 7mGTP's overlapping fluorescence. In this equation, the fluorescence intensity (F) is expressed as a function of the total guest concentration (G). Other parameters include the association constant (K_a), total concentration of peptide (H), the difference between the fluorescence efficiencies of the free peptide and the peptide•7mGTP complex ($\Delta\phi$), and the fluorescence efficiency of the guest ($\phi_{lig\text{-}free}$). This equation was also used to acquire an initial binding constant for the interaction between peptide and 7mGTP.

Figure 1.24: Corrected Fluorescence Titration for 7mGTP and WTWT-K (17.5 μM) in 10 mM Phosphate Buffer, pH 7.5 at 298 K.

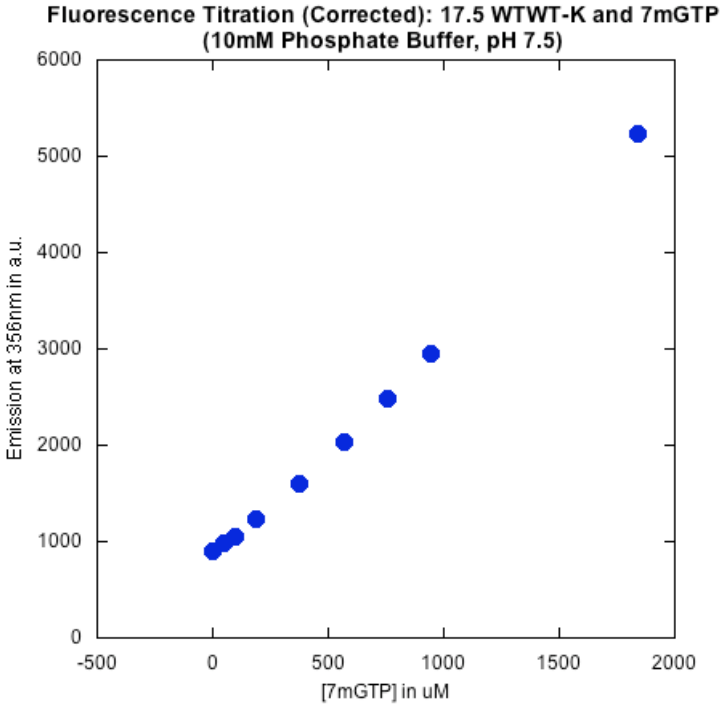

Figure 1.25: Comparison of Corrected and Uncorrected Fluorescence Data for 7mGTP and WTWT-K (17.5 μM) in 10 mM Phosphate Buffer, pH 7.5 at 298 K.

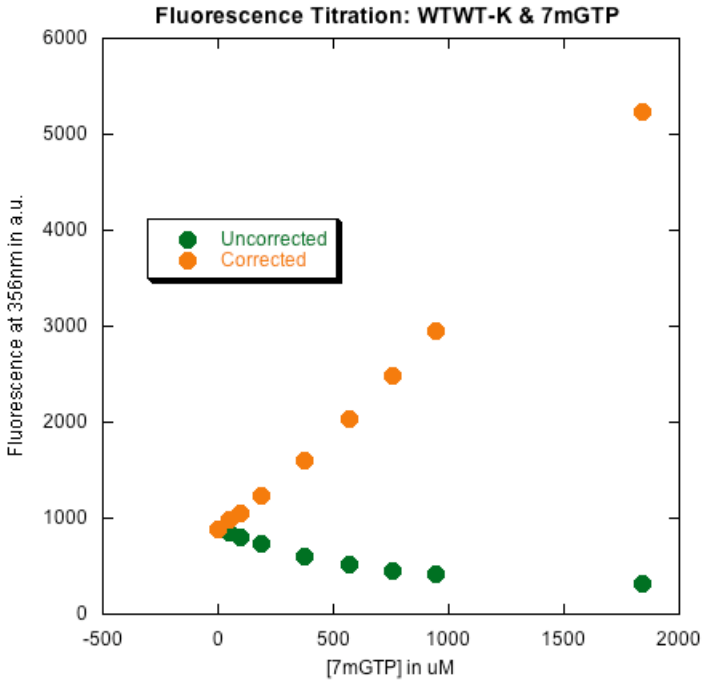

Figure 1.26: Corrected Fluorescence Titration for 7mGTP and WQWQ-K (19.0 μM) in 10 mM Phosphate Buffer, pH 7.5 at 298 K.

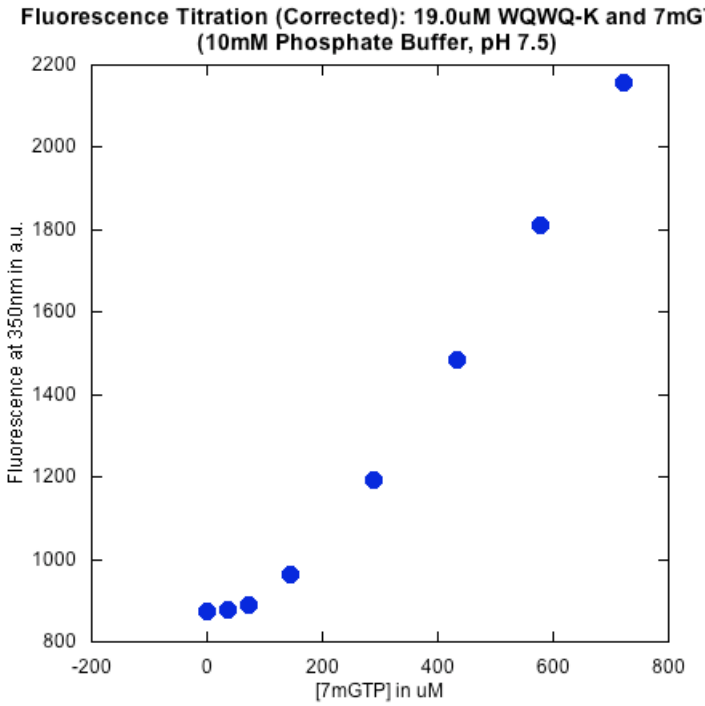

Figure 1.27: Comparison of Corrected and Uncorrected Fluorescence Data for 7mGTP and WQWQ-K (19.0 μM) in 10 mM Phosphate Buffer, pH 7.5 at 298 K.

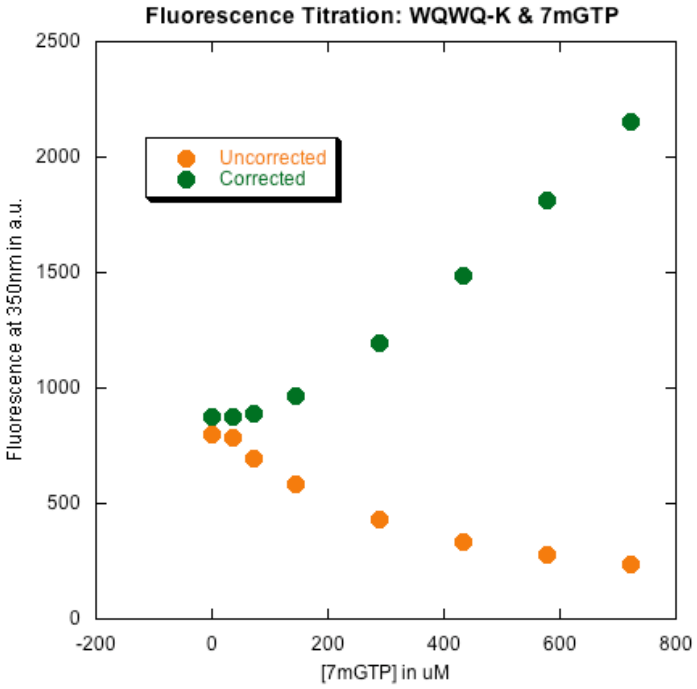

The uncorrected fluorescence emission of Trp, as a function of 7mGTP, was fit to equation 1.3 using Kaleidegraph.

Figure 1.28: Uncorrected Fluorescence Titration for 7mGTP and KKG-WTWT (14.0 μM) in 10 mM Phosphate Buffer, pH 7.5 at 298 K.

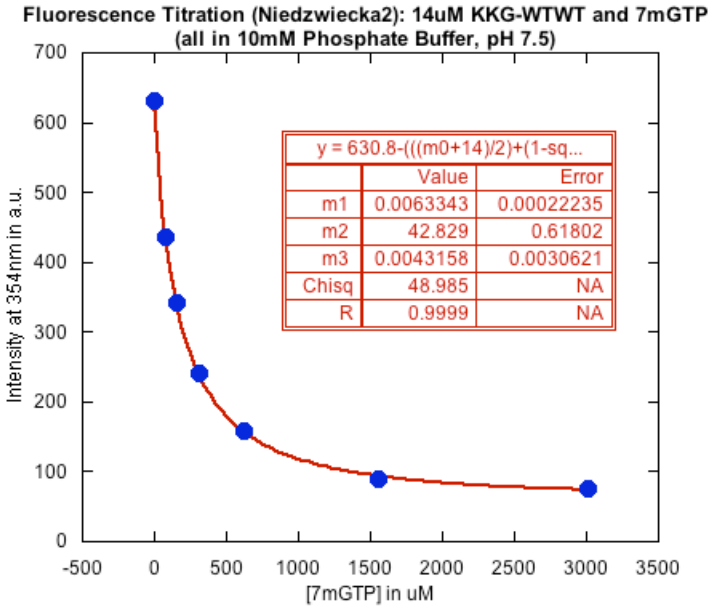

Figure 1.29: Uncorrected Fluorescence Titration for 7mGTP and WTWT-K (15.0 μM) in 10 mM Phosphate Buffer, pH 7.5 at 298 K.

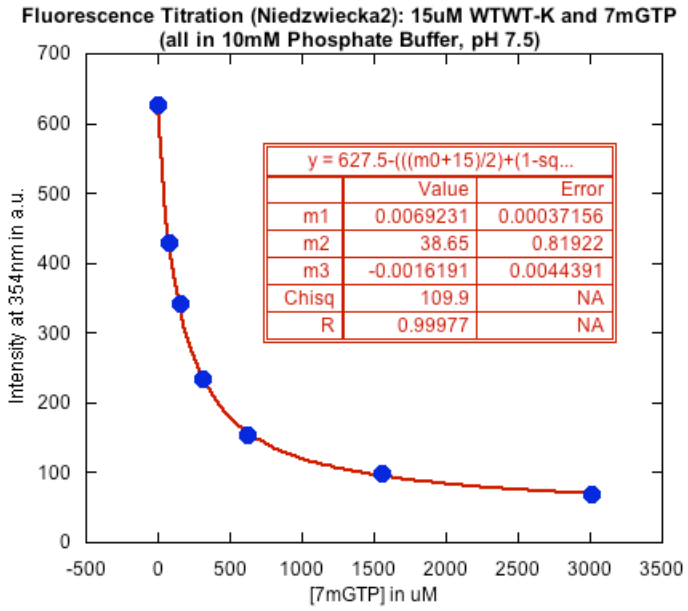

C. Competitive Binding Assay

Peptide samples were prepared in 10 mM phosphate buffer, pH 7.5, and their concentrations were determined in 6 M guanidine hydrochloride using the absorbance of the

tryptophan residues at 280nm ($\varepsilon_{280,\,Trp}$ = 5690 M^{-1}•cm^{-1}).[30] Fluorescent dye solutions were prepared in 10mM phosphate buffer, pH 7.5, and their concentrations were determined using the molar extinction coefficients for the fluorescent dyes. $\varepsilon_{474,\,fluorescein}$ = 5,800 M^{-1}•cm^{-1}, $\varepsilon_{445,\,Flavin}$ = 11,800 M^{-1}•cm^{-1}, $\varepsilon_{543,\,B}$ = 106,000 M^{-1}•cm^{-1}, $\varepsilon_{543,\,6G}$ = 116,000 M^{-1}•cm^{-1}) Fluorescence scans were obtained at ambient temperature using the appropriate excitation wavelength for each dye: 493 nm for 5(6)-Carboxyfluorescein, 445 nm for Flavin Mononucleotide, 549 nm Rhodamine B, 529 nm for Rhodamine 6G. The emission intensities of each dye as a function of peptide concentration were fit to the following binding equation on Kaleidegraph.[32]

$$F = [F_o + F_\infty (H/K_i)] / [1 + (H/K_i)] \quad (\mathbf{1.4})$$

F is the observed fluorescence intensity, F_o is the initial fluorescence intensity, F_∞ is the fluorescence intensity at binding saturation, H is the concentration of peptide, and K_i is the dissociation constant. Figures 1.xx through 1.xx are sample binding curve fits for the fluorescence titration data.

Figure 1.30: Titration of KKG-WTWT into 5(6)-Carboxyfluorescein (0.499 μM) in 10 mM Phosphate Buffer, pH 7.5 at 298 K.

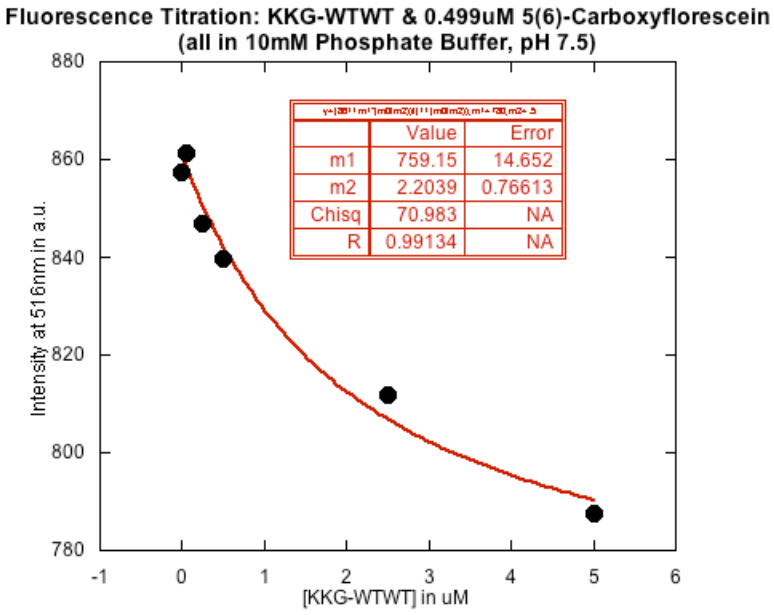

Figure 1.31: Titration of WTWT-K into 5(6)-Carboxyfluorescein (0.496 μM) in 10 mM Phosphate Buffer, pH 7.5 at 298 K.

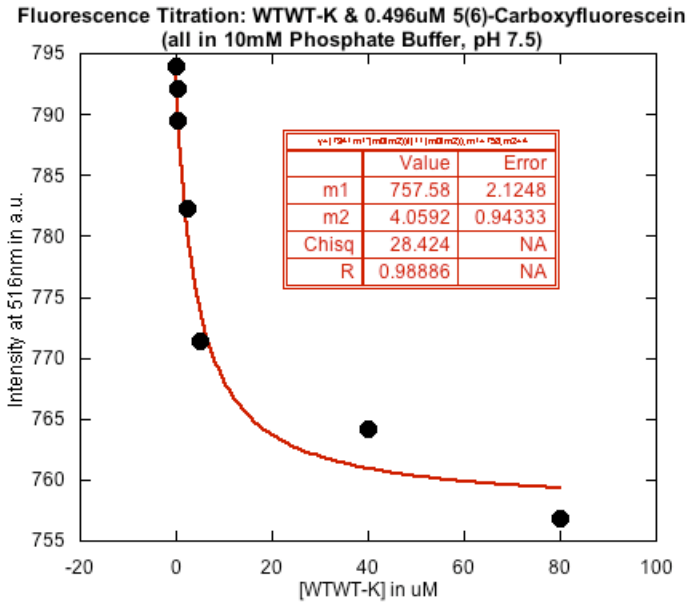

Figure 1.32: Titration of WTWK into 5(6)-Carboxyfluorescein (0.51 μM) in 10 mM Phosphate Buffer, pH 7.5 at 298 K.

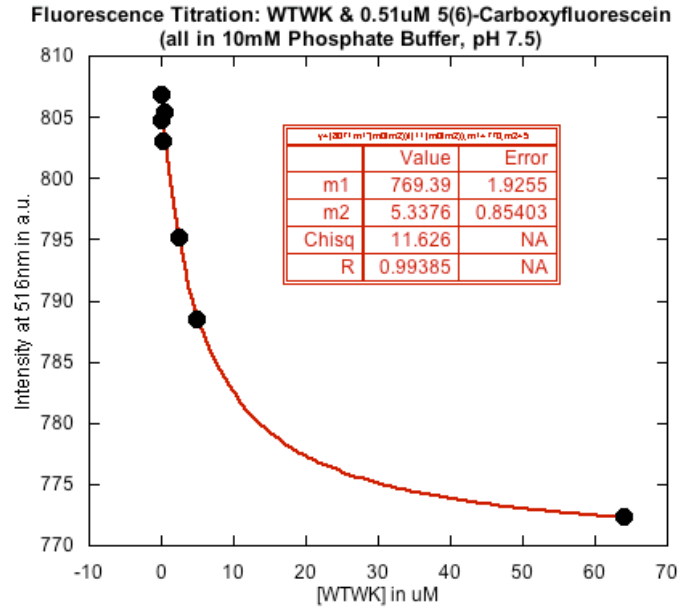

Figure 1.33: Titration of WTWT-K into Rhodamine B (1.0 μM) in 10 mM Phosphate Buffer, pH 7.5 at 298 K.

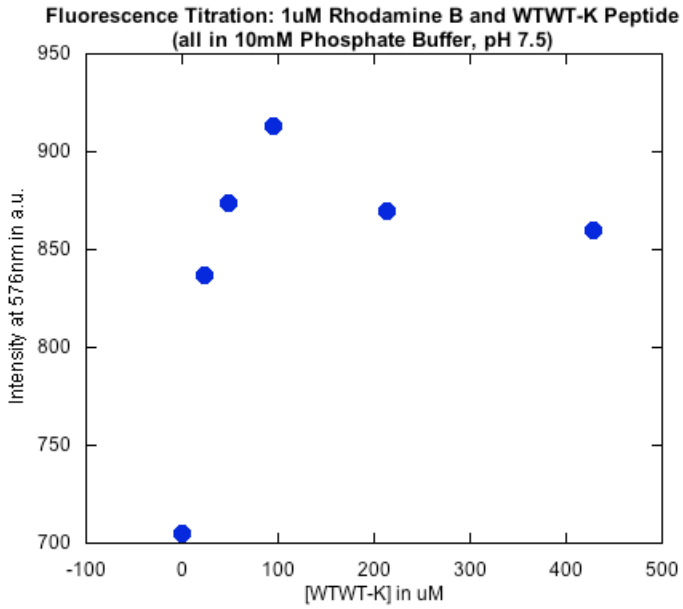

Figure 1.34: Titration of WTWT-K into Rhodamine 6G (1.0 μM) in 10 mM Phosphate Buffer, pH 7.5 at 298 K.

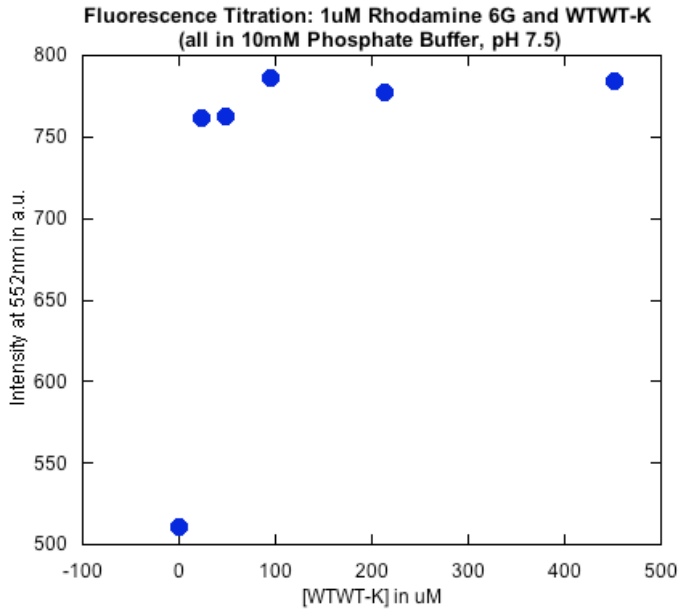

Figure 1.35: Titration of WTWK into Flavin Mononucleotide (34.0 μM) in 10 mM Phosphate Buffer, pH 7.5 at 298 K.

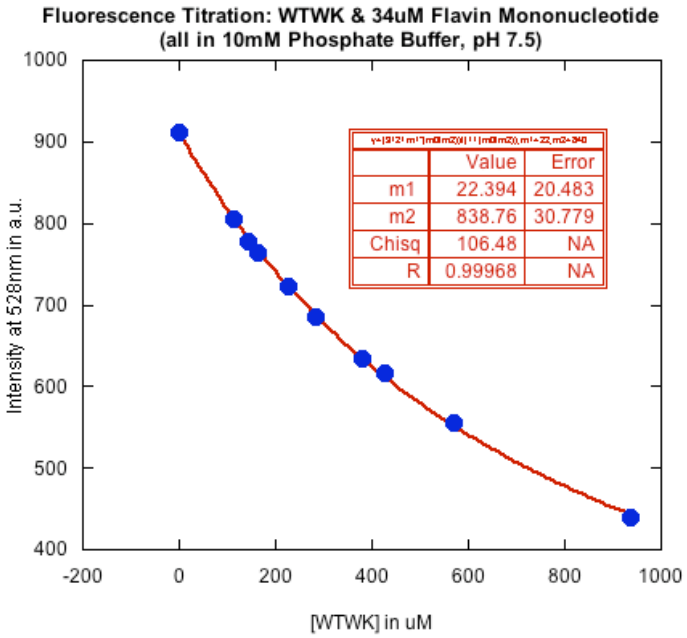

In order to determine K_d (**1.x**), a different binding equation was required.[29] K_d can be obtained by fitting the FMN emission intensities as a function of 7mGTP concentration to the following binding equation using Kaleidograph.

$$F = F_o + [(F_\infty - F_o)\,(H\bullet I)] \quad (\mathbf{1.5})$$

$$\text{where } H\bullet I = \frac{\sqrt{(I+H)(H+K_d)+K_d(G+H+K_d)-[(I+H)(H+K_d)+K_d(G+H+K_d)]^2-4\times I\times H(H+K_d)^2}}{2(H+K_d)}$$

F, F_o, F_∞, H, and K_i are the same as in Equation 1.x. I and G correspond to the FMN and 7mGTP concentrations, respectively. K_d is the dissociation constant between H and G.

Figure 1.36: Titration of 7mGTP into Flavin Mononucleotide (34.0 μM) and WTWK (626 μM) in 10 mM Phosphate Buffer, pH 7.5 at 298 K.

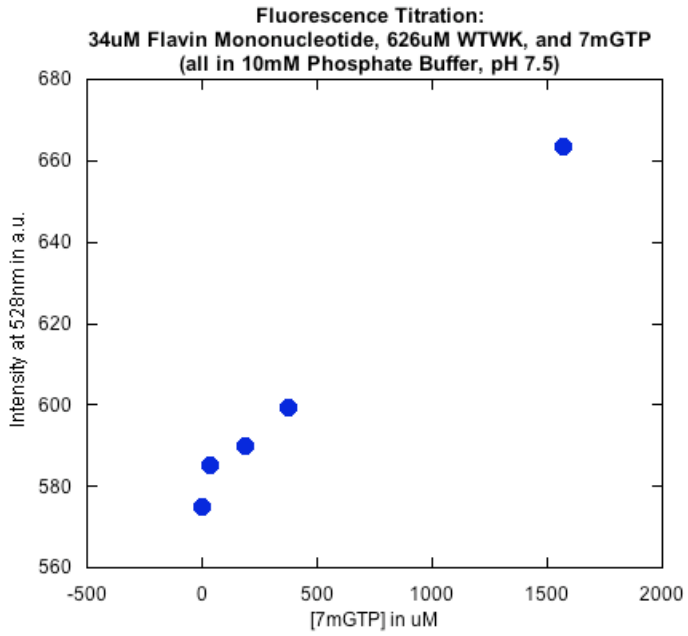

D. Isothermal Titration Calorimetry

Peptide samples were prepared in 10 mM phosphate buffer, pH 7.5, and their concentrations were determined in 6 M guanidine hydrochloride using the absorbance of the tryptophan residues at 280nm ($\varepsilon_{280,\,Trp}$ = 5690 M^{-1}•cm^{-1}).[30] 7mGTP samples were prepared in 10 mM phosphate buffer, pH 7.5. Concentrations were determined by UV spectroscopy using the molar extinction coefficient of 7mGTP ($\varepsilon_{297,\,7mGTP}$ = 3537 M^{-1} cm^{-1}).[31]

Calorimetry experiments were performed on a VP-ITC Microcalorimeter. Solutions were degassed for 10-15 minutes prior to the experiment. A degassed solution of peptide (WQWQ-K or WTWT-K) was loaded in a 2 mL reaction cell, while a degassed solution of 7mGTP was loaded into a 500 μL injection syringe. The 7mGTP solution was titrated into the reaction cell in 5 μL increments every 3 or 5 minutes, with a total of 55 injections, with mechanical stirring. All experiments were conducted at 25°C with a reference power of 10 μcal/sec and an initial delay of 5 minutes. The titration data was analyzed using the Origin

software by non-linear least squares fitting the heats of binding as a function of

7mGTP:Peptide molar ratio to the selected binding model.

Figure 1.37: ITC Raw Data for 7mGTP (9.8 mM) Heat of Dilution Experiment in 10 mM Phosphate Buffer, pH 7.5, at 298 K.

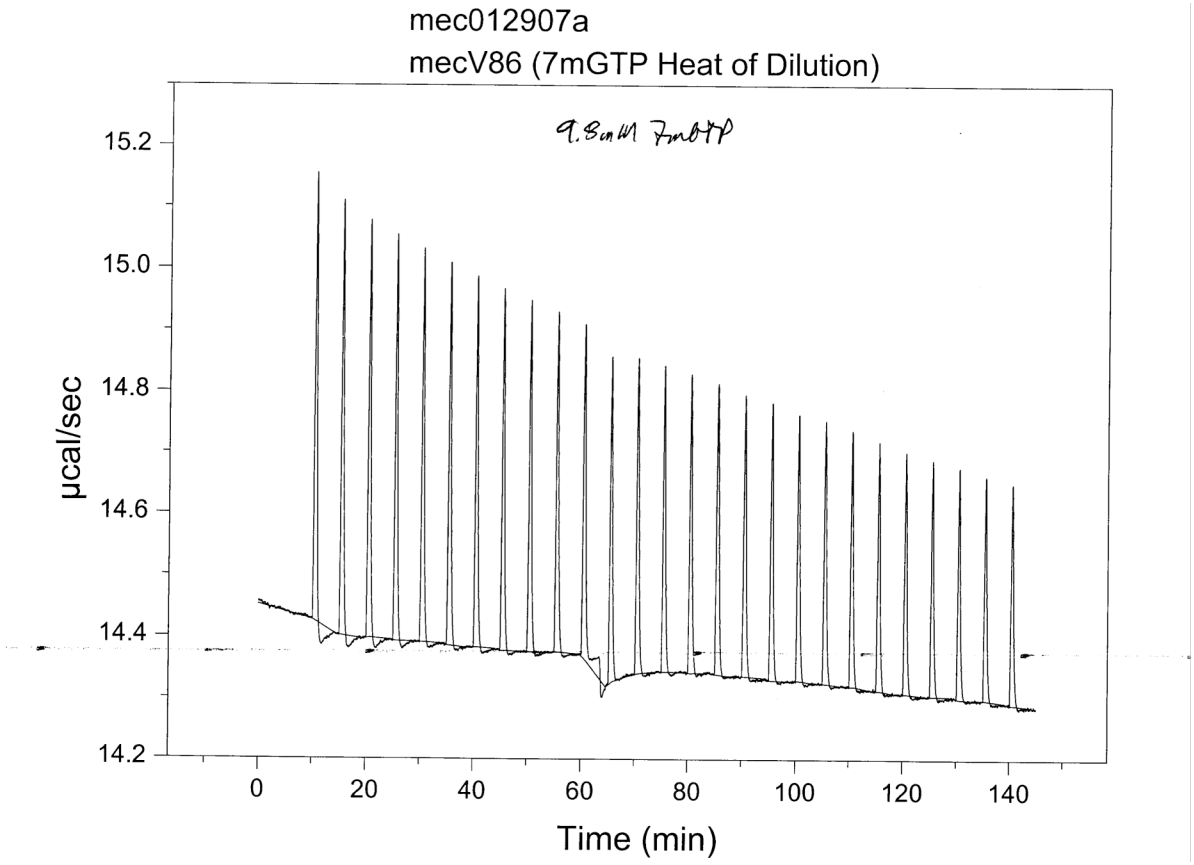

Figure 1.38: ITC Data for 7mGTP (9.8 mM) titration into WQWQ-K (440 µM) in 10 mM Phosphate Buffer, pH 7.5, at 298 K. Corrected for 7mGTP heat of dilution.

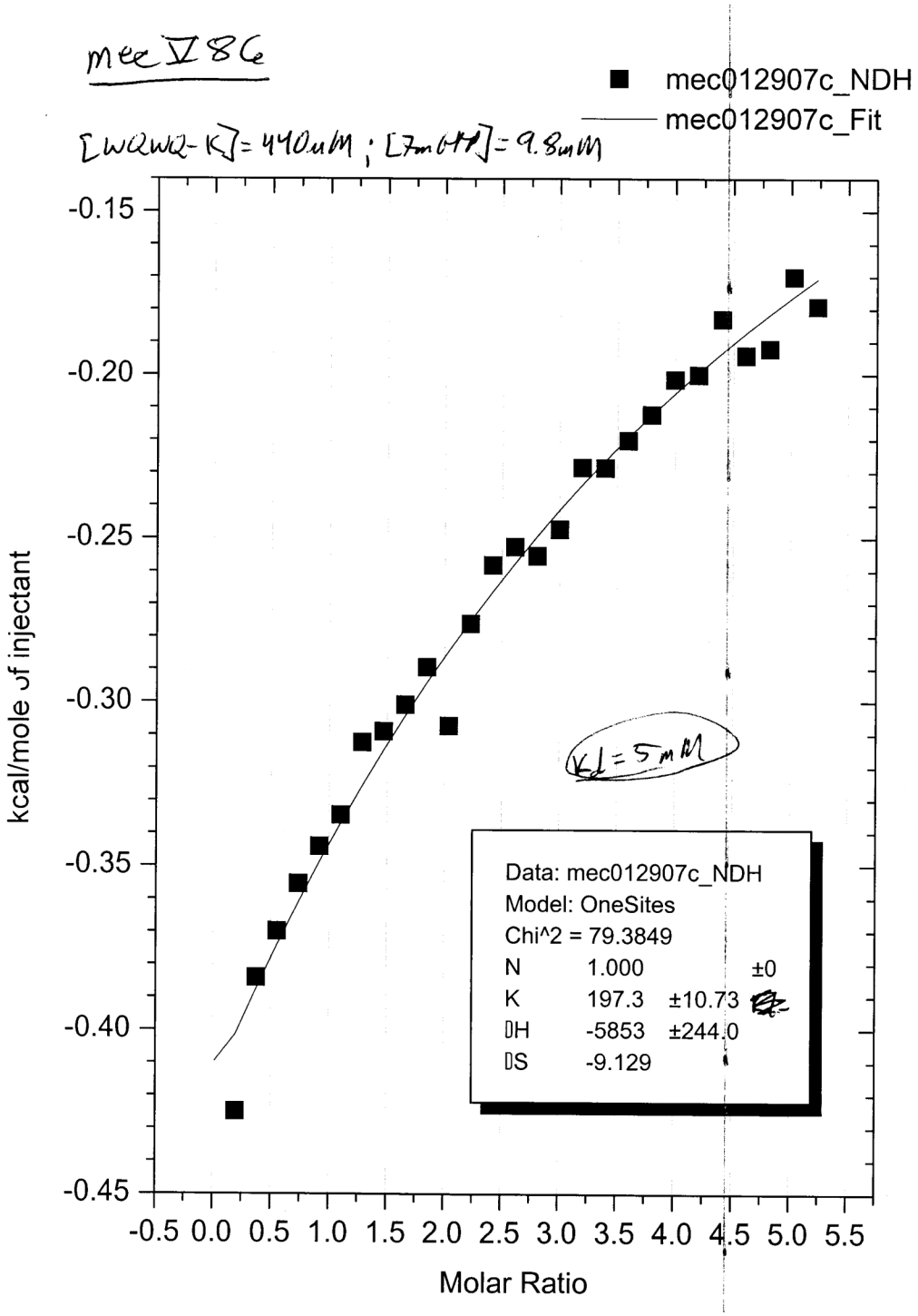

E. NMR Titration

Peptide samples were prepared in 10 mM phosphate buffer, pH 7.5 (in D_2O), and their concentrations were determined in 6 M guanidine hydrochloride using the absorbance

of the tryptophan residues at 280nm ($\varepsilon_{280,\,Trp}$ = 5690 M^{-1}•cm^{-1}).[30] Nucleotide stock solutions were prepared in 10 mM phosphate buffer, pH 7.5. Concentrations were determined by UV spectroscopy using the molar extinction coefficient of the nucleotides ($\varepsilon_{253,\,GTP}$ = 13700 M^{-1} cm^{-1}; $\varepsilon_{297,\,7mGTP}$ = 3537 M^{-1} cm^{-1}).[31] All ^{1}H NMR spectra were acquired on a 600 MHz Varian spectrometer using 8-64 scans depending on the sample concentration, with water presaturation. Due to the high concentration of nucleotide stock solutions, multiple samples, with increasing amount of nucleotide, were made. Binding was measured by fitting the upfield shifting of the tryptophan H-6 or H-7 aromatic protons to the following equation for 1:1 binding on Kaleidegraph, using nonlinear least-squares fitting,[33]

$$\delta_{obs} = \delta_R + \Delta_o / 2[R_o]\{[R_o]+[S_o]+1/K - \sqrt{(([R_o]+[S_o]+1/K)^2 - 4[R_o][S_o])}\} \quad \textbf{(1.6)}$$

where δ_{obs} is the observed chemical shift of a single tryptophan proton, δ_R is the chemical shift of the tryptophan proton in the absence of nucleotide, Δ_o is the maximum change in chemical shift at 100% complexation, $[R_o]$ is the concentration of the peptide receptor, $[S_o]$ is the concentration of nucleotide substrate, and K is the binding constant. All titrations were performed at 25 °C.

Table 1.6: NMR titration data for WQWQ-K + 7mGTP (WQWQ-K = 279 μM)

[7mGTP] in uM	Trp H-7 Shift in ppm
0	7.460
783	7.450
1570	7.439
3130	7.426

[33] Davies, J. E. D.; Ripmeeester, J. A. *Comprehensive Supramolecular Chemistry*; Vol. 8, Physical Methods in Supramolecular Chemisry; Pergamon Press: Oxford, UK, **1996**; p. 434.

6270	7.407
9400	7.396

Table 1.7: NMR titration data for WQWQ-K + GTP (WQWQ-K = 279 μM)

[GTP] in uM	Trp H-7 Shift in ppm
0	7.462
1090	7.449
2180	7.441
4350	7.433
8700	7.425
13000	7.420

Table 1.8: NMR titration data for WTWT-K + 7mGTP (WTWT-K = 257 μM)

[7mGTP] in uM	Trp H-6 Shift in ppm
0	7.057
850	7.041
1700	7.033
3400	7.023
6800	7.008
10200	7.000

Table 1.9: NMR titration data for WTWT-K + GTP (WTWT-K = 257 μM)

[GTP] in uM	Trp H-6 Shift in ppm
0	7.057
1290	7.037
2590	7.034
5180	7.025
10400	7.020
15500	7.014

Figure 1.39: Titration of 7mGTP into WQWQ-K (279 μM), in 10 mM Phosphate Buffer (D_2O), pH 7.5 at 298 K.

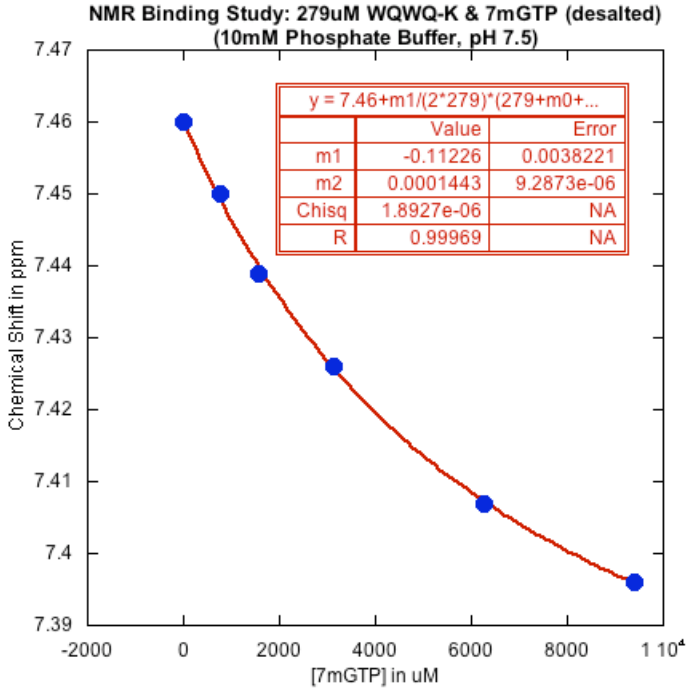

Figure 1.40: Titration of GTP into WQWQ-K (279 μM), in 10 mM Phosphate Buffer (D_2O), pH 7.5 at 298 K.

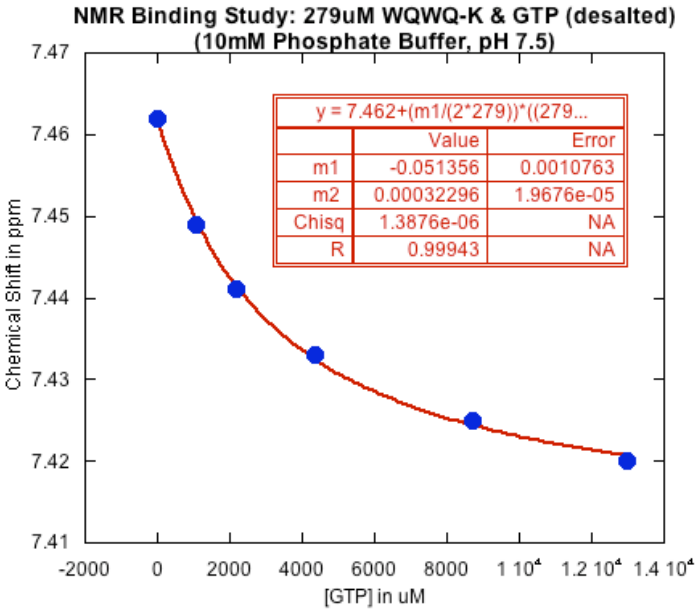

Figure 1.41: Titration of 7mGTP into WTWT-K (257 μM), in 10 mM Phosphate Buffer (D_2O), pH 7.5 at 298 K.

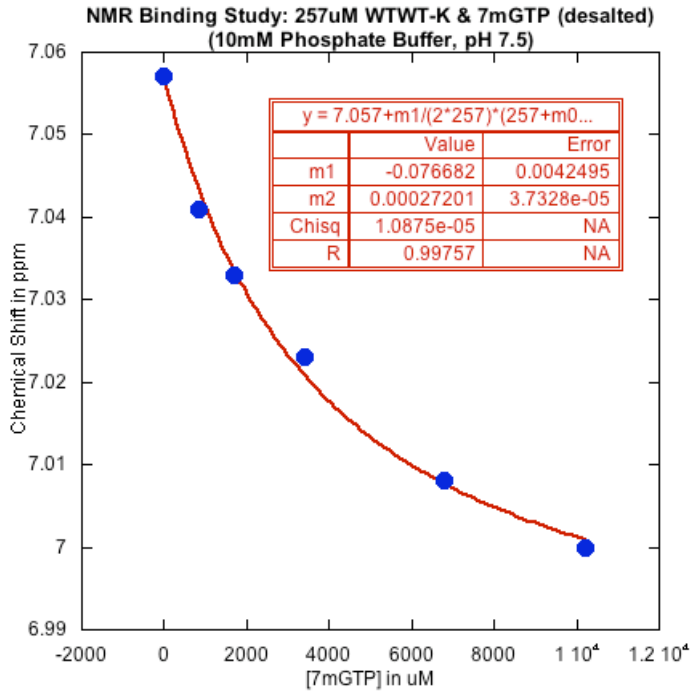

Figure 1.42: Titration of GTP into WTWT-K (257 μM), in 10 mM Phosphate Buffer (D_2O), pH 7.5 at 298 K.

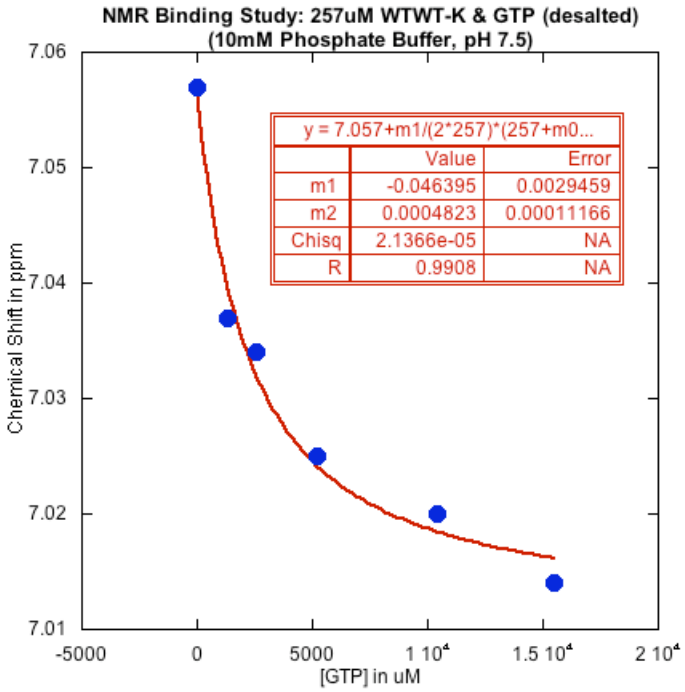

F. Trp Analog Synthesis

Synthesis of all building blocks and intermediates was performed analogous to the reported procedure.[27]

Chapter 2

Investigation of Prolyl Aromatic Interactions Using a Peptide Model System

I. Background and Introduction

A. Polyproline Helix Recognition

The polyproline (PPII) helix ($\Phi = -78°$ and $\Psi = +146°$)[34] is a secondary structure formed from sequences rich in proline (Figure 2.1).[35] The structure is left-handed and can form in the absence of proline. Typically proline is found in at least every third amino acid position and the resulting structure resembles a triangular prism. The pyrrolidine rings from the side chains form a hydrophobic interface along one edge of the prism. Despite its hydrophobic nature, the PPII helix does form in aqueous solution.

Figure 2.1: The PPII left-handed helix structure (PPLPPP) and proline amino acid

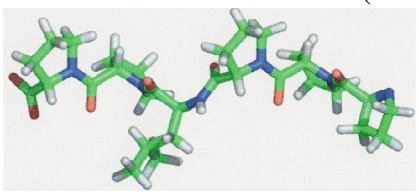

The recognition of PPII helices is a key protein-protein interaction in signaling.[36] Several modules are known to recognize PPII helices: the Src-homology 3 (SH3) domains, the WW domains, the Ena/VASP Homology 1 (EVH1) domains, the GYF domains, the UEV

---

[34] Cowan, P. M.; McGavin, S. *Nature* **1955**, *176,* 501-503.

[35] Williamson, M. P. *Biochem. J.* **1994**, *297*, 249-260.

[36] Li, S. S. C. *Biochem. J.* **2005**, *390*, 641-653.

domains, and the single-domain profilin proteins.[37] These recognition domains are involved in various biological processes, e.g. cell growth, cytoskeleton regulation, and transcription. The K_d values for these binding events are typically weak, 1-500 μM, but possess high specificity. One characteristic of all Proline Rich Motif (PRM)-binding domains is highly conserved clusters of exposed aromatic residues. These residues are necessary for the recognition of specific PRMs. The orientation of the aromatic residues determines the specificity of PRM recognition. The requirement of aromatic residues in the binding cleft suggests a role for C-H-π interactions in binding, as discussed below.

The nature of the proline side chain also plays a role in its recognition. Upon forming a PPII helix no intramolecular hydrogen bonding is observed because the amide hydrogen is replaced by a $-CH_2-$ group. This allows the backbone carbonyl groups of the polyproline helix to hydrogen bond with the PRM domains. Proline is a very good hydrogen bond acceptor because its carbonyl group is more electron-rich than the carbonyl group of the other natural amino acids. Proline also has a low number of degrees of freedom, and as a result proline rich peptides form well defined structures. These structures have a low entropic cost of binding which leads to a greater overall binding compared to more flexible peptides. The unique features of proline contribute to its hydrogen bonding capability and binding energy.

B. C-H-π Interaction

The recognition of PPII helices has been proposed to proceed through C-H-π interactions because the aromatic clusters are conserved in PRM-binding domains.[38] The C-

[37] Ball, L. J.; Kühne, R.; Schneider-Mergener, J.; Oschkinat, H. *Angew. Chem. Int. Ed.* **2005**, *44*, 2852-2869.

[38] Bhattacharyya, R.; Chakrabarti, P. *J. Mol. Biol.* **2003**, *331*, 925-940.

H-π interaction[39] is a weak, attractive force between a soft acid and a soft base. Typically soft acids are hydrogens on sp^3 or sp^2 hydbridized carbons. Soft bases include unsaturated bonds and aromatic groups. The more electron rich the aromatic group, the more favorable the interaction. This is different from a traditional hydrogen bond that is between a hard acid (OH, NH) and a hard base (lone pair of electrons).

There are characteristics of the C-H-π interaction that make it different, and in some cases, superior to the hydrogen bond.[40] Every organic molecule possesses CH groups; aromatic groups are abundant as well. The enthalpic contribution of the C-H-π interaction is small when compared to the traditional hydrogen bond but many CH groups can interact with the aromatic compound and the total enthalpic contribution is additive. The organization required for a C-H-π interaction between a methyl group and an aromatic compound is less than for a traditional hydrogen bond. The methyl group has C_3 symmetry and the aromatic ring is a flat, planar compound. When combined with the cooperative effect for enthalpy, this reduced entropy of binding can lead to a lower overall binding energy. Lastly the C-H-π interaction is effective in polar, protic solvents like water. The energy of the C-H-π interaction primarily stems from the dispersion force, whereas the traditional hydrogen bond gets most of its energy from the Coulombic force, which is dampened by polar, protic solvents. This explains why hydrogen bonding is more difficult in water relative to organic solvents. Since the Coulombic component is not an important contributor of the C-H-π interaction, polar protic solvents don't have the same effect. As a result, the C-H-π interaction has great importance in biochemical systems.

---

[39] Nishio, M.; Umezawa, Y.; Hirota, M; Takeuchi, Y. *Tetrahedron* **1995**, *51*, 8665-8701.

[40] Nishio, M. *Cryst. Eng. Commun.* **2004**, *6*, 130-158.

Zondlo has investigated prolyl-aromatic interactions using a peptide model system.[41] He synthesized a series of peptides with the sequence TXPN (Figure 2.2), where T is Threonine (Thr), P is Proline (Pro), and N is Asparagine (Asn). X was one of three types of aromatic residues: electron-rich, electron-neutral, or electron-poor. He determined the ratio of the cis and trans configurations using NMR and showed that the cis conformation was slightly favored when electron-rich aromatic residues were used. He concluded this electronic control might be due to a polarized C-H-π interaction between the proline sidechain and the aromatic residue.

Figure 2.2: Zondlo's peptide model system. (a) Sequence of peptide used, (b) Cis-trans isomerization of an aromatic-prolyl amide bond, (c) Different substitutions at X and their energetic contribution.

(a)

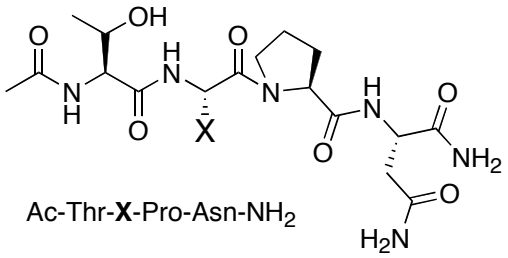

(b)

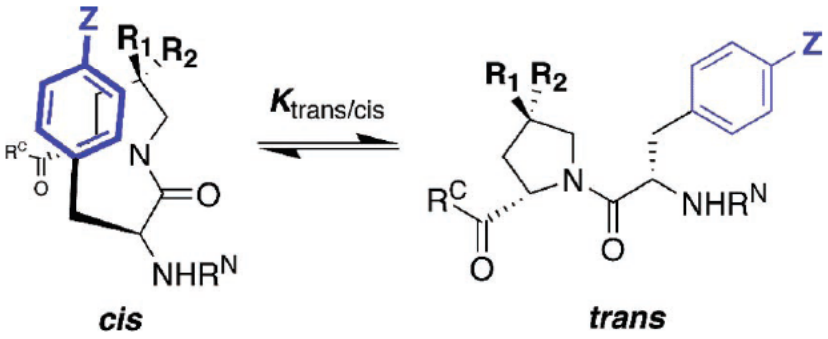

(c)

TXPN, X =	$K_{trans/cis}$	$\Delta G_{trans/cis}$ (kcal/mol)
Cyclohexylalanine (Cha)	8.0	-1.22

[41] Thomas, K. M.; Naduthambi, D.; Zondlo, N. J. *J. Am. Chem. Soc.* **2006**, *128*, 2216-2217.

F5-Phe	4.4	-0.87
Phe (F)	3.2	-0.68
Trp (W)	1.8	-0.35

C. EVH1 Domains

The Ena/VASP Homology 1 (EVH1) domains[42] are found in multi-domain signaling proteins and are divided into two classes based on the consensus sequence of their ligands. The Ena/VASP and WASP families (Class I) modulate the actin cytoskeleton and recognize the consensus sequence FPxΦP, where Φ is a hydrophobic residue and x is any amino acid residue. Typically this sequence is FPPPP. The Homer-Vesl family (Class II) has a role in signal transduction in postsynaptic compartments and recognizes the consensus sequence xPPxxF. Both classes of PRM domains have similar structures and the major variations occur in the turn and loop regions.

A conserved recognition domain is observed for all EVH1 domains (Figure 2.3). It contains three aromatic residues: tyrosine (Tyr), tryptophan (Trp), and phenylalanine (Phe). The Trp residue is not only important for ligand docking, but also makes core hydrophobic contacts essential for correct folding. In the Homer-Vesl EVH1 domains, Tyr is replaced by Ile, an aliphatic residue.

Figure 2.3: EVH1 domain (Mena, EVl, VASP, and Homer-1a) interacting with PPII helix ligand.[9] Both class I and class II represented in stereoview image.

[42] Ball, L. J.; Jarchau, T.; Oschkinat, H.; Walter, U. *FEBS Lett*. **2002**, *513*, 45-52.

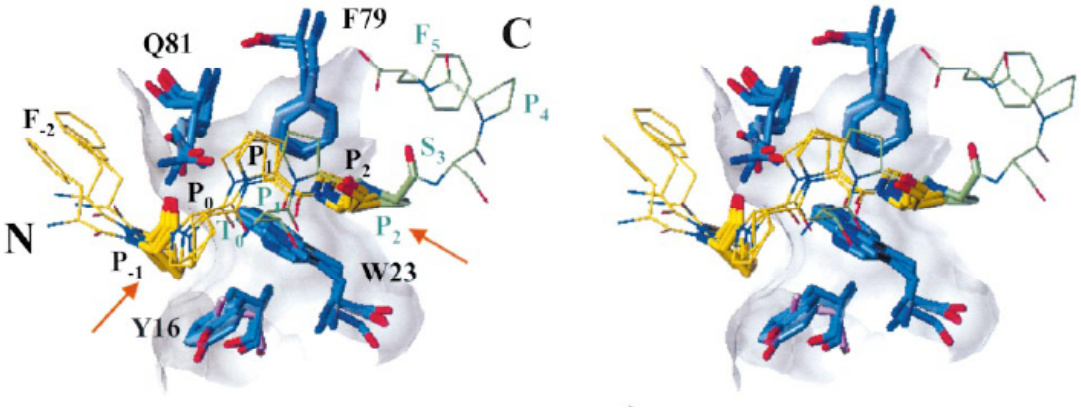

The crystal structure of the Homer 1a EVH1 domain indicates that the main recognition elements occur on the surface of a beta sheet (Figure 2.4). Tryptophan (Trp) and phenylalanine (Phe) residues are the main contributors to the binding event. The aromatic residues are located on two separate beta strands in a diagonal orientation. The TrpZip beta hairpin peptide developed by Cochran[43] has four Trp residues located on two beta strands. Two of the Trp residues are located in a diagonal fashion, similar to the Homer 1a EVH1 protein. When TrpZip is overlayed with the protein, the aromatic residues align well.

Figure 2.4: Comparison of EVH1 domain and TrpZip Peptide. (a) EVH1 domain (gray) from Homer 1a bound to PPII helix TPPSPF (green) (pdb: 1DDV); (b) trpzip peptide (pdb: 1LE0); (c) PPII binding cleft from the Homer EVH1 domain (gray) bound to PPII helix TPPSPF (green) overlayed with the trpzip peptide (yellow).

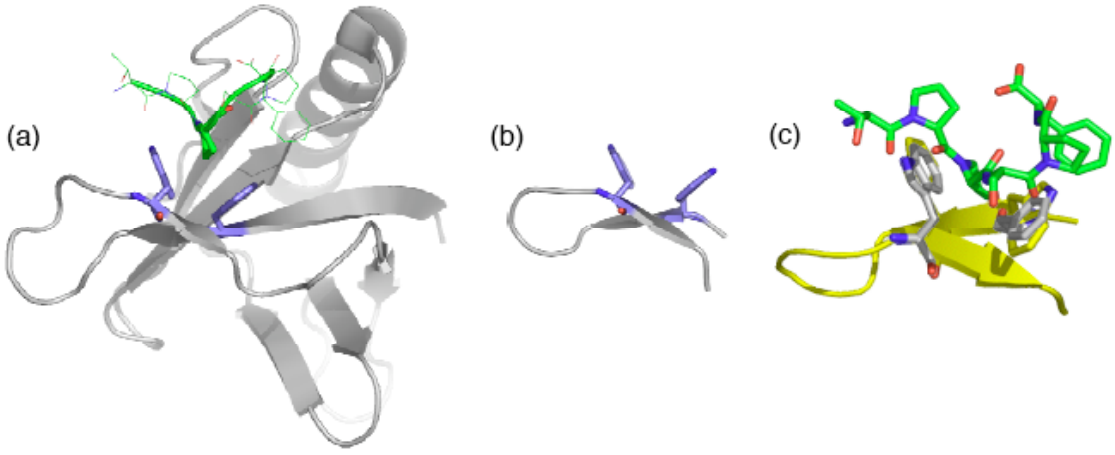

The goals of the present study are to use the TrpZip beta-hairpin peptide as a model for the beta sheet region of the Homer 1a EVH1 protein. The ligand for the Homer1a protein has the sequence TPPSPF. The binding of this ligand and that of a generic PPII helix by the model protein (beta-hairpin) were investigated and quantified.

II. Experiment Design

A. Disulfide Exchange

In order to achieve these goals, a few experiment designs were attempted. All the designs involve the use of disulfide exchange, a reversible reaction that occurs readily in aqueous solution. For example, if two compounds (A & B) containing free thiols are mixed together under oxidizing conditions a series of disuflide products can form (Figure 2.5). An individual compound can form a homodimer (A-A or B-B) or the compounds can combine to form a heterodimer (A-B). A and B will correspond to the PPII helix and beta-hairpin peptides (see below). The use of disulfide exchange can probe helix-hairpin interactions by looking at the perturbation from a statistical distribution.

Figure 2.5: Generic Disulfide Exchange

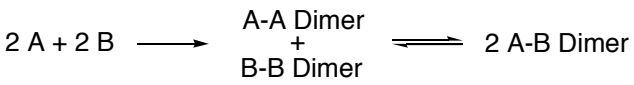

B. Design of Peptide Model System

Kim[44] used the disulfide exchange assay to investigate the preferred helix orientation in a coiled-coil peptide model system (Figure 2.6). In that study, he was investigating whether an anti-parallel or a parallel coiled-coil orientation was preferred based on the non-covalent interactions between the α-helices. To use the disulfide exchange in their peptide

---

[43] Cochran, A. G.; Skelton, N. J.; Starovasnik, M. A. *Proc. Nat. Acad. Sci., U.S.A.* **2001**, *98*, 5578-5583.

[44] Oakley, M. G.; Kim, P. S. *Biochemistry* **1998**, *37*, 12603-12610.

system, a cysteine (Cys) residue was incorporated in each helix. Two glycine (Gly) residues functioned as a spacer between the α-helix and the Cys residue.

Figure 2.6: (a) Kim's disulfide exchange assay; (b) Strutctures of cysteine and glycine

(a)

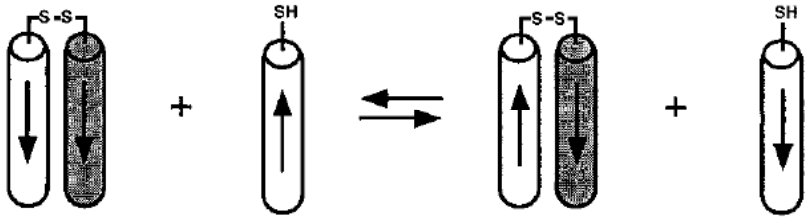

(b)

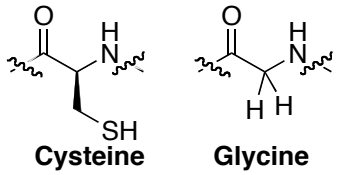

In the present study, Cochran's TrpZip beta hairpin peptide was used as a model for the Homer 1a EVH1 domain (Figure 2.7). Gly and Cys were incorporated to function as a spacer and to perform disulfide exchange, respectively. Lysine (Lys) residues were incorporated to improve the water solubility of the peptide. The final modified peptide contained Cys-Gly-Gly at the N-terminus and Lys-Lys at the C-terminus. In addition, the TrpZip peptide containing only the N-terminal modifications was studied as well. The beta hairpin peptides served as a model for the beta sheet recognition element of the protein-protein interaction.

Figure 2.7: Beta hairpin peptides used for model system: CGG-TrpZip-KK and CGG-TrpZip. Trp residues (red) align with Trp and Phe in EVH1 domain, Lys residues in orange, Cys residues in green, Gly residues in blue.

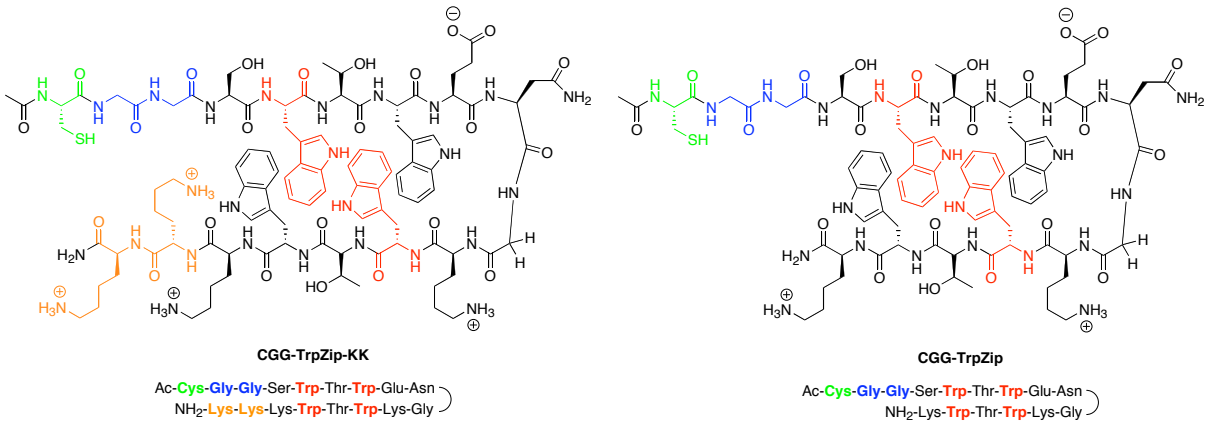

A series of peptides were synthesized to serve as a model for the polyproline (PPII) helix element (Figure 2.8). Cys and Gly residues were incorporated for the disulfide exchange assay and to serve as a spacer, respectively. In addition, Trp was used as a chromophore for concentration determination. First, a polyproline peptide (Ac-CWGGP$_n$-NH$_2$) was synthesized containing four to seven proline residues (n=4, 5, 6, 7). These peptides were used to investigate the length of the PPII helix needed for recognition. In addition to the generic PPII helix, the consensus sequence (TPPSPF), recognized by the Homer 1a protein, was synthesized to test the model system. The Phe was mutated to Trp for chromophore consistency. Again, Cys and Gly are incorporated for use in the disulfide exchange assay and to function as a spacer, respectively.

Figure 2.8: PPII helix peptides used for model system. (a) P4, (b) P7, (c) Homer1a_consensus. Cys residues in green, Gly residues in blue, Trp residues in red. Pro residues in black.

(a)

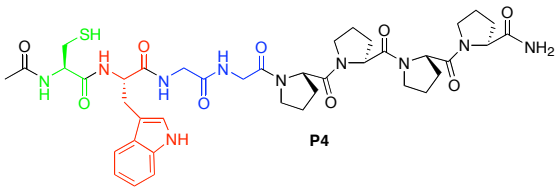

(b)

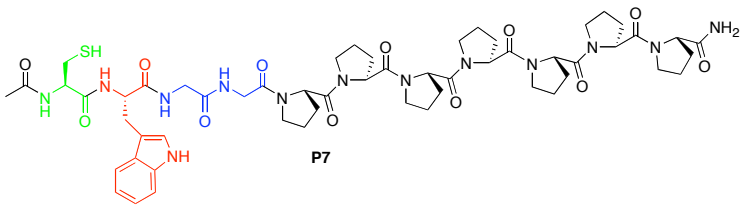

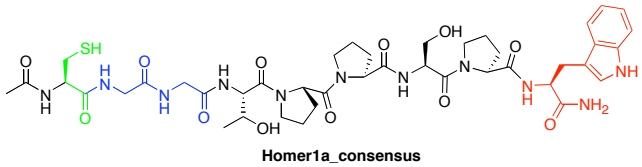

(c)

C. Disulfide exchange in peptide model system

The disulfide exchange assay was used to investigate the affinity of the PPII helix by the beta hairpin. The peptides were dissolved in either 20 mM Phosphate Buffer, pH 8.5 or Phosphate Buffered Saline (PBS: 10 mM Phosphate, 2.7 mM KCl, 137 mM HCl), pH 7.3 and pushed through a syringe filter (0.2 μm, PTFE). The peptides were combined in equal ratios (100 μM each) and allowed to equilibrate via air oxidation (Figure 2.9). In addition, each individual peptide was diluted to the appropriate concentration (100 μM) to serve as a control to help identify peaks in the experiment mixture. A number of products can form as a result of air oxidation, and one of those products is the heterodimer containing the PPII helix and beta hairpin. This disulfide exchange assay was investigated at pH 7.3 and 8.5. Results are discussed below.

Figure 2.9: Disulfide exchange assay using air oxidation

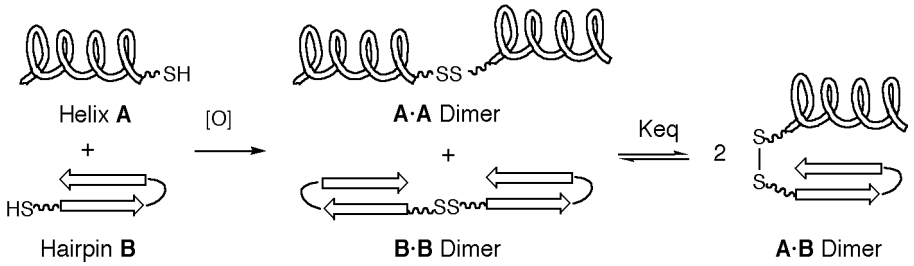

A second disulfide exchange assay (Figure 2.10) was also investigated. It required the use of a glutathione (GSH) REDOX buffer. For this experiment the peptides were dissolved in PBS buffer, pH 7.4 containing 125 μM glutathione (oxidized) and 500 μM glutathione (reduced)[45] and pushed through a syringe filter (0.2 μm, PTFE). In general, similar oxidation products are observed. The peptides were combined in equal ratios (100 μM each) and allowed to equilibrate via glutathione oxidation. However, the REDOX buffer results in the formation of glutathione containing products: glutathione-helix dimer (GS-A), glutathione-hairpin dimer (GS-B), and glutathione dimer (GS-SG).

Figure 2.10: Disulfide exchange assay using REDOX buffer

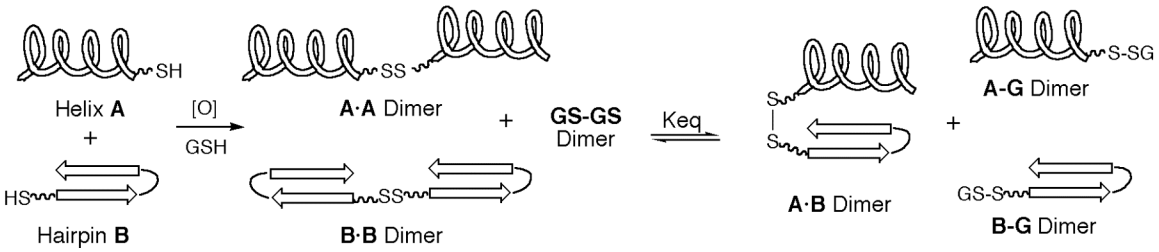

D. Data Analysis

High performance liquid chromatography (HPLC) or ultra performance liquid chromatography (UPLC) was used to analyze the experiments. The absorbance of each chromatogram was acquired at 280 nm. Each experiment was conducted with appropriate control experiments to identify all peaks. The only peak that could not be identified using the control experiments is the heterodimer (helix-hairpin dimer) because the control mixtures contain only one peptide from the assay. Therefore the heterodimer peak cannot form in the control experiment. When available, ESI-MS (Positive Ion Mode) was also used to confirm peak identity, in line with UPLC.

[45] Bilgicer, B.; Xing, X.; Kumar, K. *J. Am. Chem. Soc.* **2001**, *123*, 11815-11816.

All peaks were integrated to determine their total area. The peak areas were normalized using the extinction coefficient for Trp (5690 M^{-1}) since each peak contained a different number of Trp residues. The resulting normalized values were used to calculate K_{eq} using the appropriate equation.

When air oxidation was used, three products could be formed: helix dimer, hairpin dimer, and helix-hairpin dimer. When the helix and hairpin are combined in a 1:1 ratio, the statistical distribution of products is 2:1:1 for the helix-hairpin dimer, helix dimer, and hairpin dimer. An equation for the equilibrium constant (K_{eq}) can be written to reflect this (Figure 2.11). In the case of a statistical mixture, $K_{eq} = 4$. A K_{eq} greater than 4 implies a favorable interaction between the helix and the hairpin. A K_{eq} less than 4 implies an unfavorable interaction between the helix and the hairpin. This analysis assumes that there is no free thiol in solution, which was confirmed by HPLC for pH 8.5 experiments (top trace in Figures 2.17 and 2.18).

Figure 2.11: Equilibrium constant expression using air oxidation for Helix (**A**) and Hairpin (**B**)

$$K_{eq} = \frac{[\mathbf{A{\cdot}B}]^2}{[\mathbf{A{\cdot}A}][\mathbf{B{\cdot}B}]}$$

($K_{eq} = 4$ for a statistical mixture)

When glutathione oxidation was used, three additional products can form. When the helix, the hairpin, and the glutathione are combined in a 1:1:1 ratio, the statistical distribution of products is 1:1:1:1:1:1 for the helix-hairpin dimer, gluatathione-hairpin dimer, glutathione-helix dimer, helix dimer, hairpin dimer, and glutathione dimer. The resulting K_{eq} equation (Figure 2.12) is different than the one used for air oxidation (Figure 2.11). In the case of a statistical mixture, $K_{eq} = 1$.

Figure 2.12: Equilibrium constant expression using REDOX buffer (Glutathione, **C**) oxidation for Helix (**A**) and Hairpin (**B**)

$$K_{eq} = \frac{[\mathbf{A{\cdot}B}][\mathbf{A{\cdot}C}][\mathbf{B{\cdot}C}]}{[\mathbf{A{\cdot}A}][\mathbf{B{\cdot}B}][\mathbf{C{\cdot}C}]}$$

(K_{eq} = 1 for a statistical mixture)

Upon inspecting the components of K_{eq}, it became evident that the glutathione dimer ([C•C]) quantity could not be determined using the LC/MS method described above for two reasons. First, the glutathione dimer is polar and quickly elutes from the column. Second, the glutathione dimer does not contain a chromophore so there is no associated absorbance at 280 nm. Therefore, the glutathione dimer quantity needed to be expressed in a measurable form. Inspection of the experimental setup indicates that the glutathione dimer was coming from both the helix and hairpin stock solutions (Figure 2.13). Assuming no interaction between the peptide (helix or hairpin) and glutathione, a statistical distribution for each interaction should result. Therefore, $K_1 = K_2 = 4$.

Figure 2.13: Individual equilibrium constant expressions for Helix (**A**) and Hairpin (**B**) using REDOX buffer (Glutathione, **C**) oxidation

$$\mathbf{A{\cdot}A} + \mathbf{C{\cdot}C} \overset{K_1}{\rightleftharpoons} 2\,\mathbf{A{\cdot}C} \qquad\qquad \mathbf{B{\cdot}B} + \mathbf{C{\cdot}C} \overset{K_2}{\rightleftharpoons} 2\,\mathbf{B{\cdot}C}$$

$$K_1 = \frac{[\mathbf{A{\cdot}C}]^2}{[\mathbf{A{\cdot}A}][\mathbf{C{\cdot}C}]_1} \qquad\qquad K_2 = \frac{[\mathbf{B{\cdot}C}]^2}{[\mathbf{B{\cdot}B}][\mathbf{C{\cdot}C}]_2}$$

Assuming that the total glutathione dimer concentration came from these stock solutions, an expression for the total glutathione dimer concentration was derived (Figure 2.14).

Figure 2.14: [**C•C**] expressed in terms of measurable quantities. Helix (**A**), Hairpin (**B**), Glutathione (**C**)

$$[\mathbf{C{\cdot}C}]_1 = \frac{[\mathbf{A{\cdot}C}]^2}{4\,[\mathbf{A{\cdot}A}]} \qquad [\mathbf{C{\cdot}C}]_2 = \frac{[\mathbf{B{\cdot}C}]^2}{4\,[\mathbf{B{\cdot}B}]}$$

$$[\mathbf{C{\cdot}C}]_{total} = [\mathbf{C{\cdot}C}]_1 + [\mathbf{C{\cdot}C}]_2$$

$$[\mathbf{C{\cdot}C}]_{total} = \frac{1}{4}\left(\frac{[\mathbf{A{\cdot}C}]^2}{[\mathbf{A{\cdot}A}]} + \frac{[\mathbf{B{\cdot}C}]^2}{[\mathbf{B{\cdot}B}]}\right)$$

Substituting this value in the original expression for K_{eq} gives an equation that consists of measurable quantities (Figure 2.15). In the case of a statistical mixture, $K_{eq} = 2$. This value differs from the original value for statistical distribution (Figure 2.12). A coefficient of 4 results from the assumed statistical distribution between glutathione and each peptide ($K_1 = K_2 = 4$). This coefficient is incorporated into the expression for $[\mathbf{C{\bullet}C}]_{total}$ and ultimately the refined expression for K_{eq}.

Figure 2.15: Refined equilibrium constant expression using REDOX buffer (Glutathione, **C**) oxidation for Helix (**A**) and Hairpin (**B**)

$$K_{eq} = \frac{4\,[\mathbf{A{\cdot}B}][\mathbf{A{\cdot}C}][\mathbf{B{\cdot}C}]}{[\mathbf{A{\cdot}C}]^2\,[\mathbf{B{\cdot}B}] + [\mathbf{B{\cdot}C}]^2\,[\mathbf{A{\cdot}A}]}$$

($K_{eq} = 2$ for a statistical mixture)

In both cases (air oxidation & REDOX buffer), K_{eq} can be converted to ΔG using the equation $\Delta G = -RT \ln (K_{eq})$. The ΔG value can be corrected, relative to a statistical distribution, by dividing the acquired K_{eq} by the K_{eq} value for a statistical distribution (Figure 2.16). Therefore the strength of binding for this interaction can be quantified.

Figure 2.16: Corrected expression for ΔG

$$\Delta G(\mathbf{A{\cdot}B}) = - RT \ln (K_{eq}/x)$$

x = 4 for Air Oxidation
x = 2 for Glutathione Oxidation

III. Results

A. Air oxidation at pH 7.5

The first method, air oxidation at pH 7.5, was investigated. Both beta hairpin peptides (CGG-TrpZip and CGG-TrpZip-KK) were tested with the polyproline helices (P4, P5, P6, P7, Homer1a_consensus). However, peptide degradation occurred before equilibrium was reached and the results were not quantified.

B. Air oxidation at pH 8.5

The second method also used air oxidation but elevated pH (8.5) was used to speed up the equilibration time. The equilibration time was faster but the peptides began to degrade as well. As a result, it is unknown whether equilibrium was reached before the peptides began to degrade. CGG-TrpZip-KK (Table 2.1) and CGG-TrpZip (Table 2.2) were investigated.

Table 2.1: Results using air oxidation at pH 8.5 for CGG-TrpZip-KK, t = 5 days

	K_{eq}	**ΔG(A•B) in kcal/mol**
P4 Helix Ac-CWGGPPPP-NH_2	3.6	**0.06**
P5 Helix Ac-CWGGPPPPP-NH_2	13	**-0.7**
P6 Helix Ac-CWGGPPPPPP-NH_2	47	**-1.4**
P7 Helix Ac-CWGGPPPPPPP-NH_2	60	**-1.6**
Homer1a_consensus Ac-CGGTPPSPW-NH_2	4.6	**-0.08**

Table 2.2: Results using air oxidation at pH 8.5 for CGG-TrpZip, t = 6 days

	K_{eq}	**ΔG(A•B) in kcal/mol**
P4 Helix Ac-CWGGPPPP-NH_2	0.69[a]	**1.0**
P5 Helix Ac-CWGGPPPPP-NH_2	5[b]	**-0.13**
P6 Helix Ac-CWGGPPPPPP-NH_2	24[b]	**-1.0**
P7 Helix	n/a[c]	**n/a[c]**

Ac-CWGGPPPPPPP-NH_2		
Homer1a_consensus Ac-CGGTPPSPW-NH_2	6.7	**-0.3**

a: Data acquired at 15 days, b: Data acquired at 10 days, c: Data couldn't be acquired because of peak overlap

C. REDOX Buffer at pH 7.5

The third method uses a glutathione REDOX buffer to oxidize the cysteines to disulfides. Equilibration time was much faster (4 days) but since more peaks were present in the mixture, different gradients were needed to avoid peak overlap. Only CGG-TrpZip-KK (Table 2.3) was evaluated for this assay because its water solubility was superior to CGG-TrpZip.

Table 2.3: Results using REDOX buffer and CGG-TrpZip-KK, t = 4 days

	K_{eq}	**ΔG(A•B) in kcal/mol**
P4 Helix Ac-CWGGPPPP-NH_2	n/a	**n/a**
P5 Helix Ac-CWGGPPPPP-NH_2	9.7	**-0.93**
P6 Helix Ac-CWGGPPPPPP-NH_2	27.4	**-1.5**
P7 Helix Ac-CWGGPPPPPPP-NH_2	25.7	**-1.5**
Homer1a_consensus Ac-CGGTPPSPW-NH_2	5.4	**-0.59**

IV. Discussion

A. Air oxidation at pH 7.5

The peptide monomers were still present after 5 days, indicating that the disulfide exchange was proceeding very slowly. Degradation was suspected because peak heights were decreasing over time but no new peaks were created. The degradation products could not be identified. It is possible that the degradation products eluted off the column at the beginning

of the run (void volume) or after the gradient was complete. Another possible reason for decreasing peak heights could be peptide aggregation.

B. Air oxidation at pH 8.5

Again peak heights began to decrease over time, suggesting peptide degradation. However, the peptide monomers were fully oxidized to their dimeric state, contrary to the pH 7.5 results. It is not conclusive that equilibrium was reached because of the changing peak heights. Conclusive evidence would be a reproducible peak area over a number of days. Nevertheless, the observed results serve as a starting point to understanding the effectiveness of the model system. The results indicate that a favorable interaction is created as the number of proline residues increase, in the case of the generic PPII helix (Table 2.1 and Table 2.2). This effect appears to level off after the seventh proline residue. In the case of the Homer1a_consensus peptide, only a slight preference for the helix:hairpin heterodimer is observed.

C. REDOX Buffer at pH 7.5

In this experiment, the peak heights did not decrease over time. The use of the REDOX buffer inhibited the degradation and allowed accurate evaluation of the equilibrium distribution of peptide dimers. ΔG values (Table 2.3) are similar to those determined by air oxidation (pH 8.5) even though GS dimers exist. Observing a similar result gives credence to the K_{eq} equation derived for this REDOX buffer oxidation process. Increasing the number of prolines increases the strength of binding. As the number of prolines increases, more favorable contact with the hairpin, presumably the Trp residues, is being made. The favorable contact could be a result of one or more C-H-π interactions between the proline side chain

and Trp's indole ring. Once again, the Homer1a consensus sequence shows only a slight deviation from a statistical mixture.

V. Conclusions

This study set out to achieve two objectives. The first was the use of the TrpZip peptide as a model for the recognition domain of the Homer 1a EVH1 protein. Achievement of this goal relied on the peptide's ability to recognize the PPII helix ligands. The second goal was the development and use of a disulfide exchange assay to investigate the effectiveness of the model system and quantify the binding event. The results with the generic PPII helix (P_n, n = 4 - 7) indicate that both goals were achieved. Five Pro residues are needed in the helix to favor the heterodimer structure over a statistical distribution. The strength of the favorable interaction (between helix and hairpin) plateaus when six or seven Pro residues are in the helix. The best K_{eq} observed (Table 2.3) is 13-fold greater than a statistical distribution and Zondlo's best K_{eq} is 4-fold greater than his control peptide (Figure 2.2). These results suggest that a stronger prolyl-π interaction exists between the PPII helix and the beta-hairpin peptide, compared to Zondlo's peptide model system.

The results with the Homer 1a consensus sequence indicate that there is room for improvement. The crystal structure of the Homer1a ligand with the EVH1 domain indicates that the C-terminal end of the ligand curls upward and possibly forms favorable contacts with another portion of the Homer 1a EVH1 protein. Unfortunately that interaction could not be modeled using the given system. However it may be possible to incorporate additional components of the consensus sequence at the N-terminus (Ala and Leu) to improve binding of the Homer 1a consensus. The results with the generic PPII helix suggest that the Pro residues, for the Homer 1a consensus, are not in the right positions for binding.

This work demonstrates the use of the disulfide exchange assay to investigate non-covalent interactions in a peptide model system. In addition, the assay was modified to tolerate the use of a glutathione REDOX buffer. The power of ultra high performance liquid chromatography (UPLC) was demonstrated by shortening the analysis time of the assays from 30 minutes to 5 minutes.

VI. Experimental Procedures

A. Peptide Synthesis and Purification

Peptides were synthesized by automated solid phase peptide synthesis on an Applied Biosystems Pioneer Peptide Synthesizer using Fmoc (9-fluorenylmethoxycarbonyl) protected amino acids on a PAL-PEG-PS resin. The amino acids residues were activated for coupling with HBTU (O-benzotriazole-N,N,N',N',-tetramethyluronium hexafluorophosphate) and HOBt (N-hydroxybenzotriazole) in the presence of DIPEA (diisopropylethylamine) in solvent DMF (N,N-dimethylformamide). Deprotections were carried out in 2% DBU (1,8-diazabicyclo[5.4.0]undec-7-ene), 2% piperdine in DMF for approximately 10 minutes. Extended cycles (75 minutes) were used for each amino acid coupling step. The N-terminus was acetylated with 5% acetic anhydride, 6% lutidine in DMF for 30 minutes. Cleavage of the peptide from the resin was performed in 94:2.5:2.5:1 TFA (trifluoroacetic acid): TIPS (Triisopropylsilane): water: EDT (Ethanedithiol) for 3-4 hours. TFA was evaporated and ether was used to precipitate the cleavage products. The water soluble peptides were extracted with water and lyophilized. Peptides were purified by reversed phase HPLC, using a Waters Atlantis dC_{18} (5μm, 10 x 100mm) column and a gradient of 1 to 60% B in 50 minutes, where solvent A was 95:5 water:acetonitrile, 0.1 % TFA and solvent B was 95:5 acetonitrile:water, 0.1 % TFA. Once purified, the peptides were lyophilized to powder and the peptide identity was confirmed by electrospray ionization (ESI) mass spectrometry in the positive ion mode.

B. HPLC Analysis

HPLC/UV analyses were performed using an Alliance HPLC system fitted with a quaternary pump, autosampler, a thermostated column compartment, and a diode array

detector controlled by Empower 2 v6.1 (Waters Corporation, USA). Chromatography was carried out using a Waters XBridge C18 column (4.6 mm x 75 mm; particle size 2.5µm; Waters, USA). The mobile phase was composed of a mixture of 0.1% trifluoroacetic acid in 95:5 water: acetonitrile (Solvent A) and 0.1% trifluoroacetic acid in 95:5 acetonitrile:water (Solvent B). The gradient was delivered at 1 mL/min as follows: 0 min, 15% B; 40 min, 30% B. The column was maintained at ambient temperature. The diode array detector was set at 220 and 280 nm. One hundred microliters of sample was injected onto the column by an auto liquid sampler. Figures 2.17 through 2.18 are sample data acquired from HPLC.

Figure 2.17: HPLC chromatogram of air oxidation experiment (pH 8.5) using CGG-TrpZip-KK (100 µM) and P6 (100 µM) at 35 °C. Top trace is a mixture of CGG-TrpZip-KK and P6, middle trace is P6 control, bottom trace is CGG-TrpZip-KK control. Absorbance recorded at 280 nm.

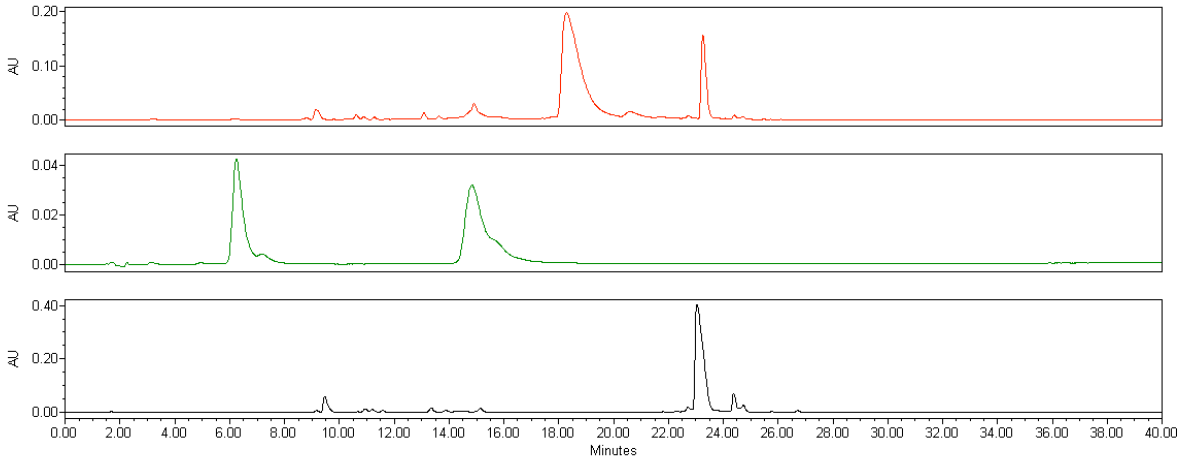

Figure 2.18: HPLC chromatogram of air oxidation experiment (pH 8.5) using CGG-TrpZip-KK (100 µM) and Homer1a_consensus (100 µM) at 35 °C. Top trace is a mixture of CGG-TrpZip-KK and Homer1a_consensus, middle trace is Homer1a_consensus control, bottom trace is CGG-TrpZip-KK control. Absorbance recorded at 280 nm.

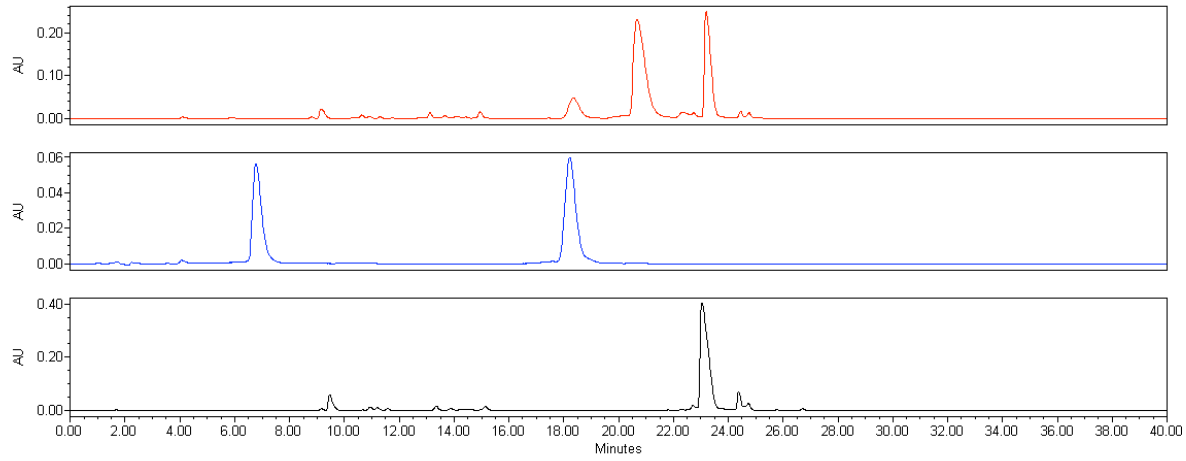

C. UPLC Analysis

UPLC/UV analyses were performed using an Acquity UPLC system fitted with a binary pump, a plate autosampler, a thermostated column compartment, sample organizer, and an Acquity photodiode array detector controlled by Masslynx v4.1 (Waters). Chromatography was carried out using an Acquity UPLC BEH C18 column (2.1 mm x 100mm; particle size 1.7μm; Waters). The mobile phase was composed of a mixture of 0.2% formic acid in water (solvent A) and 0.2% formic acid in acetonitrile (solvent B). For pH 8.5 experiment, the gradient was delivered at 0.6 mL/min as follows: 0 min, 15% B; 10 min, 50% B. For REDOX buffer and pH 7.3 experiments, the gradient was delivered as follows: 0 min, 15% B; 2 min, 22% B; 3 min, 24% B; 5 min, 50% B. The column was maintained at 35 °C. The diode array detector was set at 220 and 280 nm. Five to ten microliters of sample was injected onto the column by an auto liquid sampler. Following UV detection, the flow was directed to the mass spectrometer without a split. Figures 2.19 through 2.25 are sample data acquired from UPLC.

Figure 2.19: UPLC chromatogram of air oxidation experiment (pH 7.3) using CGG-TrpZip-KK (100 μM) and P6 (100 μM) at 35 °C. Top trace is a mixture of CGG-TrpZip-KK and P6,

middle trace is P6 control, bottom trace is CGG-TrpZip-KK control. Absorbance recorded at 280 nm.

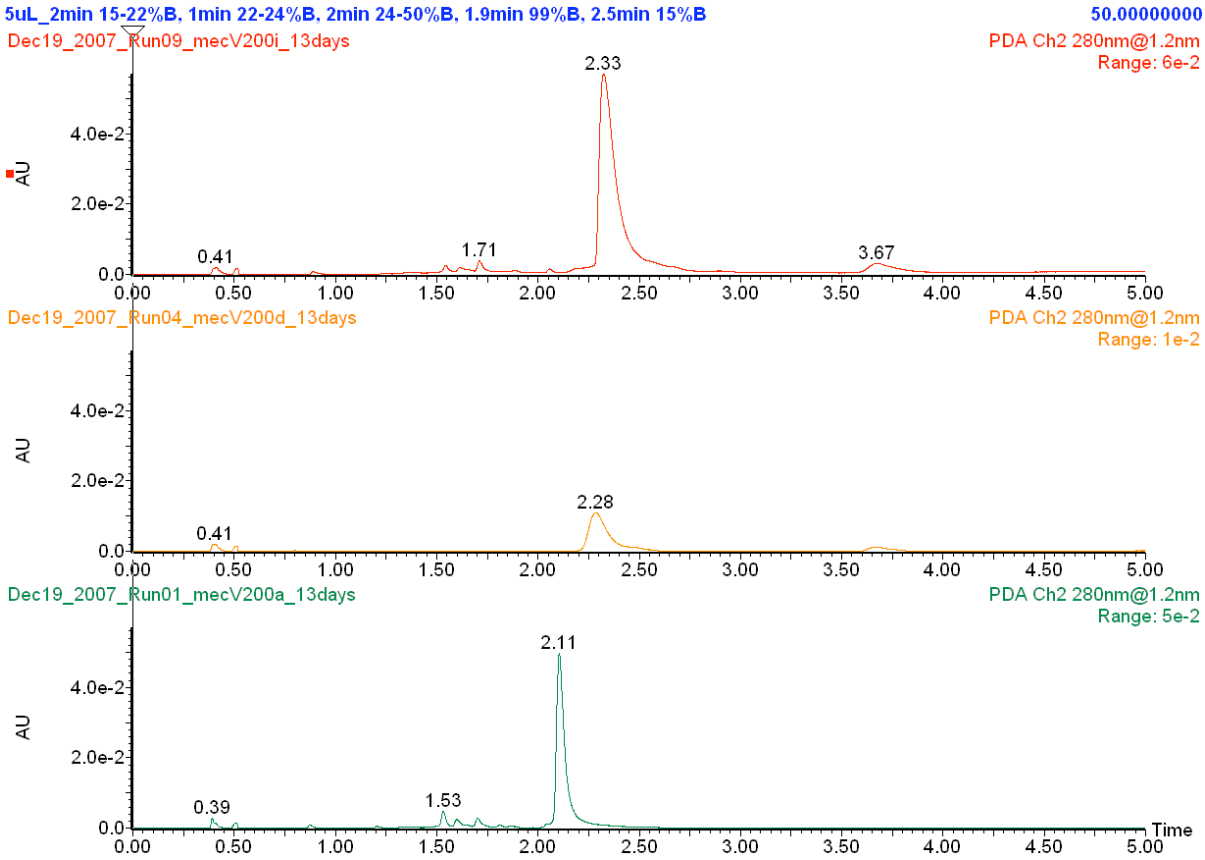

Figure 2.20: UPLC chromatogram of air oxidation (pH 7.3) experiment using CGG-TrpZip-KK (100 μM) and Homer1a_consensus (100 μM) at 35 °C. Top trace is a mixture of CGG-TrpZip-KK and Homer1a_consensus, middle trace is Homer1a_consensus control, bottom trace is CGG-TrpZip-KK control. Absorbance recorded at 280 nm.

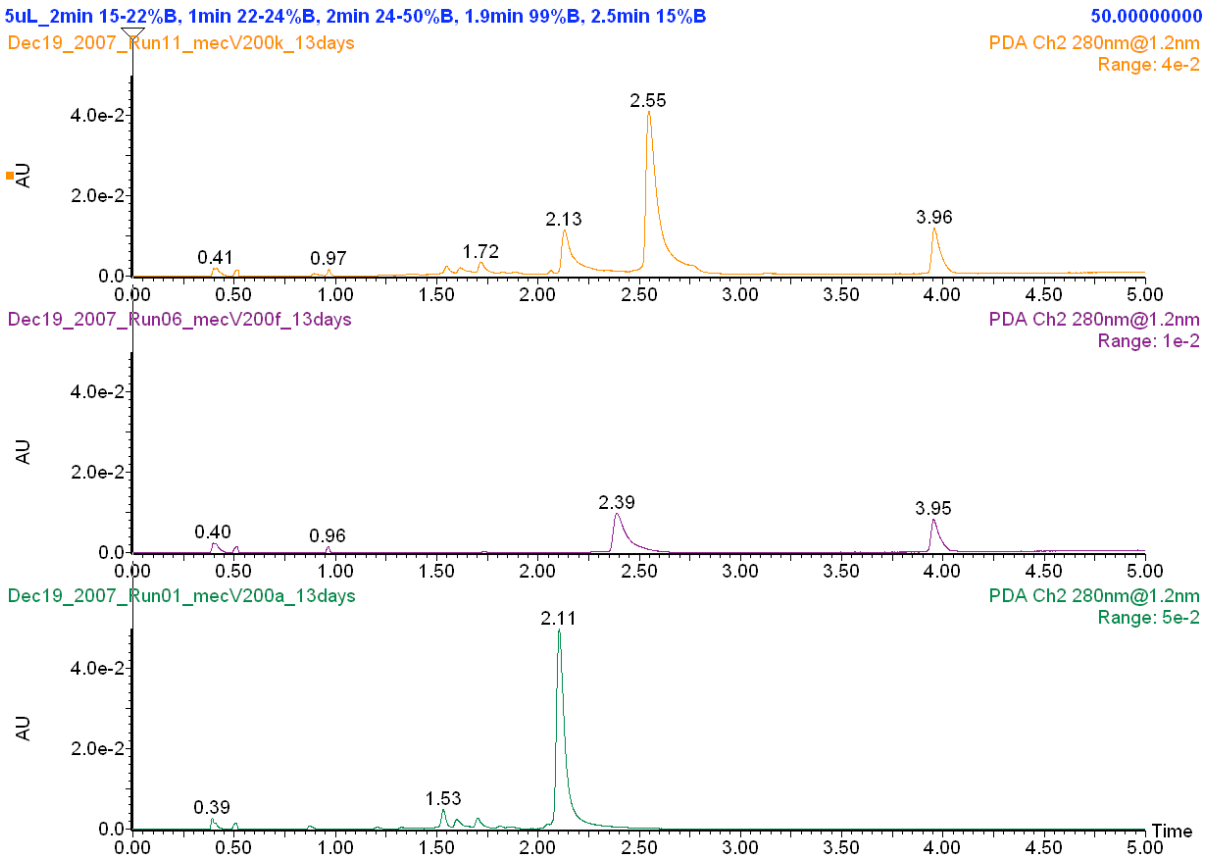

Figure 2.21: UPLC chromatogram of REDOX buffer (pH 7.4) experiment using CGG-TrpZip-KK (100 μM) and P4 (100 μM) at 35 °C. Top trace is a mixture of CGG-TrpZip-KK and P4, middle trace is P4 control, bottom trace is CGG-TrpZip-KK control. Absorbance recorded at 280 nm.

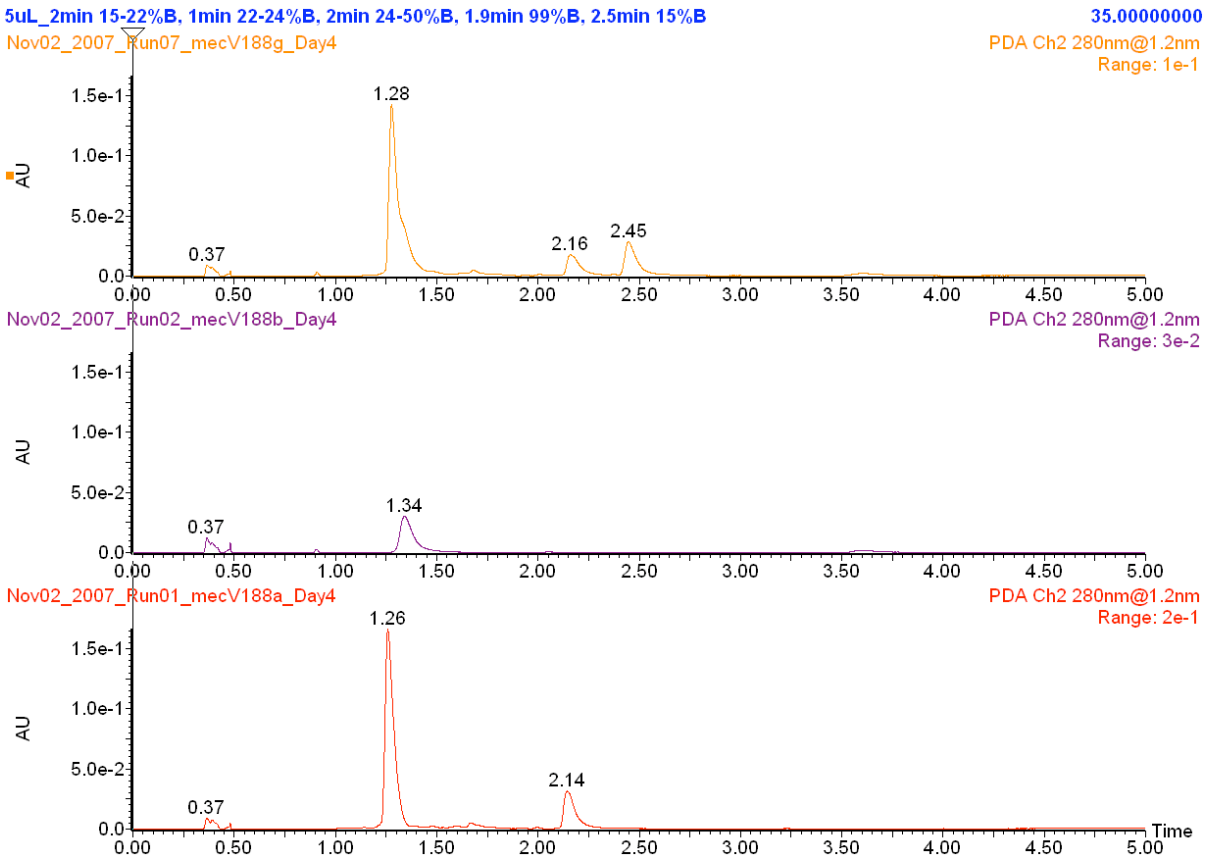

Figure 2.22: UPLC chromatogram of REDOX buffer (pH 7.4) experiment using CGG-TrpZip-KK (100 μM) and P5 (100 μM) at 35 °C. Top trace is a mixture of CGG-TrpZip-KK and P5, middle trace is P5 control, bottom trace is CGG-TrpZip-KK control. Absorbance recorded at 280 nm.

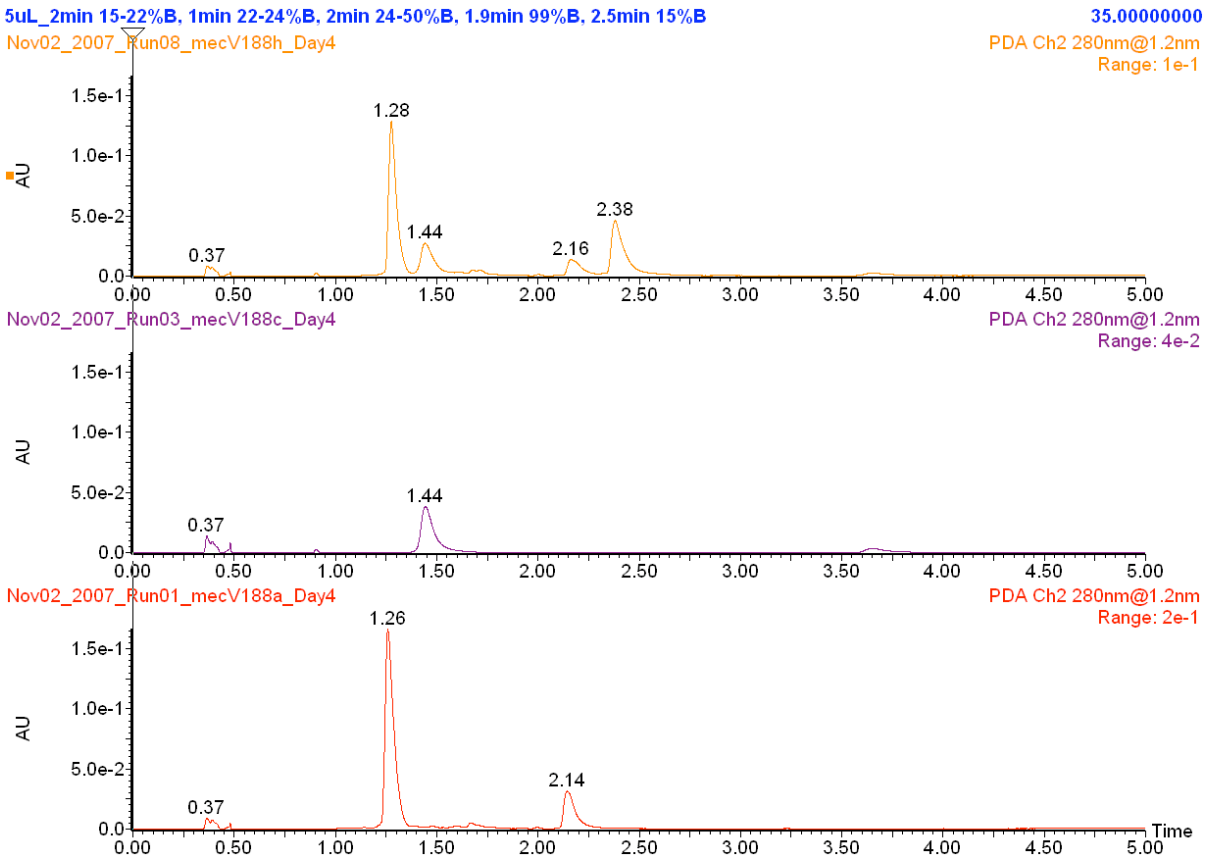

Figure 2.23: UPLC chromatogram of REDOX buffer (pH 7.4) experiment using CGG-TrpZip-KK (100 μM) and P6 (100 μM) at 35 °C. Top trace is a mixture of CGG-TrpZip-KK and P6, middle trace is P6 control, bottom trace is CGG-TrpZip-KK control. Absorbance recorded at 280 nm.

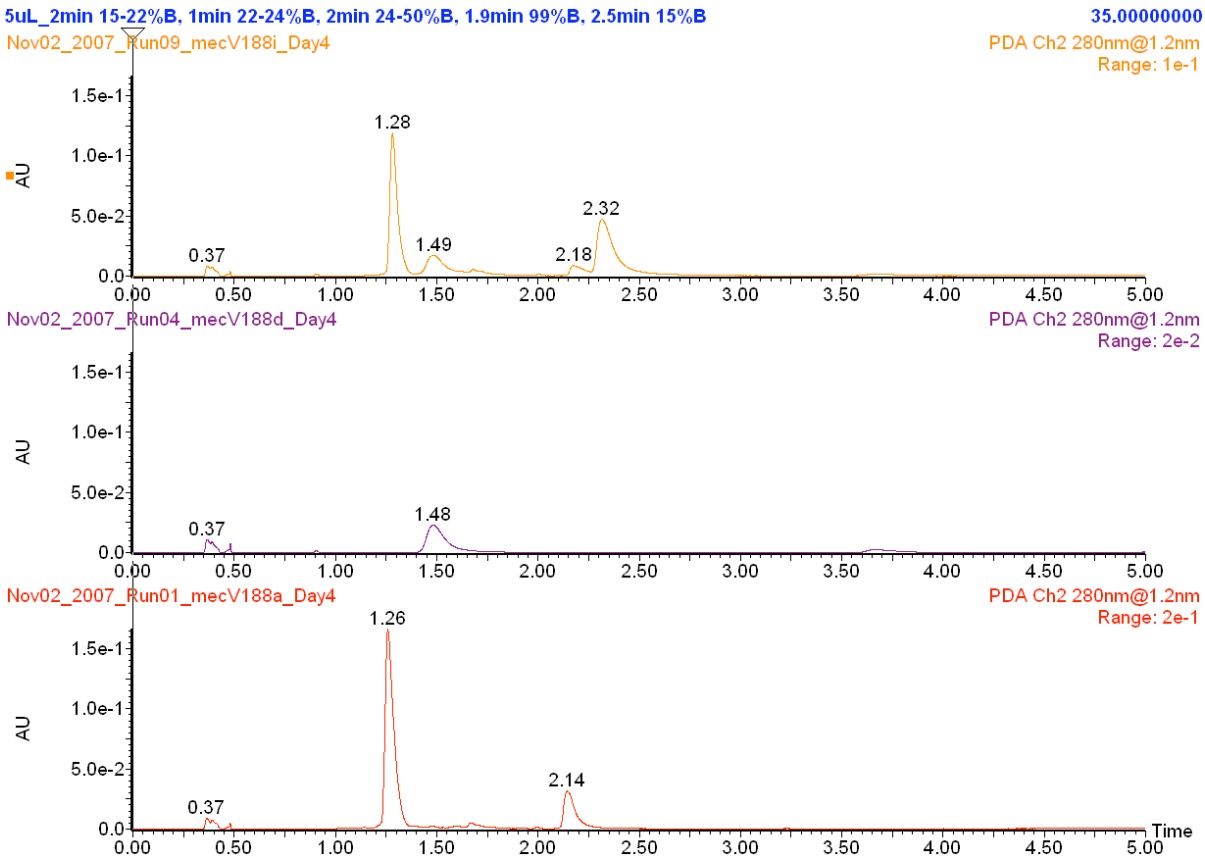

Figure 2.24: UPLC chromatogram of REDOX buffer (pH 7.4) experiment using CGG-TrpZip-KK (100 μM) and P7 (100 μM) at 35 °C. Top trace is a mixture of CGG-TrpZip-KK and P7, middle trace is P7 control, bottom trace is CGG-TrpZip-KK control. Absorbance recorded at 280 nm.

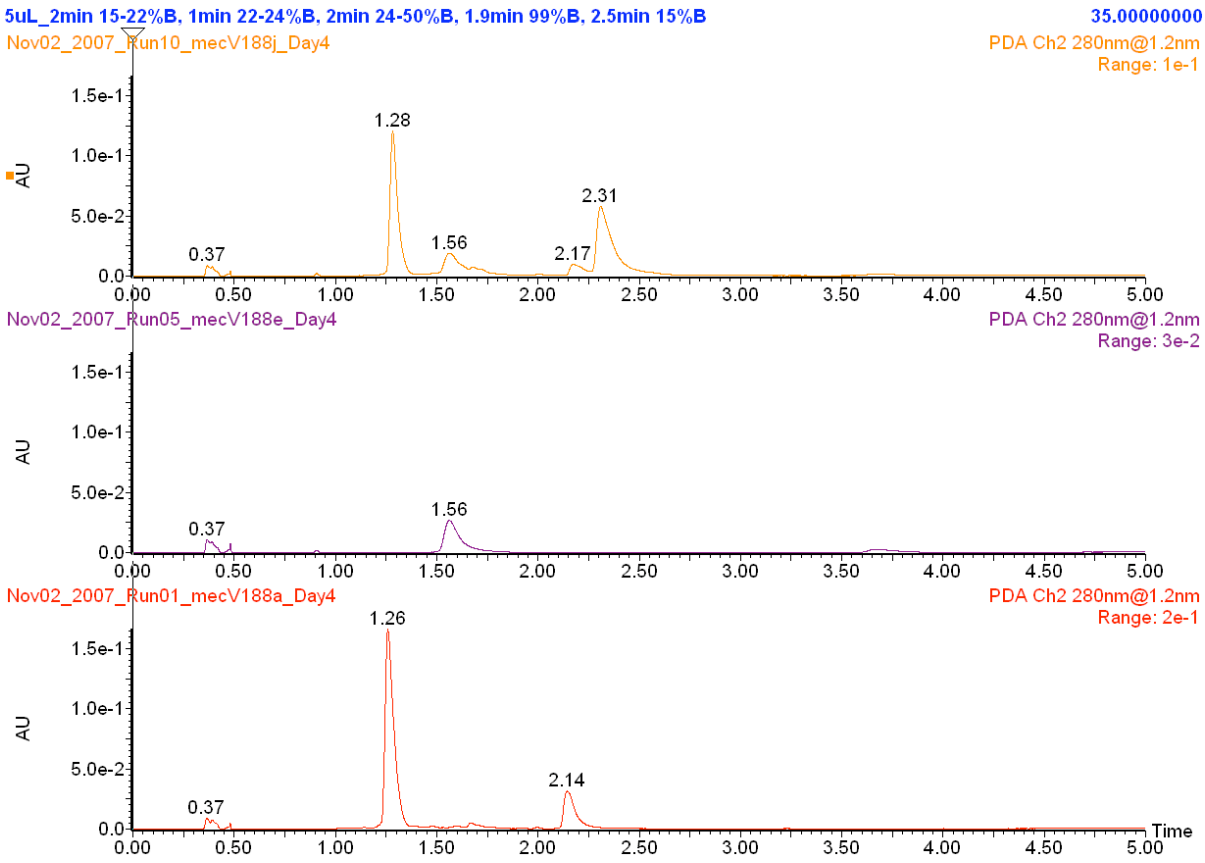

Figure 2.25: UPLC chromatogram of REDOX buffer (pH 7.4) experiment using CGG-TrpZip-KK (100 μM) and Homer1a_consensus (100 μM) at 35 °C. Top trace is a mixture of CGG-TrpZip-KK and Homer1a_consensus, middle trace is Homer1a_consensus control, bottom trace is CGG-TrpZip-KK control. Absorbance recorded at 280 nm.

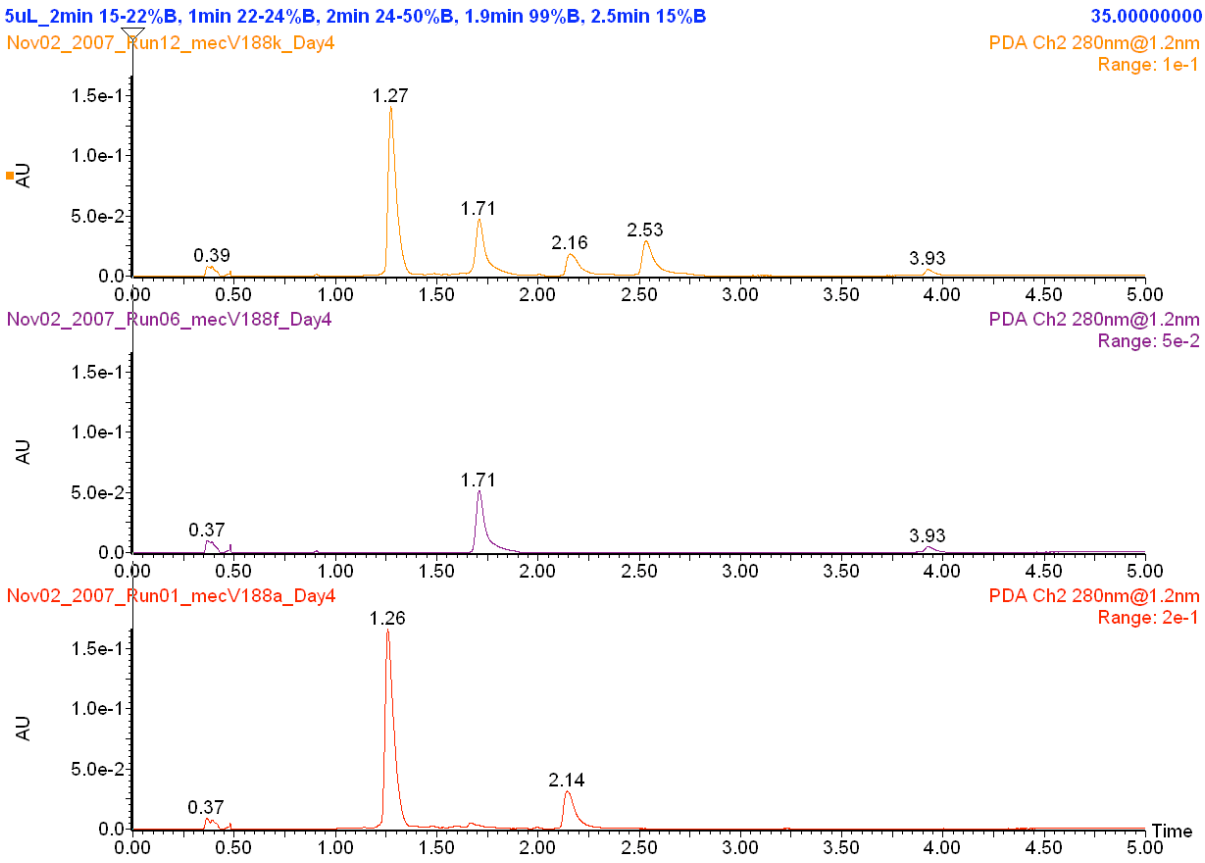

D. MS Analysis

Mass spectrometry was performed on a Micromass ZQ single quadrupole (Waters) using a standard electrospray ionization (ESI) source operated in positive ion mode. The desolvation gas rate was set to 700 L/hr at a temperature of 350 °C, the cone gas rate was set to 0 L/hr and the source temperature at 150 °C. The cone and desolvation gas flows were obtained from an in-house nitrogen source. The capillary voltage and the cone voltage were set at 1100 V and 50 V, respectively. The extractor voltage and RF lens were set at 3 V and 0 V, respectively. Scan times were 1.0 s with a delay of 0.02 s. Data was collected in continuum mode from *m/z* 500 to *m/z* 1800.

Chapter 3

The Use of Dynamic Combinatorial Chemistry (DCC) to find Nucleotide Receptors and Peptide Receptors

I. Background and Introduction

A. Dynamic Combinatorial Chemistry (DCC)

Dynamic combinatorial chemistry (DCC) uses reversible covalent bond formation to create a library of compounds.[46] The use of reversible reactions enables the library to be under thermodynamic control because the library can continuously respond to changes in its composition to reach the lowest energy state. The ability of the library to respond to changes in its environment makes this a dynamic process. The first example of DCC was reported in 1996 by Sanders,[47] so DCC is a young field of research in which the scope and limitations are still being defined.

DCC is a useful tool for molecular recognition because the library can respond to a stimulus such as a potential guest molecule (Figure 3.1). The potential hosts are formed by reaction of all the building blocks with each other. Upon addition of a guest molecule, the library adjusts to find the lowest energy state. This state could be in the form of a receptor for that particular guest molecule. Since the library is an equilibrium mixture, Le Chatelier's principle applies and the library will adjust to reestablish the thermodynamically lowest

---

[46] Corbett, P. T.; Leclaire, J.; Vial, L.; West, K. R.; Wietor, J.; Sanders, J. K. M.; Otto, S. *Chem. Rev.* **2006**, *106*, 3652-3711.

[47] Brady, P. A.; Bonar-Law, R. P.; Rowan, S. J.; Suckling, C. J.; Sanders, J. K. M. *Chem. Commun.* **1996**, 319-320.

energy state. Therefore, if a favorable interaction between one of the library compounds (host) and the guest exists, then that host will be amplified. The building blocks needed to make more of this host come from the other library components. In other words, the synthesis of the favorable host occurs at the expense of the less favorable hosts. This is possible because all the library components are synthesized using reversible reactions.

Figure 3.1: A small dynamic combinatorial library and the energetic effect of adding a template that binds to one of the equilibrating species.[48]

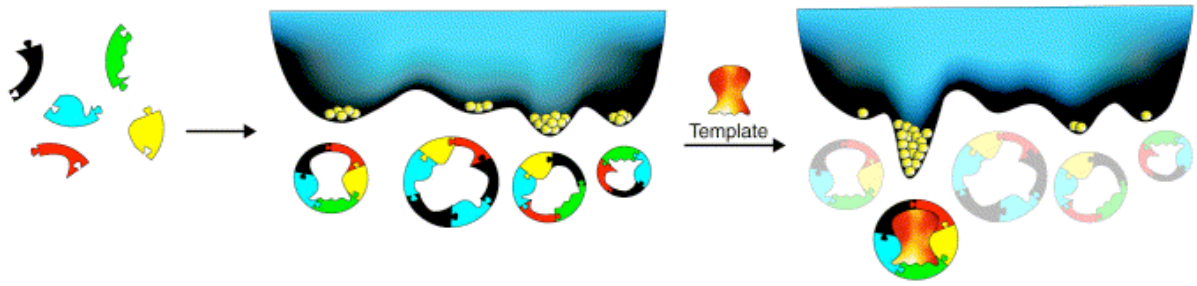

A key feature of DCC is that the desired compound(s) are amplified at the expense of undesired ones. In addition, the amplified host can be separated and isolated directly from the library mixture. Both of these are major advantages over traditional combinatorial chemistry, where identified hosts need to be synthesized after their identification. Traditional combinatorial chemistry still presents advantages over DCC.[49] The number of reversible reactions available for DCC is a limiting factor for its use. Traditional combinatorial chemistry has many irreversible reactions available. In DCC, all library members need to be soluble during the screening process because insoluble components can shift the equilibrium of the library mixture significantly. In traditional combinatorial chemistry, the insolubility of some library members is less of an issue. The use of reversible reactions for DCC limits the control of the reactions. In traditional combinatorial chemistry, each individual step can be

[48] Otto, S.; Furlan, R. L. E.; Sanders, J. K. M. *Curr. Opin. Chem. Biol.* **2002**, *6*, 321-327.

[49] Otto, S.; Furlan, R. L. E.; Sanders, J. K. M. *Drug Discov. Today* **2002**, *7*, 117-125.

controlled. DCC has some disadvantages but its advantages (amplification of host and isolation of library members) make it a technique worth considering in the field of molecular recognition.

B. Disulfide Exchange and DCC

Disulfide exchange is one of the few reversible reactions used in DCC that can occur under physiological conditions. Reversible disulfide exchange is mediated by thiolate anions, which are created by deprotonation of free thiol. These anions can continuously undergo substitution reactions to create more disulfide bonds. This exchange process can be switched on and off by manipulating the pH of the library. Exchange is rapid at pH 7-9 but negligible at pH 2.5.[50]

Disulfide exchange has been used to find receptors for a variety of guests, most of which contain ammonium groups. Sanders reported the use of this reaction to generate a library of compounds composed of dithiol building blocks **A**, **B**, and **C** (Figure 3.2). The design of these building blocks was based on Dougherty's cyclophane receptors.[51]

Sanders combined these building blocks in equimolar (3.3 mM) ratios and generated a DCC library in aqueous solution at pH 8.5.[52] The two major products were a cyclic dimer (BC) and a cyclic trimer (ABC). These products, along with others, can be separated and analyzed by HPLC. Using this DCC library, he showed that two different guests (**1**, **2**) could template and amplify the formation of two different hosts: A_2B and A_3, repectively. (Figure 3.2).

---

[50] Otto, S.; Furlan, R. L. E.; Sanders, J. K. M. *J. Am. Chem. Soc.* **2000**, *122*, 12063-12064.

[51] Petti, M. A.; Shepodd, T. J.; Barrans, R. E.; Dougherty, D. A. *J. Am. Chem. Soc.* **1988**, *110*, 6825-6840.

[52] Otto, S.; Furlan, R. L. E.; Sanders, J. K. M. *Science* **2002**, *297*, 590-593.

Figure 3.2: Results from disulfide exchange based DCC libraries. Selective amplification of three different hosts with three different ammonium guests.

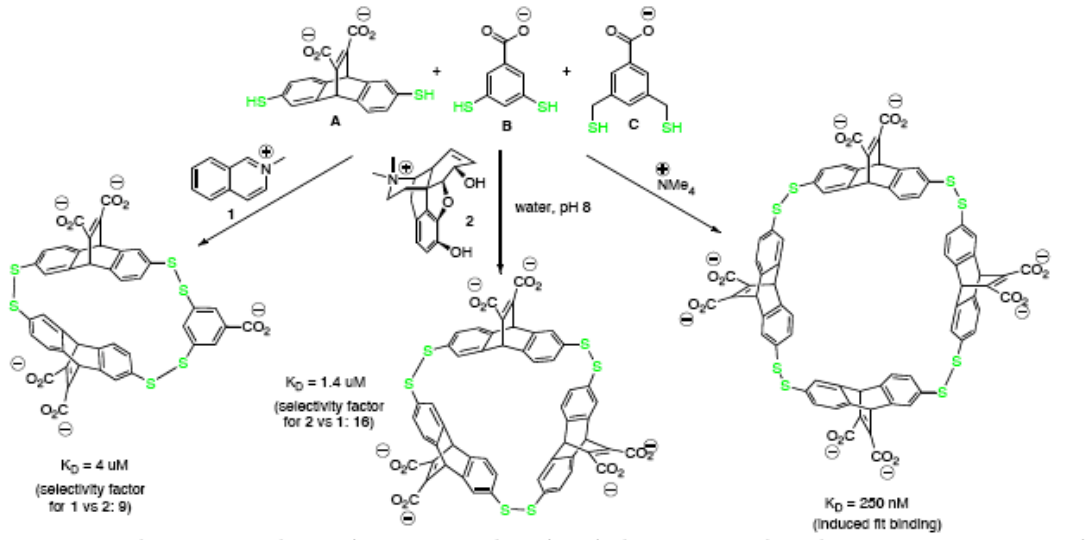

A second generation (biased) library was assembled to maximize the synthetic yield of each host. For host A_2B, dithiols A and B were combined in a 2:1 ratio. For host A_3, only dithiol A was used for the library. After isolation of the receptors, the binding of each guest was quantified by isothermal titration calorimetry (ITC). The binding constant for the matched pairs was significantly stronger than for the mismatched pairs (Figure 3.2).

In a similar study, Otto reported the use of the disulfide exchange reaction to find a receptor for tetramethylammonium iodide.[53] Addition of this guest amplified the tetrameric structure, A_4. Use of the biased library showed that the amplification was around 400-fold, relative to the untemplated mixture. Further analysis determined the amplified structure was the meso compound rather than the racemic. The binding was quantified by ITC and, again, the binding observed was very strong (Figure 3.2).

In both cases, the binding was strongly enthalpy driven. The cation-π interaction was hypothesized to be the dominant driving force for binding. These results establish DCC as a

[53] Corbett, P. T.; Tong, L. H.; Sanders, J. K. M.; Otto, S. *J. Am. Chem. Soc.* **2005**, *127*, 8902-8903.

way to identify and synthesize receptors for different guests. The fact that the guests contained ammonium groups was particularly interesting because previous efforts were aimed at using the cation-π interaction to bind 7mGTP (Chapter 1), which contains an ammonium group. As a result, DCC was investigated as a way to synthesize and amplify a disulfide containing receptor for 7mGTP. As an initial study, natural nucleotides were used as targets for DCC libraries.

C. Histone Post-Translational Modifications in Gene Expression

The DNA within our cells exists in the form of chromatin. The building block of chromatin is the nucleosome, a structure consisting of an octamer of four histone proteins (H2A, H2B, H3, and H4) around which DNA is wrapped.[54] The N-terminus of the histone proteins (histone tail) is unstructured and extends out of the protein-DNA complex (Figure 3.3). These histone tails are subject to covalent modification including acetylation, methylation, and phosphorylation. Histone methylation can occur on lysine or arginine residues.[55] Lysine methylation occurs on the H3 and H4 histone tails and this methylation can signal either transcriptional activation or repression, depending on the sites of methylation.[56]

Figure 3.3: Structure of the nucleosome, consisting of histone proteins complexed with DNA (magenta).

[54] Kornberg, R. D.; Lorch, Y. *Cell* **1999**, *98*, 285-294.

[55] Martin, C. Zhang, Y. *Nat. Rev. Mol. Cell Biol.* **2005**, *6*, 838-849.

[56] Zhang, Y.; Reinberg, D. *Genes Dev*. **2001**, *15*, 2343-2360.

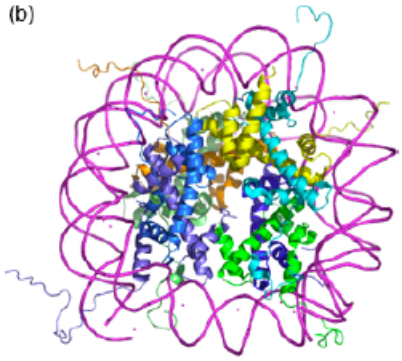

Lysine residues on the histone tail can be fully (KMe_3) or partially (KMe_2, KMe) methylated (Figure 3.4) and these modified histone tails are recognized by effector proteins. Three effector proteins recognize KMe_3: Chromodomains, Tudor domains, and PHD domains.[57]

Figure 3.4: The different methylation states of lysine

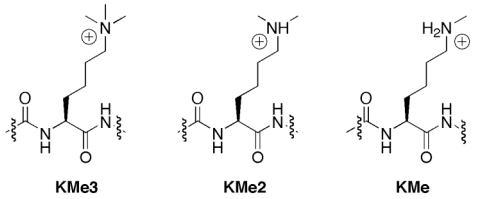

These proteins have been shown to be highly selective with regard to the methylation state of the modification. Selectivity for different methylation states of a Lys sidechain, by different effector proteins, has been shown to arise from differences in the number of aromatic residues versus acidic sidechains. KMe3 is typically bound in an aromatic pocket (Figure 3.5a). Acidic residues form salt bridges to the protonated amines in KMe2 and KMe (Figure 3.5b). Previous work in our lab has shown that the charge on the Lys is required for binding,

[57] Taverna, S. D.; Li, H.; Ruthenburg, A. J.; Allis, C. D.; Patel, D. J. *Nat. Struct. Mol. Biol*. **2007**, *14*, 1025-1040.

indicating that the driving force for binding is a cation-π interaction and not the hydrophobic effect.[58]

Figure 3.5: Binding pockets for PTMs. (a) Histone 3 K9Me3 (green) bound to HP1 chromodomain (gray) via cation-π with three aromatic sidechains (pdb code 1KNE); (b) Histone 3 K4Me2 (green) bound to the 3-MBT domain (gray) via cation-π interactions with three aromatic rings and a hydrogen bond to Glutamate (blue) (pdb code 2RHI).

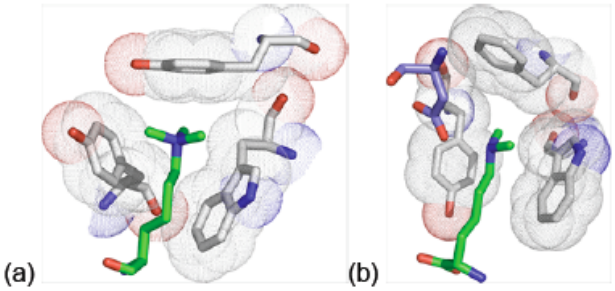

The KMe3 modification is similar in structure to the tetramethylammonium cation. Otto's DCC study showed that an aromatic cage was templated by the tetramethylammonium cation. The binding affinity observed in their study was in the nanomolar range (Figure 3.2). Binding affinities of the effector proteins to modified histone tails is in the micromolar range,[12] a weaker interaction than the templated receptor. These results suggest that DCC could be used to find a receptor for modified lysine residues. The reported dithiol building blocks (**A**, **B**, **C**) provided a nice starting point because each building block contained an aromatic ring that could form cation-π interactions with the methylated lysine residue. All of the building blocks contain one or two carboxylic acids, which improve the water solubility of these aromatic molecules. The carboxylates could form salt bridges with the protonated amines in KMe2 and KMe residues. This interaction coupled with the cation-π interaction could create a receptor that mimics the aromatic cage found in the effector proteins.

[58] Hughes, R. M.; Wiggins, K. R.; Khorasanizadeh, S.; Waters, M. L. *Proc. Nat. Acad. Sci. U.S.A.* **2007**, *104*, 11184-11188.

Furthermore, a different receptor for each methylation state is possible: an aromatic cage for KMe3 and an aromatic cage with hydrogen bonding carboxylate for KMe2 and KMe.

The primary goals of this project are to use DCC for the discovery and synthesis of receptors for nucleotide and peptide guests. The nucleotide guests (Figure 3.6) are a starting point for future DCC studies using 7mGTP. The peptide guests (Figure 3.9) are a starting point for future DCC studies using the modified histone tail. Disulfide mediated DCC is used because the exchange reaction occurs in aqueous solution and its application in finding receptors for ammonium guests has been established. These projects are the first use of DCC in our group's research. As a result, other goals of the project include the synthesis of dithiol starting material and the development of methodology for library analysis.

II. Experiment Design

A. Synthesis of Dithiol Building Blocks

The reported synthesis of dithiol **A** (Scheme 3.1) begins with $NaBH_4$ reduction of quinone **3** to anthracene **4**.[59] Substitution using *N,N,*-dimethylthiocarbamoyl chloride (**5**) to acquire **6** was followed by high temperature rearrangement resulting in **7**.[60] This thioester undergoes a Diels-Alder reaction with dimethyl acetylene dicarboxylate, at high temperature to afford **8**. Basic hydrolysis removes all protecting groups to generate dithiol **A**.

Scheme 3.1: Synthesis of Dithol A.[7]

[59] Boldt, P. *Chem. Ber*. **1967**, *100*, 1270-1280.

[60] Field, L.; Engelhardt, P. R. *J. Org. Chem*. **1970**, *35*, 3647-3655.

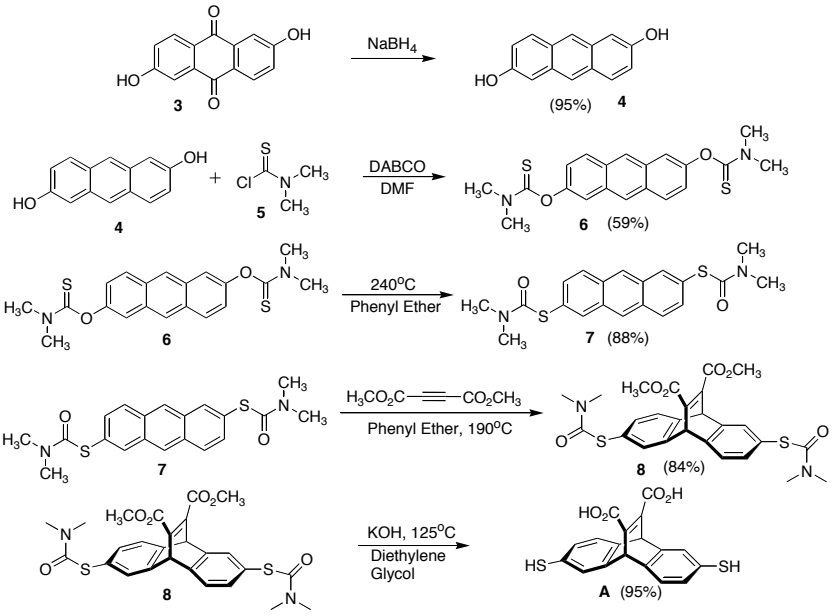

Complete reduction of quinone **3** to anthracene **4** was unsuccessful despite many attempts. One possible reason for the difficulty was the starting material: 2,6-dihydroxyanthraquinone. Only a less pure version of the starting material, anthraflavic acid technical grade, was available at the time this synthesis was started. Impurities present in this starting material may have led to the difficulty in duplicating the reported synthesis. An alternative pathway described in the literature[14] was completed to form **4**. (Scheme 3.2)

Scheme 3.2: Alternative Pathway to Anthracene-2,6-diol

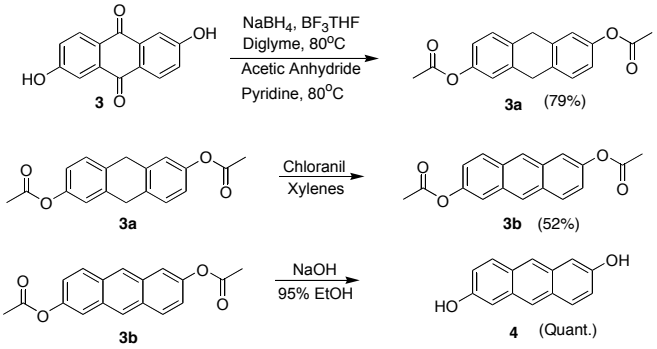

The alternative pathway (Scheme 3.2) involves partial reduction of quinone **3** followed by acetylation of the diols to acquire **3a**. Complete conversion to the anthracene was accomplished using chloranil to afford the protected diol, **3b**. Basic hydrolysis yields the

desired anthracene **4**. The remainder of the synthesis was completed in a manner analogous to the published procedure.[7]

The synthesis of dithiol **B** was performed in an analogous manner to dithol **A**. (Scheme 3.3) Commercially available dihydroxybenzoate starting material (**9**) reacts with *N,N,*-dimethylthiocarbamoyl chloride (**5**) to give the *O*-thio-carbamate (**10**) which undergoes high temperature rearrangement to give the *S*-thiocarbamate (**11**).[15] Basic hydrolysis removes all protecting groups to generate dithiol **B**.

Scheme 3.3: Synthesis of Dithiol B.[7]

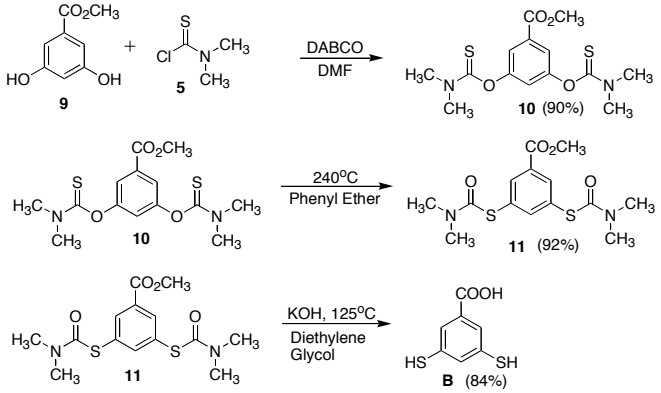

The synthesis of dithiol **C** (Scheme 3.4) follows a different procedure than dithiols **A** and **B**. 3,5-dimethylbenzoic acid (**12**) was converted to the methyl ester (**13**) under acidic conditions in methanol. This product was converted to the benzyl bromide (**15**) using *N*-bromosuccinimide (**14**).[61] The benzyl bromide underwent substitution with thiourea (**16**) followed by basic hydrolysis to yield dithiol **C**.[62]

Scheme 3.4: Synthesis of Dithiol C.[16,17]

[61] Markovac, A.; LaMontague, M. P. *J. Med. Chem.* **1980**, *23*, 1198-1201.

[62] Staab, H. A.; Kirrstetter, G. H. *Liebigs. Ann. Chem.* **1979**, 886-898.

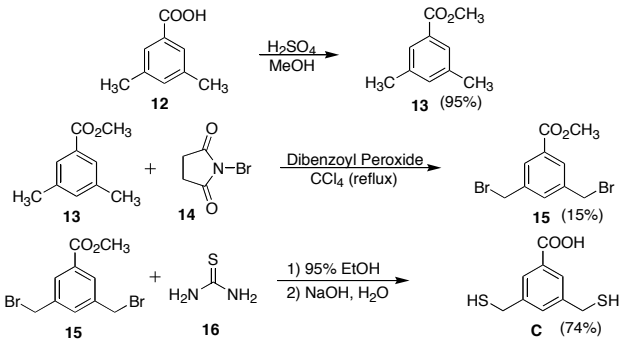

The extinction coefficient (ε value) of each dithiol was determined (see experimental) in H_2O at 315 nm (Table 3.1). The ε values were used for data analysis (see below).

Table 3.1: Experimentally determined ε values at 315 nm.

Dithiol	**ε value at 315 nm (M^{-1})**
A	1700
B	1700
C	80

B. Control Library

After the synthesis of the dithiol compounds was complete, a mixture containing all three dithiols was assembled at pH 8.5 and allowed to react via thiol mediated air oxidation. During the equilibration, the dithiols react with each other to give a mixture of species. The equilibrium mixture may be due to the formation of favorable interactions between the building blocks (π-π). Alternatively, the combinations formed may be the result of avoiding disfavorable interactions (charge-charge repulsion). This mixture of building blocks is the control library and it is important because it serves as a baseline or comparison point. Once equilibrium is reached for this mixture (3-4 weeks), it shows what favorable products exist when no guest or template are added to the mixture.

C. Templated Library

The templated library is the control library with a guest or template included in the mixture. Addition of the template can change the library's original composition. These

changes could lead to the formation of products that form favorable interactions (π-π, Coulombic, Van der Waals) with the template. As described above, amplification of favorable species occurs at the expense of unfavorable ones. The degree of amplification is determined by comparing it to the control library. This is described in detail below.

D. Biased Library

In order to quantify the binding event between product and template, the product needs to be isolated. Two advantages of DCC are that the template can synthesize its own host and this host can be isolated from the library mixture. In order to maximize the amount of product formed, a second library can be assembled that contains only the building blocks for the templated receptor in the appropriate ratio. This is referred to as a biased library. Once isolated, the product can be characterized (NMR, mass spectrometry, X-Ray) and used to measure binding to the template (ITC, NMR).

E. Data Analysis

Analysis of the library using LC/MS was not trivial. Much time was spent identifying the best conditions for library analysis. Initial attempts were directed at reversed phase (RP) HPLC separation using TFA as an ion pair agent but separation was poor. This was attributed to the strongly acidic mobile phase (pH 1) that resulted in protonation of the carboxylates. The neutral structures were either precipitating on the column or not being retained, resulting in a messy chromatogram. Higher pH for the mobile phase was investigated with formic acid (pH 2-3), ammonium acetate, NH_4OAc (pH 5), and triethylammonium acetate (pH 6) buffered mobile phases. The best separation was observed with NH_4OAc. LC conditions using NH_4OAc were incorporated but MS analysis needed to be improved. For the MS analysis, negative mode ionization was used because the carboxylates ionize better under this

mode. With the help of Curt Heine (Waters Corp.), the best ionization conditions for negative mode ionization were determined. The analytical conditions were tested, by reproducing the published work of Sanders and Otto.[7,8] Once the analytical conditions were established, DCC libraries were tested with new guests as templates.

The library mixtures were analyzed by UPLC/MS to separate, quantify, and identify the products in the library mixture. Chromatography is used to separate the library mixture on a C18 column, using an NH_4OAc mobile phase at pH 5 to aid in the separation of products. As the products elute off the column, they proceed through a UV detector where their absorbance at 315 or 320 nm is recorded. After UV detection, the separated products are directed to a mass spectrometer, where each peak is analyzed by electrospray ionization (ESI), in the negative ion mode, and its mass is determined. In summary, the library mixture is separated by UPLC, the amount of product is quantified by UV absorption at 315 nm, and the identity is determined by ESI in the negative ion mode.

The amount of amplification observed can be quantified by determining the change in peak area relative to the control. First, the area under the peak is integrated and the resulting raw values need to be normalized for comparison to each other. This can be accomplished one of two ways. One way to normalize the peak area is to determine its contribution to the total peak area of the chromatogram. The total peak area is defined as the sum of all the peaks in the chromatogram. The % Area for a peak is the individual peak area divided by the total peak area and multiplied by 100. This is calculated for both the control library and the templated library. Next, a comparison is made between the similar peaks in the control library and the templated library. This is done by, first, subtracting the control library peak area from the templated peak area. This difference is divided by the control library peak area

and multiplied by 100 to determine the percent change in peak area, relative to the control library.

An alternative way to normalize the data is through the use of extinction coefficicents (ε values). Once the identity of a peak is determined by MS analysis, it can be normalized using the ε values for the starting dithiols, as determined from the mass. Normalized peak areas can be calculated for both the control and templated libraries. The peak area is divided by the sum of all the ε values in the compound. The resulting value, corrected peak area, has the corrected value for the control library subtracted from it. The difference is divided by the corrected peak area for the control library and multiplied by 100 to determine the change in peak area. In both normalization methods, if the change in peak area is greater than zero, then the product corresponding to that peak was amplified as a result of the template. If the change in peak area is less than zero, then the product corresponding to that peak was consumed as a result of the template.

III. Nucleotide Recognition using DCC

A. Templated vs Control Library

DCC was used to investigate possible binders for nucleotides. Dithiols A, B, and C were combined in an equal ratio (3.3 mM) at a total concentration of 10 mM. Templated libraries containing each nucleotide (10 mM) were assembled. The nucleotides used were GMP, GTP, ATP, CMP, and CTP (Figure 3.6). After the library reached equilibrium (3-4 weeks), it was analyzed by UPLC/MS. The templated libraries were compared to the control library to investigate the effect of the template.

Figure 3.6: Nucleotides used in DCC study investigating nucleotide receptors

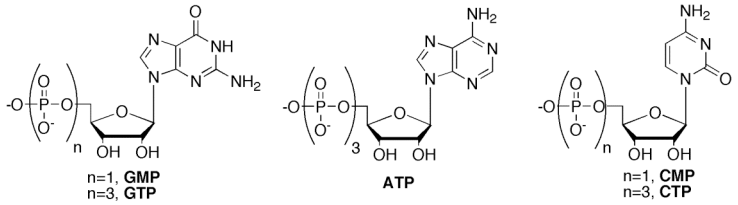

For the control library, the major products identified by LC/MS were B_3, BC, ABC, B_2C, and A_2BC. Dithiol A is used as a racemic mixture therefore any product containing two copies of dithiol A has an additional diastereomer. Second, products that contain 4 or more building blocks can potentially form constitutional isomers. In both cases, the isomers can be separated on the column but the exact isomer cannot be determined until the product is isolated. Lastly, MS cannot identify some of the peaks. The peaks that elute prior to 6.5 minutes and the peak at 9.2 minutes (see experimental) cannot be identified.

For the GMP, GTP, and ATP templated libraries similar results were observed (Figure 3.7, Table 3.2). The highest amplification was for the peak at 7 minutes: cyclic B_4. The next highest amplification was for the peak at 7.8 minutes: cyclic B_2C_2 and/or cyclic B_3C. In this case, two peaks co-elute and so one or both could be amplified by the template. All other peak amplifications observed were modest when compared to these two peaks. It is interesting to note that the unidentifiable peaks (9.2 minutes and all peaks < 6.5 minutes) disappear in these templated libraries.

For CTP, the results are the opposite of the ones for ATP, GTP, and GMP templated DCC screens (Figure 3.7, Table 3.2). The greatest amplification is at 7.8 minutes and second best is at 7 minutes. It is also interesting to note that the increase in percent observed is less than those observed for ATP, GTP, and GMP.

For CMP, the best amplification was observed for the peak at 7.9 minutes (Figure 3.7, Table 3.2). This peak was identified as A_2BC. This is one of the two possible constitutional

isomers that form. The other isomer co-elutes with B_3 at 6.6 minutes. When compared to the amplification observed with ATP, GTP, and GMP this amplification is small. All other peak area increases were within error of the control library.

Figure 3.7: Results of nucleotide templated DCC libraries after 43 days

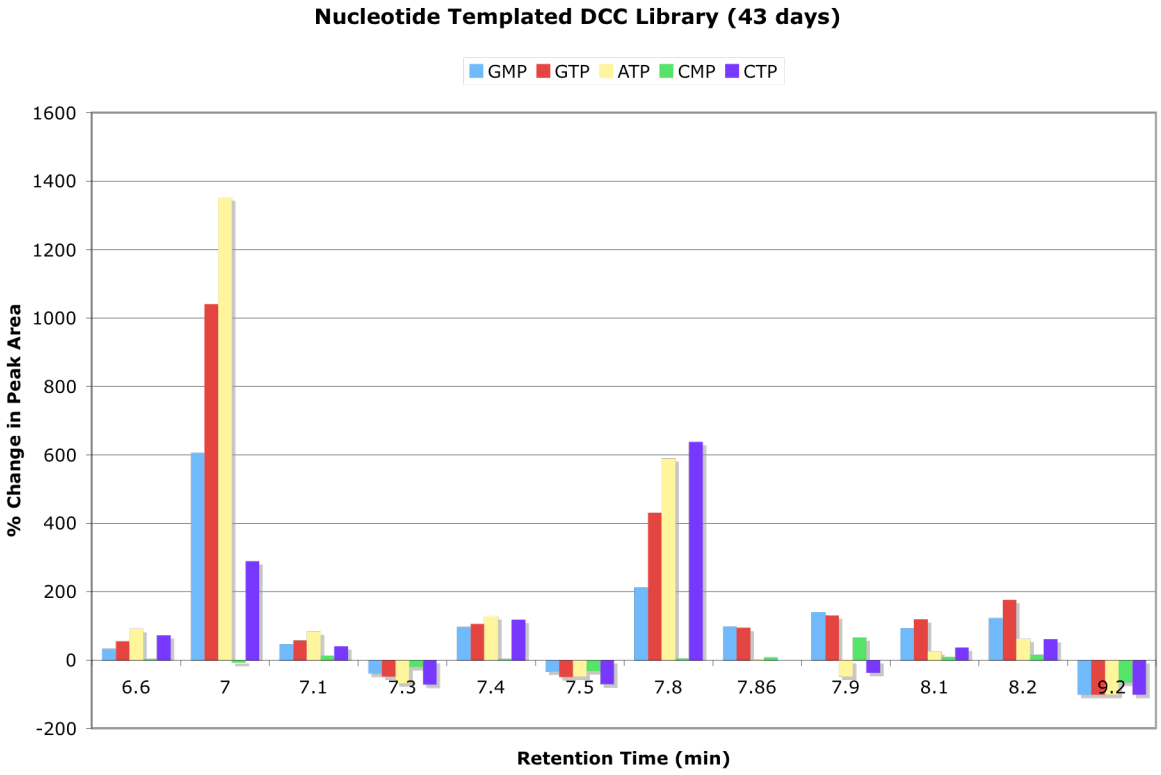

Table 3.2: Identity of peaks in Figure 3.7 determined by ESI-MS

Retention Time (min)	Structural Formula
6.6	A_2BC, B_3
7.0	B_4
7.1	B_2C
7.3	AB_2
7.4	BC
7.5	AB_3
7.8	B_2C_2, B_3C
7.86	ABC
7.9	A_2BC
8.1	AB_2C
8.2	AB_2C
9.2	Unknown

B. Biased Library

Biased libraries were assembled to further investigate the most amplified products for each nucleotide. In all cases, the total concentration of dithiols was equivalent to the concentration of nucleotide, 10 mM. In the case of ATP, GTP, and GMP the biased library consisted of only dithiol B. In the case of CTP, two biased libraries were screened containing B and C in different ratios, 1:1 and 3:1, respectively. In the case of CMP, a biased library was assembled containing A, B, and C in a 2:1:1 ratio, resepctively. These biased libraries were analyzed by UPLC/MS using the same conditions as before.

An unknown precipitate formed in both biased libraries containing CTP during the equilibration. It could be the receptor•nucleotide complex but this has not been investigated. Since the library was no longer homogeneous, no further analysis was done. The biased library for CMP was nearly identical to the control (see experimental). As a result, no further analysis was done.

The biased libraries for ATP, GTP, and GMP provided interesting results. Again B_4 (6.7 min) was the most amplified structure, but to a lesser degree than before (Figure 3.8, Table 3.3). Other amplified structures, in order of most to least amplified, included B_6, B_5, and B_3. These results support the previous finding that B_4 was the most amplified receptor.

Figure 3.8: Results of nucleotide templated biased library after 43 days

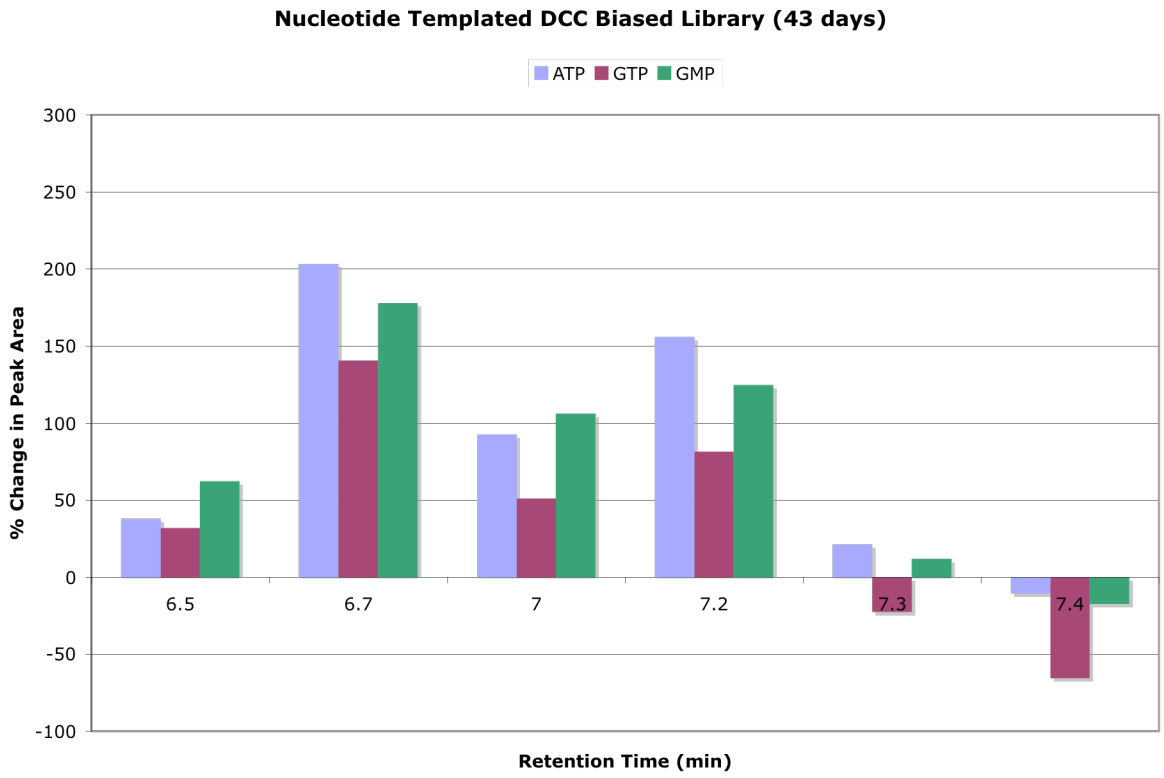

Table 3.3: Identity of peaks in Figure 3.8 determined by ESI-MS

Retention time (min)	Structural Formula
6.5	B_3
6.7	B_4
7.0	B_5
7.2	B_6
7.3	B_7
7.4	B_8

There seems to be a difference between the extent of amplification for each nucleotide. Comparison of ATP and GTP shows that amplification is greater for ATP than GTP for all species. The only difference between the two templates is the nucleotide base. Therefore, the receptor may be binding the adenine base more strongly than the guanine base.

Comparison between GTP and GMP shows that GMP amplifies the receptors more than GTP. This is different than what was observed in the original library. The only difference between these two is the length of the phosphate chain. A possible reason for the

difference in amplification is the overall charge of the nucleotide. The GMP may minimize the charge-charge repulsion between the phosphate and the carboxylate in the receptor.

ATP templated peaks are not always more amplified than those for GMP. For the receptors B_4 and B_6, the percent change in the presence of ATP is larger than with GMP templation. For the receptors B_3 and B_5, GMP templation is higher. Assuming that the percent area values are not within error of each other, a couple of points can be made. In the case of B_4 and B_6 receptors, the macrocycle may be large enough to tolerate or accommodate the additional phosphate groups in ATP. In the case of B_3 and B_5 receptors, the macrocycle may not be able to assemble in a manner to avoid charge-charge repulsion between the carboxylates and the phosphates. In both cases, there are two differences between the templates: identity of base and overall charge. Running the same biased library using AMP could provide valuable information. If the overall charge of the guest is an issue, then a difference will be observed between ATP and AMP. If the identity of the base is an issue, then a difference will be observed between AMP and GMP. This work is currently ongoing.

C. Isolation of Amplified Receptors

The next step was to isolate the amplified receptor for binding studies. B_4 was the most amplified, based on the biased library, so its isolation was investigated by HPLC. First an investigation was performed on an analytical HPLC to see how the separation compares to UPLC. Separation required longer run times but B_4 could be separated from the mixture reasonably well. After developing conditions for the analytical HPLC, the separation was completed using the semi-preparative HPLC. Separation was worse on the semi-prep column but this could be due to the age of the semi-prep column. An NMR structure of B_4 would

help confirm the MS data observed and may provide information about the mode of binding. Currently this work is ongoing.

D. Summary and Discussion

The nucleotide templated DCC studies have shown amplification of a cyclic homotetramer, B_4. This amplification is of particular interest considering that the structure is anionic in the screening experiment because of deprotonated carboxylic acids. The nucleotide's phosphate tail makes it anionic as well. Despite an anionic host and an anionic guest, a binding event appears to be occurring. This B_4 receptor is amplified in the presence of ATP to a greater extent than in the presence of GTP. This difference suggests potential selectivity of this receptor for the adenine base over the guanine base. Binding studies between the receptor and guest will confirm this hypothesis and are currently in progress.

IV. Trimethyl lysine Recognition using DCC

A. Templated vs Control Library

As an initial study into the use of DCC to find a receptor for the post-translationally modified histone tail, a simple dipeptide was used (Figure 3.9). This peptide contained a lysine residue with different methylation states (mono-, di-, and tri-). The DCC library was assembled to investigate selectivity among the different methylation states of lysine. Dithiols A, B, and C were combined in an equal ratio (3.3 mM) at a total concentration of 10 mM. Templated libraries containing each peptide (10 mM) were assembled. The library was analyzed using UPLC/MS. After the library reached equilibrium (3 weeks), the templated results were compared to the control library.

Figure 3.9: Peptides (H-Lys(xMe)-Gly-NH_2) used for DCC study investigating lysine methylation states

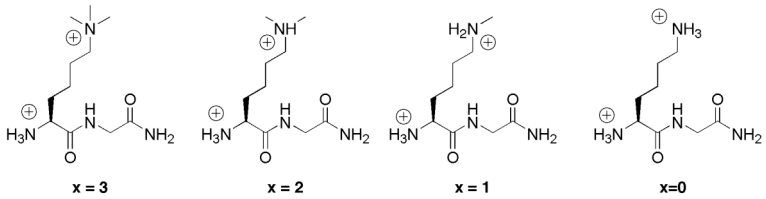

For most of the guests, the amplification observed was less than 50%. The lone exception was found in the tri-methyl lysine screen. The peak at 7.6 minutes increased 350% relative to the control. MS identifies this peak as A_2B, the same receptor Sanders isolated in his studies with **1** (Figure 3.2).[7] The amplification of this receptor for the other methylation states is less than 10%, indicating the possibility of selectivity. The next highest amplification observed for the trimethyl lysine peptide was at 7.3 minutes, corresponding to either BC or AB_3.

For the other methylation states (non-, mono-, di-), the highest amplification was observed at 6.95 and 7.3 minutes, corresponding to B_4 and either BC or AB_3, respectively (Figure 3.10, Table 3.4). Small amplification suggests that binding of these peptides by disulfide receptors may be weaker than the binding of the trimethyl lysine peptide.

Figure 3.10: Results of peptide templated DCC libraries after 21 days

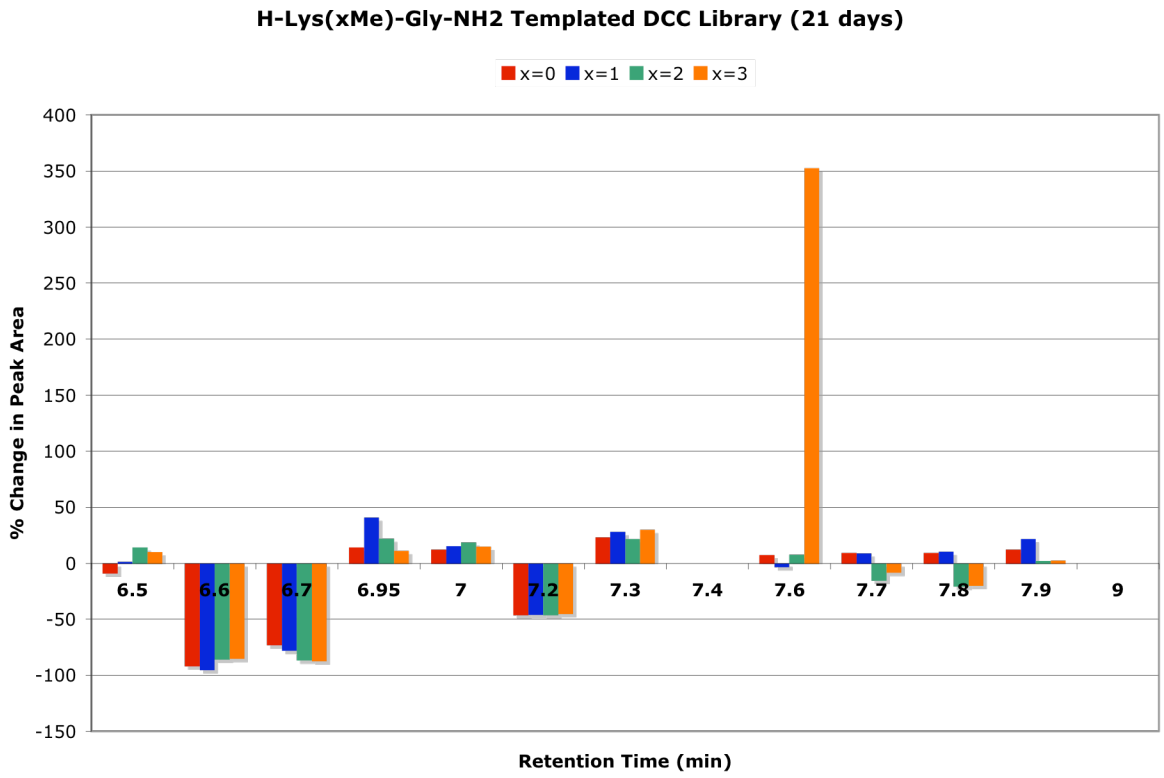

Table 3.4: Identity of peaks in Figure 3.10 determined by ESI-MS

Retention Time (min)	Structural Formula
6.5	B_3, C_2
6.6	AC
6.7	A_2
6.95	B_4
7.0	B_2C
7.2	AB_2
7.3	BC, AB_3
7.4	Unknown
7.6	A_2B
7.7	ABC, B_2C
7.8	A_2BC
7.9	AB_2C
9.0	Unknown

B. Biased Library

A biased library was assembled to further investigate the templated synthesis of A_2B. The concentration of dithiol was 10 mM but the ratio of dithiols was 2:1 (A:B). This biased

library was screened against each methylation state of lysine (10 mM) and analyzed using UPLC/MS. After the library reached equilibrium, the templated results were compared to the control library (Figure 3.11, Table 3.5).

Figure 3.11: Results of peptide templated biased library after 22 days

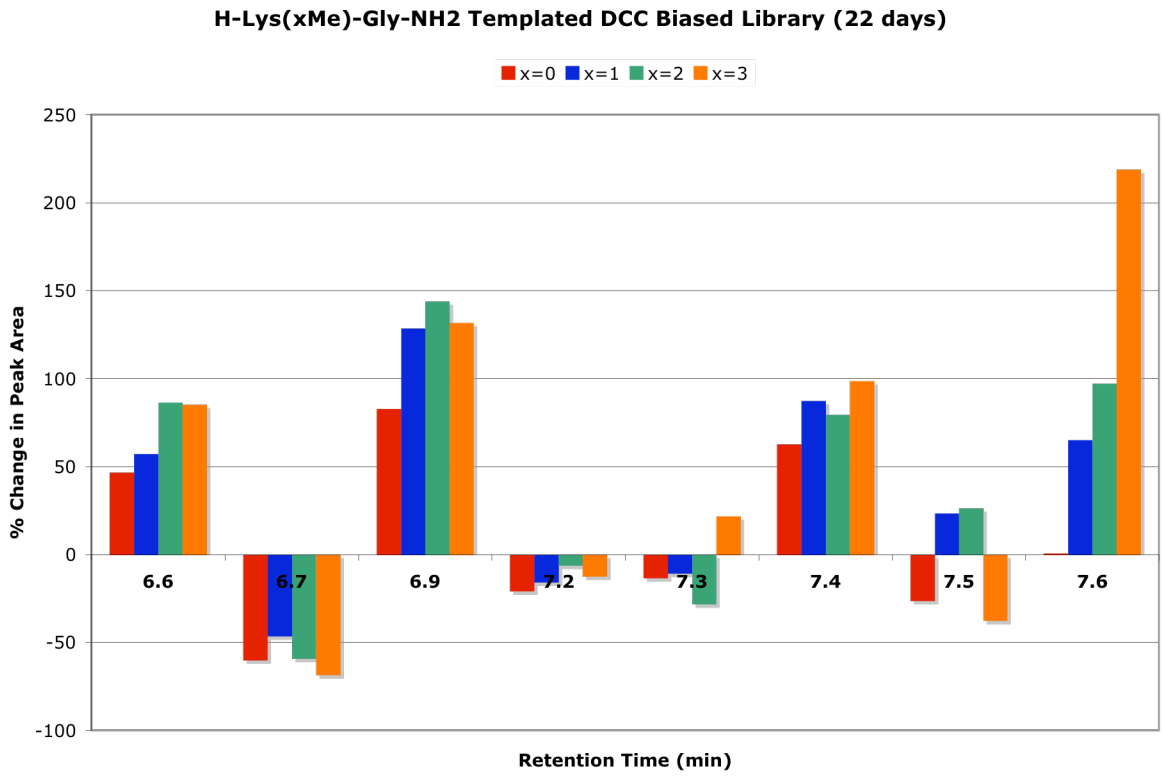

Table 3.5: Identity of peaks in Figure 3.11 determined by ESI-MS

Retention Time (min)	Structural Formula
6.6	B_3
6.7	A_2
6.9	B_4
7.2	A_2B_3, AB_2
7.3	AB_3, A_2B_3, A_2B*
7.4	A_2B, AB_3, AB_4
7.5	AB_4
7.6	A_2B

*A_2B is only found here for x=3 peptide

In the biased library, the trimethyl lysine templated library is different from the other peptides. The peak at 7.6 minutes, A_2B, is the most amplified. The other three peptides exhibit similar amplifications of the compounds at 6.9 and 7.4 minutes. The B_4 receptor (6.9 min) is the most amplified for the non-, mono-, and dimethyl lysines. Three products are observed for the peak at 7.4 minutes: A_2B, AB_3, and AB_4. Unfortunately poor separation prevents identification of the most amplified product of the three. The results observed for all the peptides are consistent with the results from the original library (Figure 3.10).

C. Summary and Discussion

Poor separation makes analysis of other peaks difficult. For the peaks at 7.2, 7.3, and 7.4 minutes more than one product was observed for each peak. One special case to note is the peak at 7.3 minutes. For the trimethyl lysine peptide library, this peak contained the other diastereomer of A_2B and showed no evidence for the A_2B_3 compound. As a result, the % change value went from negative to positive, indicating that the other diastereomer of A_2B may be enhanced.

Two diastereomers of A_2B are possible: racemic (rac) & meso (Figure 3.12) Tentatively, the amplified receptor has been identified as rac-A_2B, based on work by Otto and Sanders.[63] They report HPLC conditions to separate the diastereomers and this work is currently ongoing. After enough material has been collected, the isomer will be characterized and the binding of each dipeptide will be investigated. These initial results are particularly fascinating because diastereoselective amplification could be occurring. In addition, the diastereomer may selectively bind trimethyl lysine more strongly than the other methylation states.

[63] Corbett, P. T.; Sanders, J. K. M.; Otto, S. *Chem. Eur. J.* **2008**, *14*, 2153-2166.

Figure 3.12: Diastereomers of the A_2B receptor

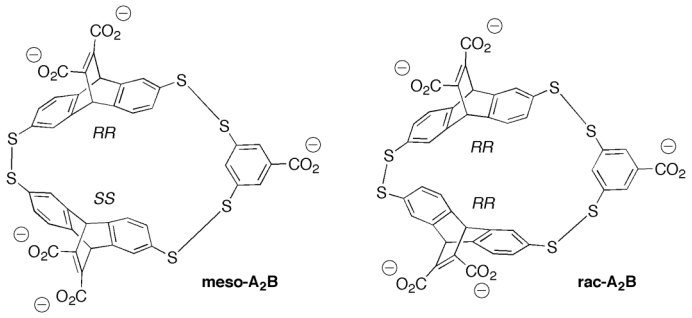

V. Conclusions

These two projects have established DCC as a viable tool to find receptors for structurally similar guests. The UPLC/MS analytical methodology has been established to analyze DCC libraries undergoing disulfide exchange. The analysis could be improved by optimizing the separation of the library mixture. The nucleotide and peptide templated DCC libraries amplified two different receptors. In the case of nucleotide templated libraries, an anionic receptor was amplified in the presence of an anionic guest. Typically this would be considered unfavorable but determining the structure of B_4 may provide insight into why this occurs. In the case of the peptide templated biased DCC libraries, enhancement of the A_2B receptor was strongest for the tri-methylated lysine residue. For the non-methylated lysine residue, no amplification was observed. This suggests that the A_2B receptor is selective for tri-methyl lysine. Current efforts are directed toward isolating both amplified receptors and quantifying binding.

VI. Experimental Procedures

A. Dithiol Building Blocks

Synthetic Procedures

Acetic acid 6-acetoxy-9,10-dihydro-anthracen-2-yl ester: To a flame dried flask containing anthraflavic acid (1.0 g, 4.2 mmol) in diglyme (30 mL) was added a 1M $NaBH_4$ solution (800 mg in 20 mL in diglyme, 21 mmol), followed by BF_3•THF (2 mL, 17 mmol, 4 eq). The resulting mixture was stirred at 60 °C for 90 minutes. After starting material was consumed, excess acetic anhydride (20 mL) and pyridine (0.7 mL, 8.4 mmol, 2 eq) were added. The reaction was warmed to 85 °C and stirred for 2 hours. The reaction was quenched by pouring over iced water and cooling to 5 °C overnight. The resulting product was filtered and rinsed with H_2O. The recovered solid was taken up in ethyl acetate, dried over $MgSO_4$, filtered, and concentrated under vacuum. 988 mg (79%) of **3a** was recovered as a beige solid and used in next step without further purification. ^{1}H NMR (400 MHz, $CDCl_3$): δ = 2.41 (s, 6H), 3.92 (d, 4H), 6.93 (dd, 2H), 7.05 (d, 2H), 7.29 ppm (d, 2H).

Acetic acid 6-acetoxy-anthracen-2-yl ester: To a flask containing **3a** (1.0 g, 3.4 mmol) in xylenes (35 mL) was added chloranil (1.0 g, 4.0 mmol, 1.2 eq) and refluxed for 5 hours. After cooling to ambient temperature, the reaction was filtered and the recovered solid washed with benzene. Recrystalization from acetic anhydride affords 430 mg (52%) of **3b** as a white solid. ^{1}H NMR (300 MHz, $CDCl_3$): δ = 2.41 (s, 6H), 7.25 (dd, 2H), 7.71 (d, 2H), 8.11 (d, 2H), 8.39 ppm (s, 2H).

Anthracene-2,6-diol: To a flask containing **3b** (300 mg, 1 mmol) in 95% ethanol (5 mL) was added 1 M NaOH (5 mL, 5 mmol, 5 eq) and heated at 90°C for 1 hour. Reaction was acidified with concentrated HCl and filtered to yield 210 mg (Quant.) of **4** as a green

solid. ^{1}H NMR (400 MHz, DMSO-d_6)[18]: δ = 7.06 (dd, 2H), 7.12 (d, 2H), 7.80 (d, 2H), 8.11 (s, 2H), 9.63 ppm (s, 2H).

Determination of Extinction Coefficient

In order to determine the ε value, a 10 mM stock solution was made in water and the pH was titrated to 8.5 using NaOH and HCl. The absorbance was recorded (315 nm) at different concentrations of ditihol. This acquired data was plotted and the best linear fit (y = mx + b) was acquired. When absorbance is below 1 a.u., its relationship to concentration can be expressed using the Beer-Lambert Law.

$$A = \varepsilon bc$$

This expression is nearly identical to the linear fit acquired for the data. As a comparison, absorbance is denoted as "y", concentration is denoted ax "x". For this experiment, the path length, b, was 1 cm. As a result, the ε value is the slope of the equation since b (y-intercept) is zero.

B. Peptide Synthesis and Purification

Peptides were synthesized by manual solid phase peptide synthesis using Fmoc (9-fluorenylmethoxycarbonyl) protected amino acids on a PAL-PEG-PS resin. The amino acids residues were activated for coupling with HBTU (O-benzotriazole-N,N,N',N',-tetramethyluronium hexafluorophosphate) and HOBt (N-hydroxybenzotriazole) in the presence of DIPEA (diisopropylethylamine) in solvent DMF (N,N-dimethylformamide). Deprotections were carried out in 2% DBU (1,8-diazabicyclo[5.4.0]undec-7-ene), 2% piperdine in DMF for approximately 10 minutes. Fmoc-Gly-OH coupled for 90 minutes followed by deprotection to generate free N-terminus. Coupling of lysine-based sidechain described below.

H-Lys-Gly-NH_2: Fmoc-Lys(Boc)-OH was coupled for 90 minutes followed by deprotection to generate free N-terminus.

H-Lys(Me)-Gly-NH_2: Fmoc-Lys(Me)(Boc)-OH was coupled overnight using same reagents as Fmoc-Gly-OH coupling. This was followed by deprotection to generate the free N-terminus.

H-Lys(2Me)-Gly-NH_2: Boc-Lys(2Me)-OH•HCl was coupled for 90 minutes using same reagents as Fmoc-Gly-OH coupling.

H-Lys(3Me)-Gly-NH_2: Boc-Lys(2Me)-OH•HCl was coupled for 90 minutes using same reagents as Fmoc-Gly-OH coupling. Lysine side chain methylated overnight using methyl iodide (11 eq) and 7-Methyl-1,5-7-triazabicyclo[4.4.0]dec-5-ene (0.5 eq) in DMF.

Cleavage of the peptide and removal of Boc groups from the resin was performed in 95:2.5:2.5 TFA (trifluoroacetic acid): TIPS (Triisopropylsilane): water for 2-3 hours. TFA was evaporated and ether was used to precipitate the cleavage products. The water soluble peptides were extracted with water and lyophilized. Peptides were purified by reversed phase HPLC, using a Waters Atlantis dC_{18} (5μm, 10 x 100mm) column and a mobile phase of 1% B for 5 minutes, where solvent A was 95:5 water:acetonitrile, 0.1 % TFA and solvent B was 95:5 acetonitrile:water, 0.1 % TFA. Once purified, the peptides were lyophilized to powder and the peptide identity was confirmed by ESI (Positive Ion mode) mass spectrometry.

C. Sample Preparation

Dithiol stock solutions were prepared in water with 2 equivalents of sodium hydroxide (relative to number of carboxylic acids) followed by sonication. The pH was adjusted to 8.5 using NaOH and HCl. The concentration of the stock solution was determined using the absorbance at 315 nm ($\varepsilon_{315,\text{ Dithiol A}} = \varepsilon_{315,\text{ Dithiol B}} = 1700\ M^{-1}$; $\varepsilon_{315,\text{ Dithiol C}} = 80\ M^{-1}$).

Nucleotides were added directly to the library mixture as their sodium salts. Peptide samples were prepared in water and their concentrations were determined by dissolving a known mass in a known volume of water.

D. UPLC Analysis

UPLC/UV analyses were performed using an Acquity UPLC system fitted with a binary pump, a plate autosampler, a thermostated column compartment, sample organizer, and an Acquity photodiode array detector controlled by Masslynx v4.1 software (Waters Corporation, USA). Chromatography was carried out using an Acquity UPLC BEH C18 column (2.1 mm x 100mm; particle size 1.7μm; Waters). The mobile phase was composed of a mixture of 5 mM NH_4OAc in water (solvent A) and 5 mM NH_4OAc in acetonitrile (solvent B). In general, the gradient was delivered at 0.4 mL/min as follows: 0 min, 1% B; 10 min, 60% B. For analysis of nucleotide biased libraries, the gradient was delivered as follows: 0 min, 1% B, 0.4 mL/min; 6 min, 35.4% B, 0.4 mL/min; 10 min, 99% B, 0.5 mL/min. The column was maintained at 30 °C. The diode array detector was set at 315 or 320 nm. Two and a half microliters of sample were injected onto the column by an auto liquid sampler. Following UV detection, the flow was directed to the mass spectrometer without a split. Figures 3.13 through 3.29 are sample data acquired from UPLC.

Figure 3.13: UPLC chromatogram for DCC library containing GMP (10 mM) and Dithiols A, B, C (3.3 mM each) at 30 °C. Bottom chromatogram is the control and the top chromatogram is the GMP templated library. Absorbance recorded at 320 nm.

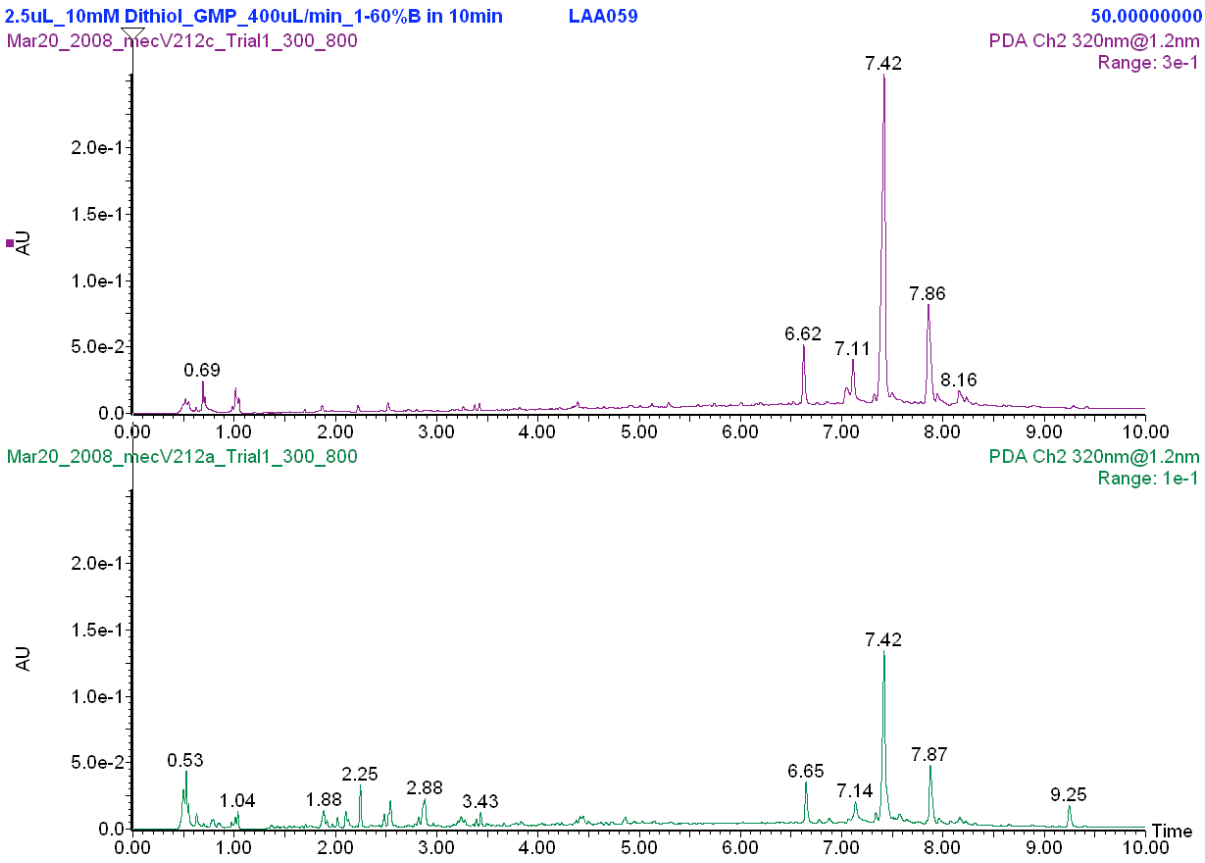

Figure 3.14: UPLC chromatogram for DCC library containing GTP (10 mM) and Dithiols A, B, C (3.3 mM each) at 30 °C. Bottom chromatogram is the control and the top chromatogram is the GTP templated library. Absorbance recorded at 320 nm.

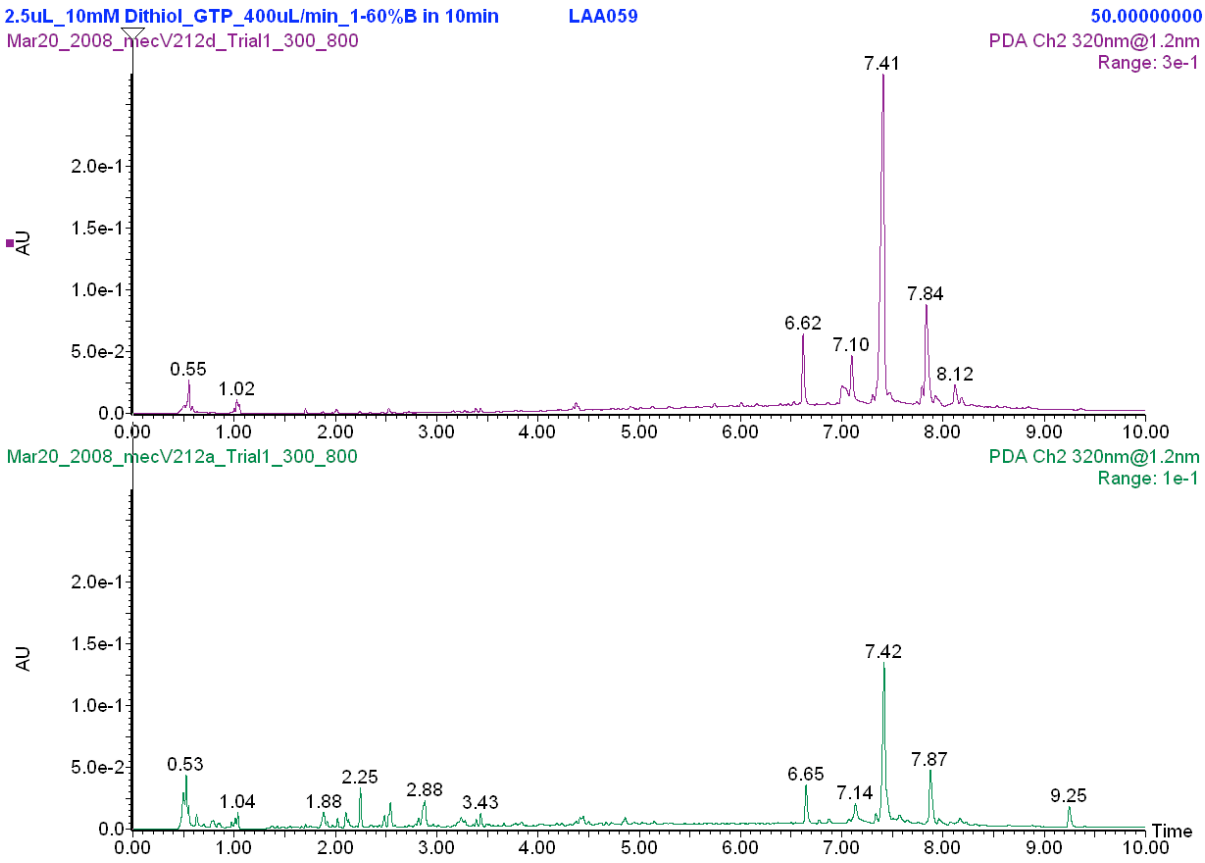

Figure 3.15: UPLC chromatogram for DCC library containing ATP (10 mM) and Dithiols A, B, C (3.3 mM each) at 30 °C. Bottom chromatogram is the control and the top chromatogram is the ATP templated library. Absorbance recorded at 320 nm.

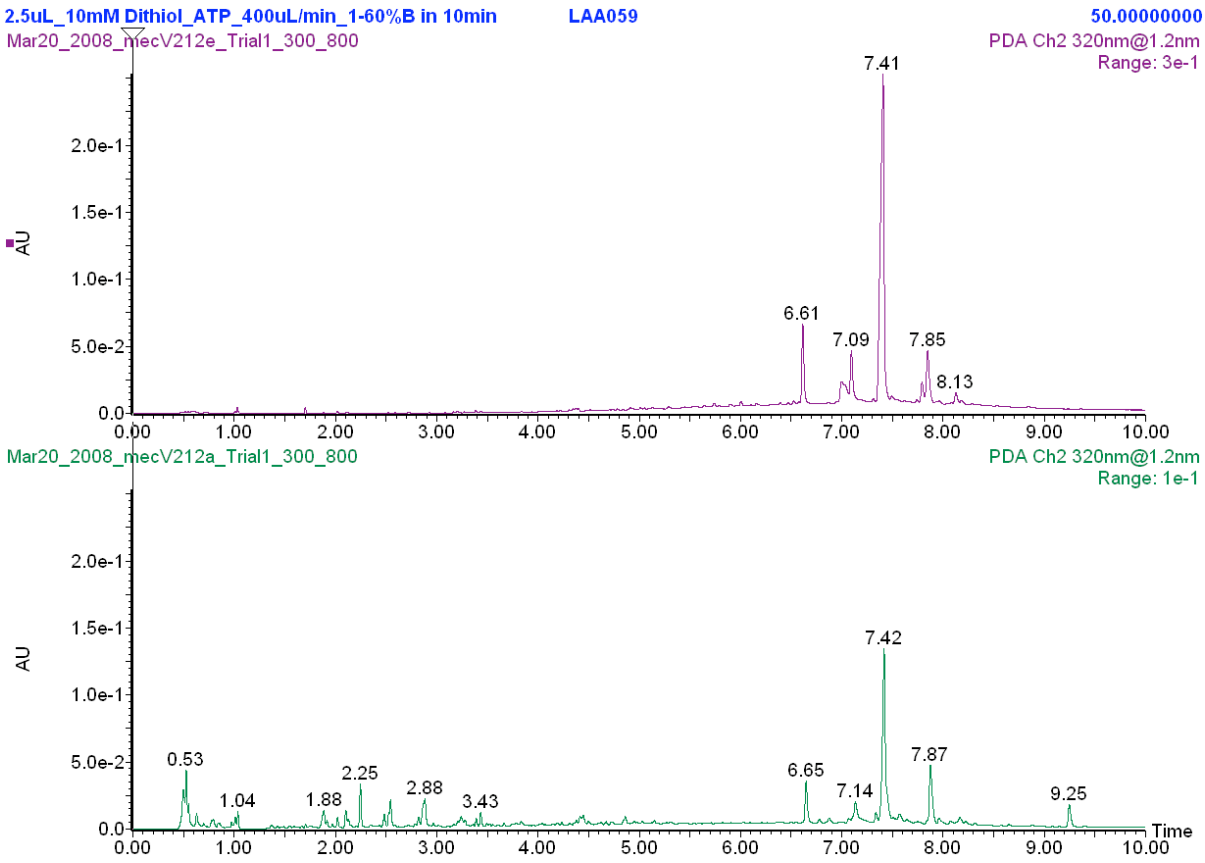

Figure 3.16: UPLC chromatogram for DCC library containing CMP (10 mM) and Dithiols A, B, C (3.3 mM each) at 30 °C. Bottom chromatogram is the control and the top chromatogram is the CMP templated library. Absorbance recorded at 320 nm.

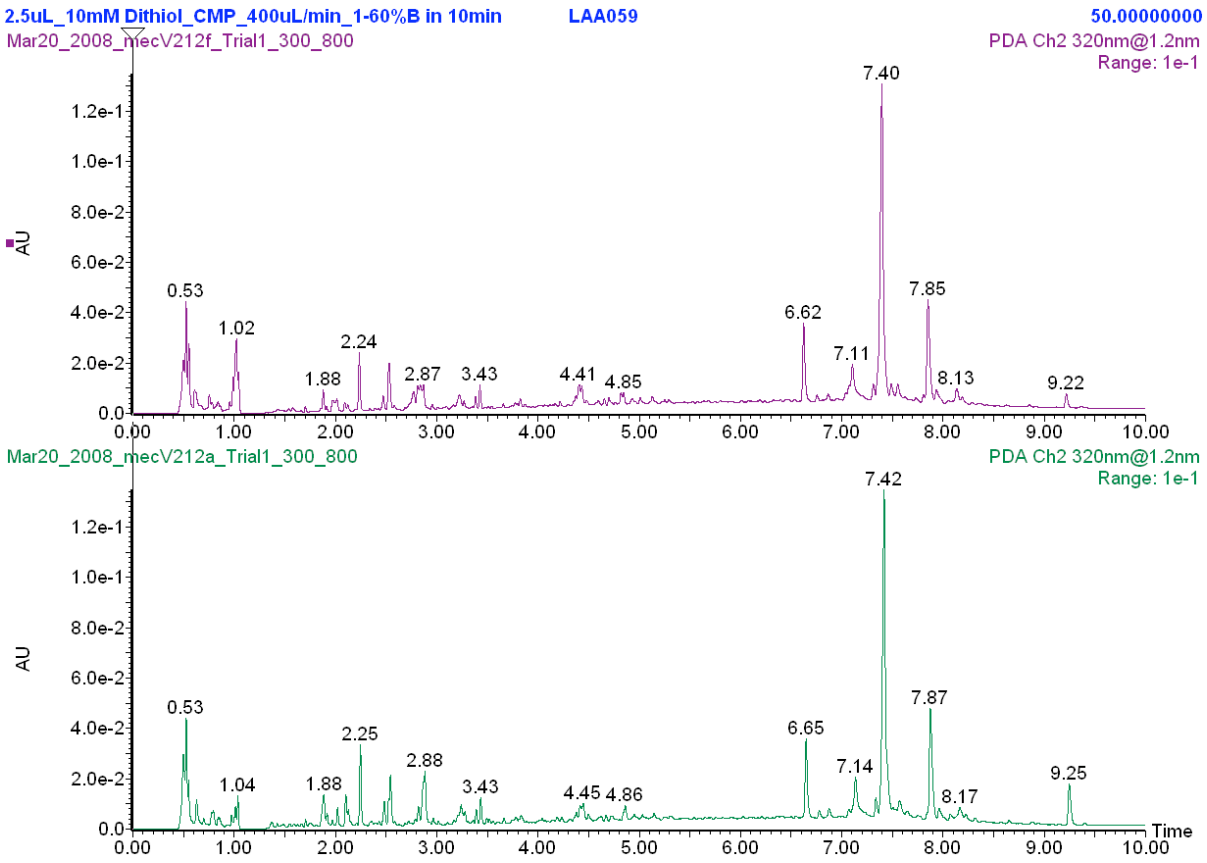

Figure 3.17: UPLC chromatogram for DCC library containing CTP (10 mM) and Dithiols A, B, C (3.3 mM each) at 30 °C. Bottom chromatogram is the control and the top chromatogram is the CTP templated library. Absorbance recorded at 320 nm.

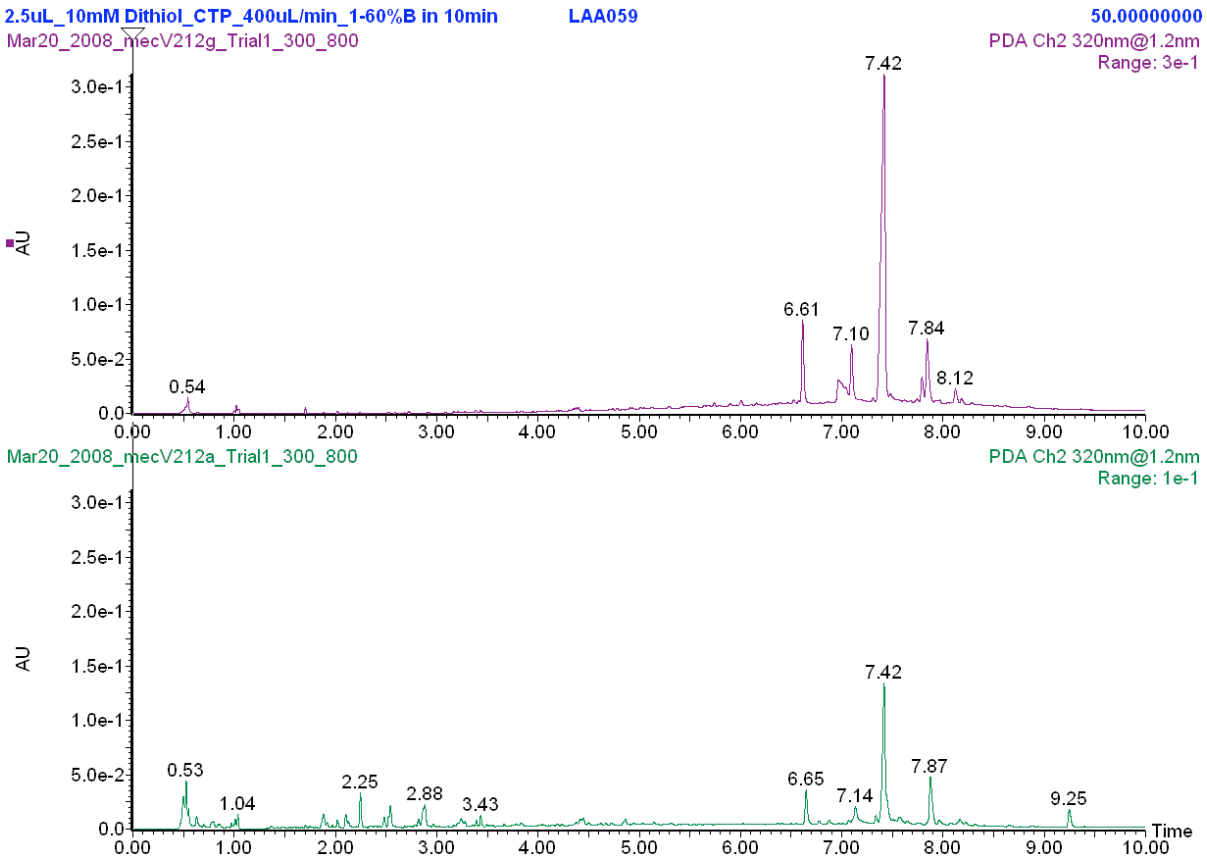

Figure 3.18: UPLC chromatogram for biased DCC library containing ATP (10 mM) and Dithiol B (10 mM) at 30 °C. Bottom chromatogram is the control and the top chromatogram is the ATP templated library. Absorbance recorded at 315 nm.

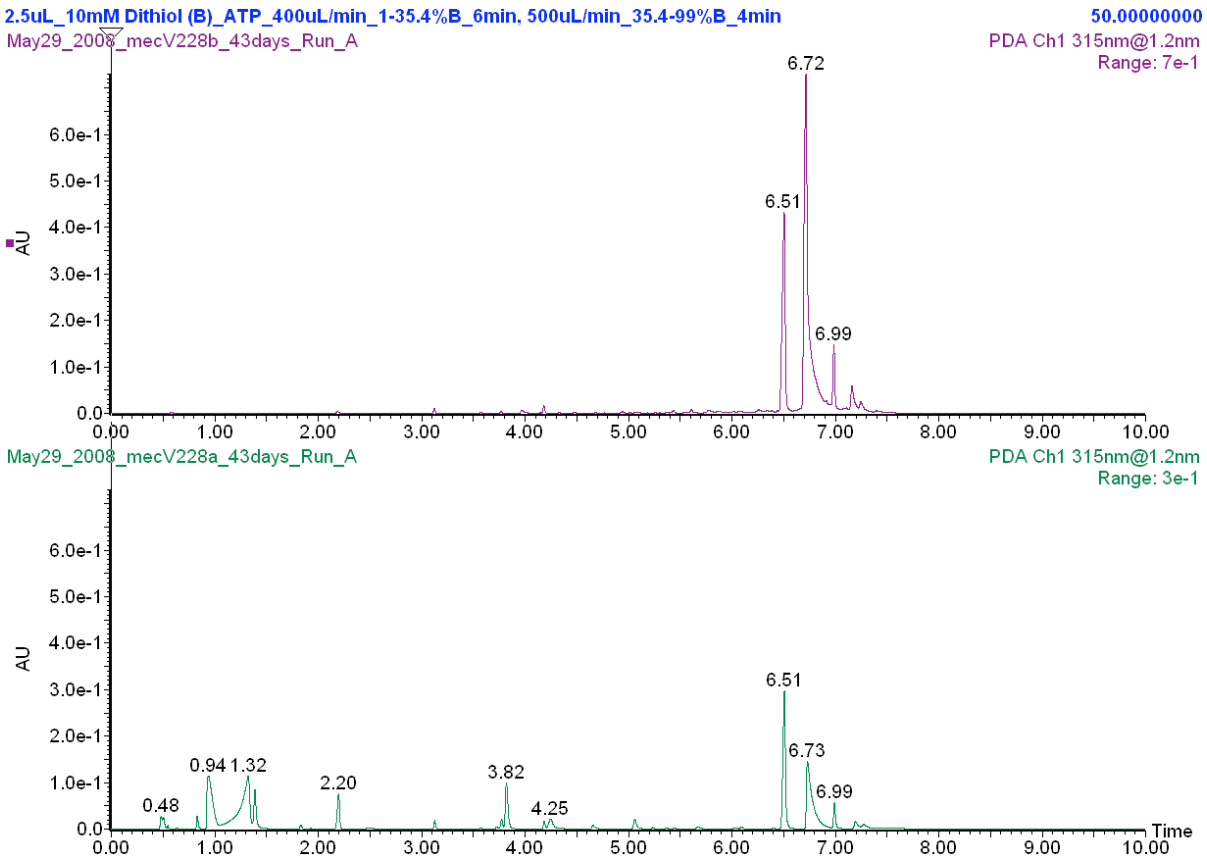

Figure 3.19: UPLC chromatogram for biased DCC library containing GTP (10 mM) and Dithiol B (10 mM) at 30 °C. Bottom chromatogram is the control and the top chromatogram is the GTP templated library. Absorbance recorded at 315 nm.

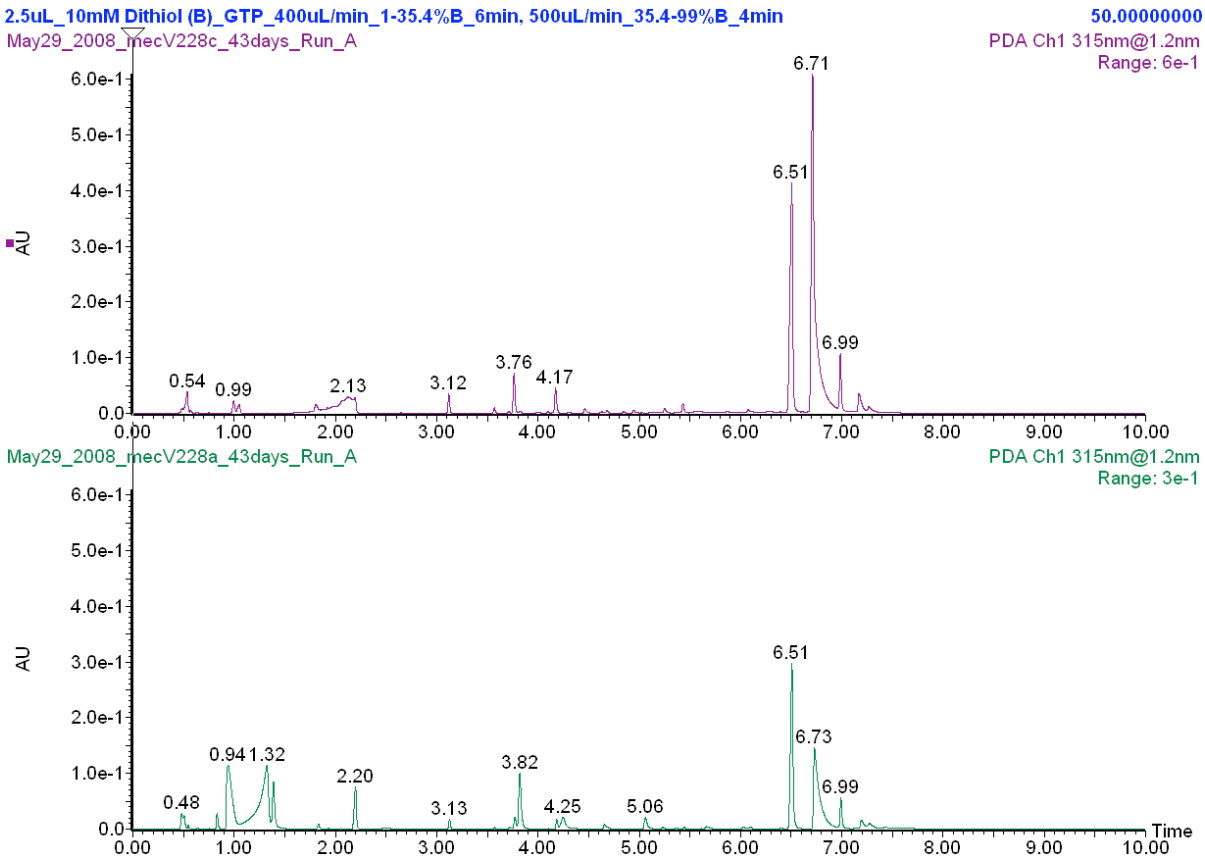

Figure 3.20: UPLC chromatogram for biased DCC library containing GMP (10 mM) and Dithiol B (10 mM) at 30 °C. Bottom chromatogram is the control and the top chromatogram is the GMP templated library. Absorbance recorded at 315 nm.

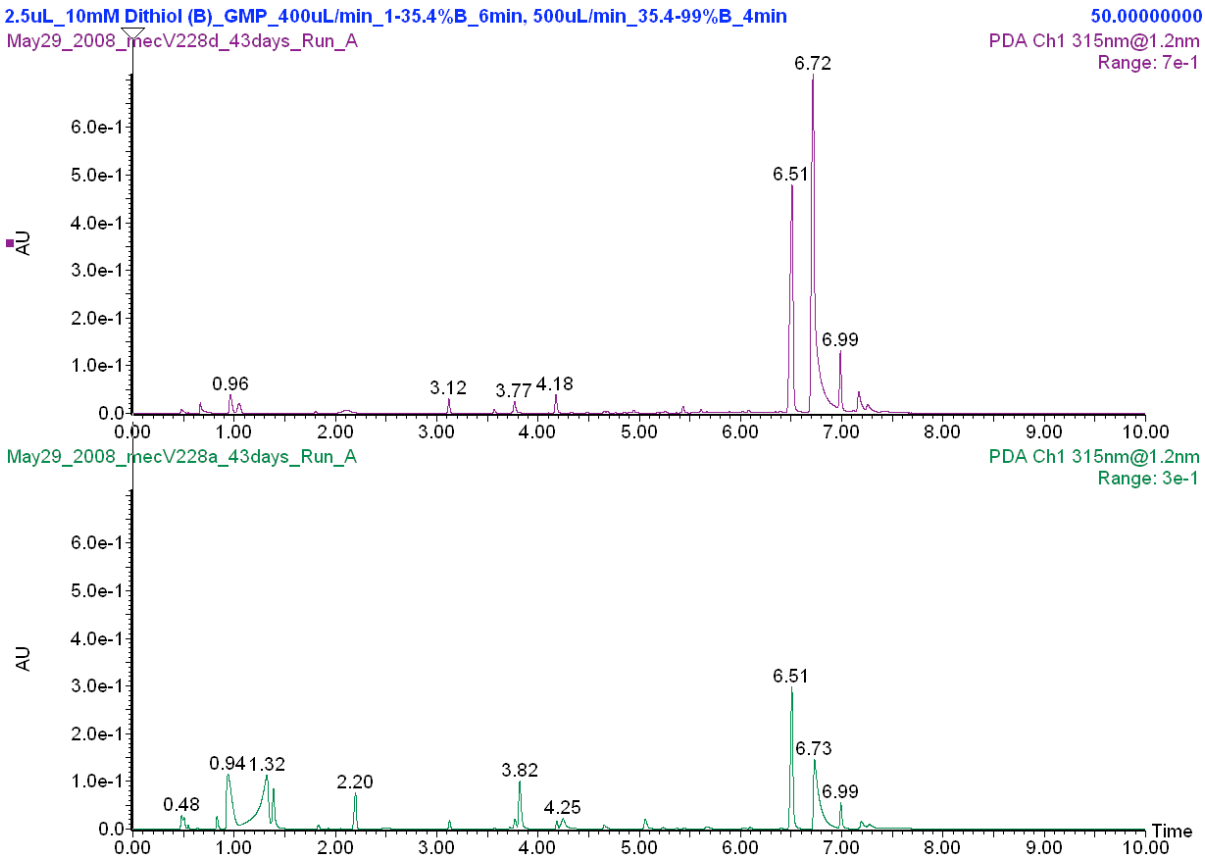

Figure 3.21: UPLC chromatogram for biased DCC library containing CMP (10 mM) and Dithiols A, A, B, C (3.3 mM each) at 30 °C. Bottom chromatogram is the control and the top chromatogram is the CMP templated library. Absorbance recorded at 315 nm.

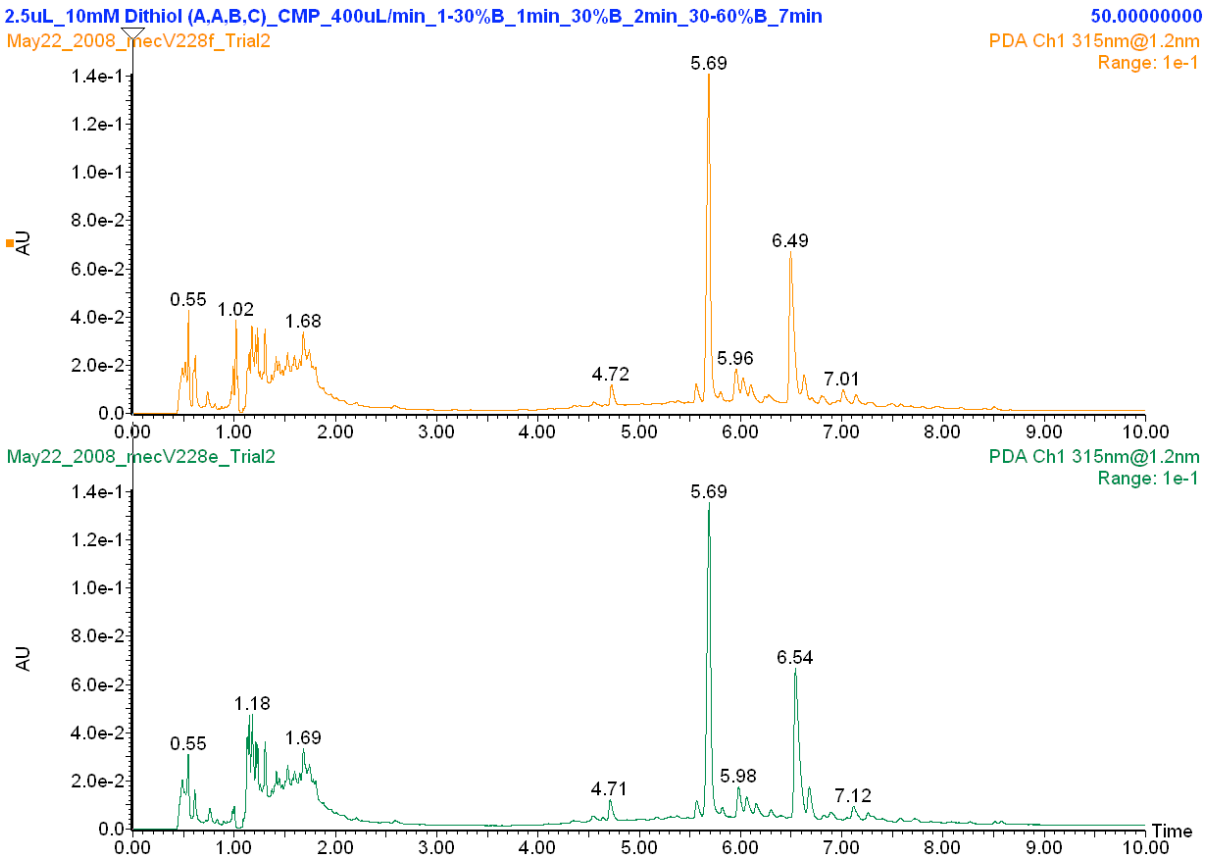

Figure 3.22: UPLC chromatogram for DCC library containing H-Lys-Gly-NH_2 (10 mM) and Dithiols A, B, C (3.3 mM each) at 30 °C. Bottom chromatogram is the control and the top chromatogram is the H-Lys-Gly-NH_2 templated library. Absorbance recorded at 315 nm.

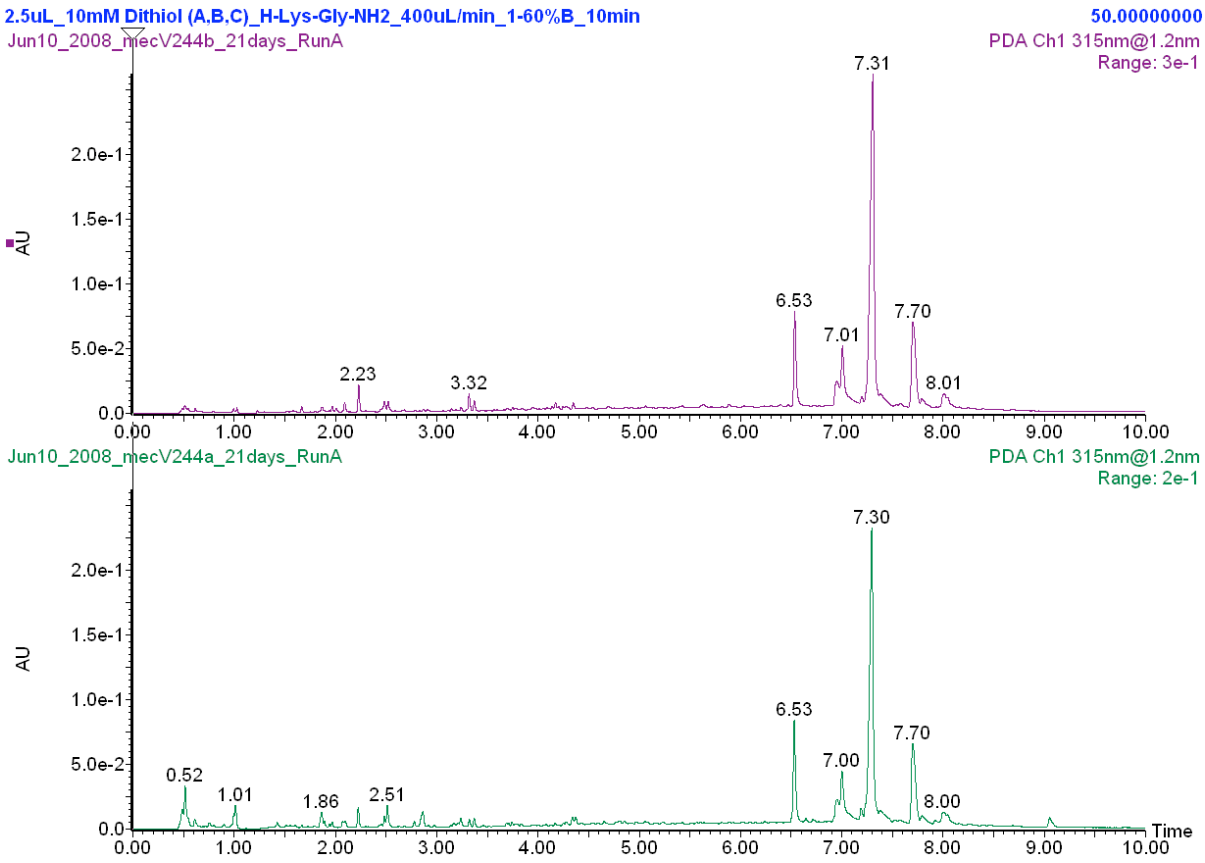

Figure 3.23: UPLC chromatogram for DCC library containing H-Lys(Me)-Gly-NH_2 (10 mM) and Dithiols A, B, C (3.3 mM each) at 30 °C. Bottom chromatogram is the control and the top chromatogram is the H-Lys(Me)-Gly-NH_2 templated library. Absorbance recorded at 315 nm.

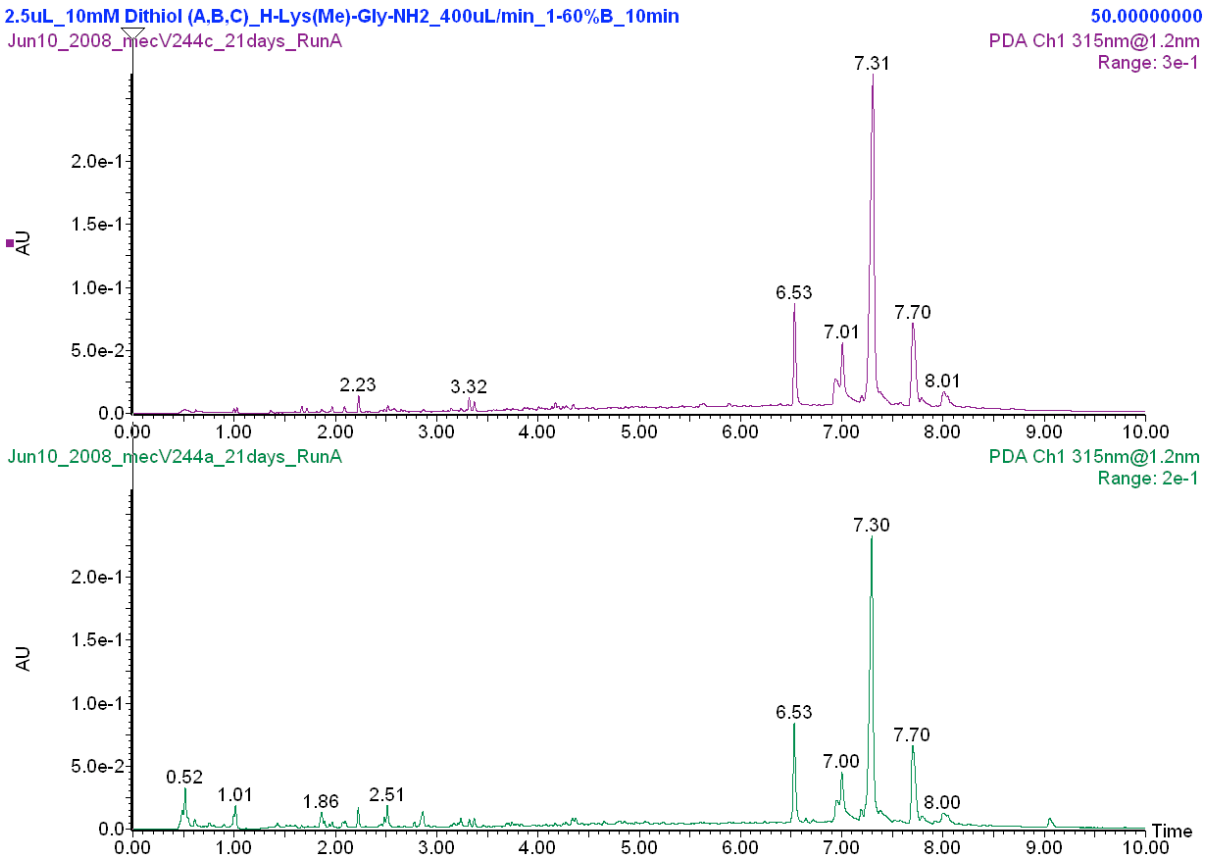

Figure 3.24: UPLC chromatogram for DCC library containing H-Lys(2Me)-Gly-NH_2 (10 mM) and Dithiols A, B, C (3.3 mM each) at 30 °C. Bottom chromatogram is the control and the top chromatogram is the H-Lys(2Me)-Gly-NH_2 templated library. Absorbance recorded at 315 nm.

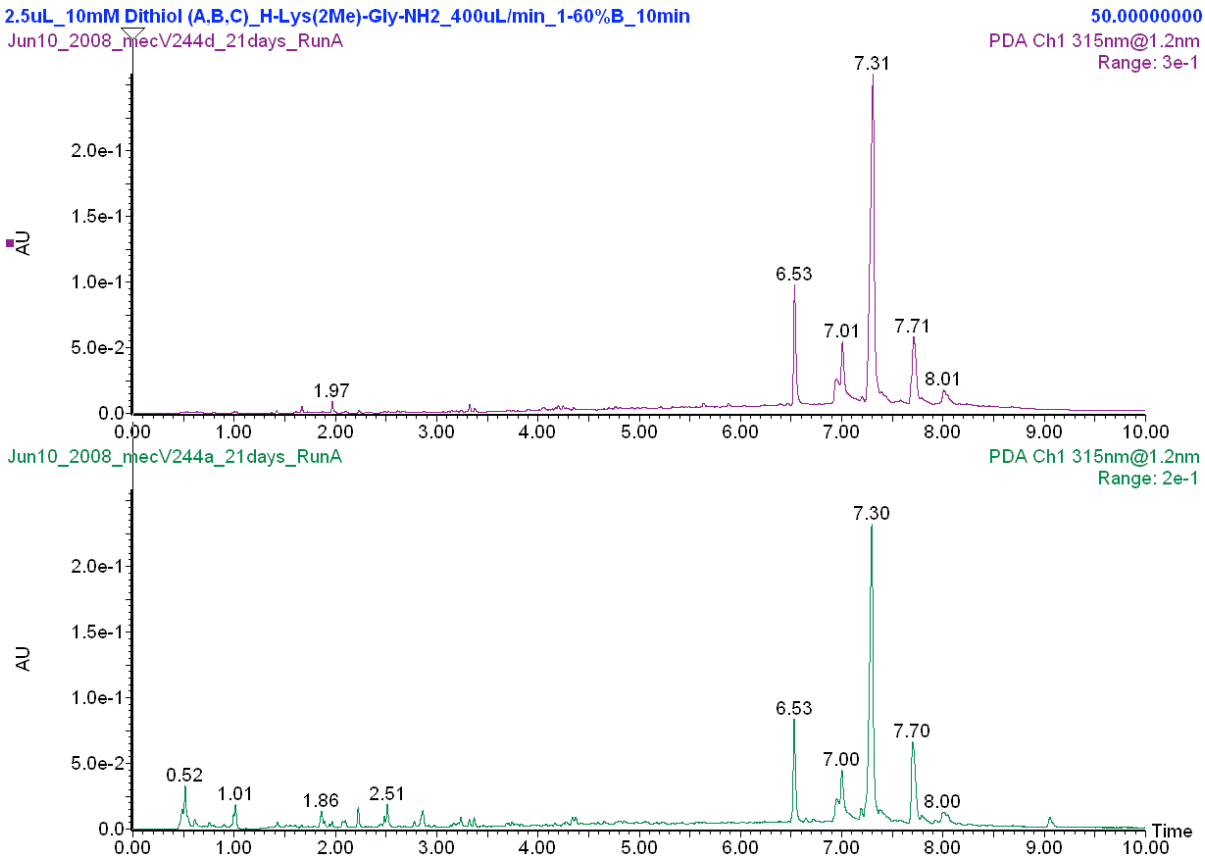

Figure 3.25: UPLC chromatogram for DCC library containing H-Lys(3Me)-Gly-NH_2 (10 mM) and Dithiols A, B, C (3.3 mM each) at 30 °C. Bottom chromatogram is the control and the top chromatogram is the H-Lys(3Me)-Gly-NH_2 templated library. Absorbance recorded at 315 nm.

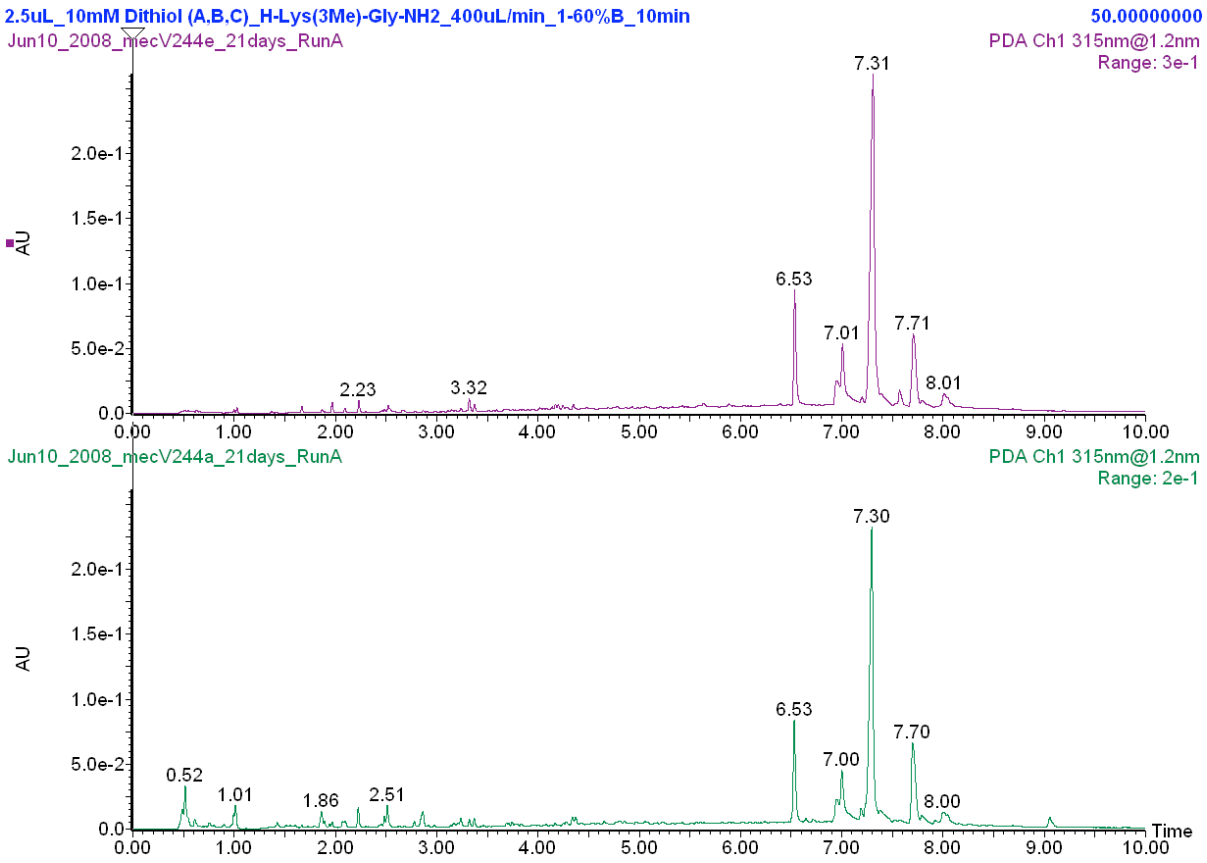

Figure 3.26: UPLC chromatogram for biased DCC library containing H-Lys-Gly-NH_2 (10 mM) and Dithiols A, A, B (3.3 mM each) at 30 °C. Bottom chromatogram is the control and the top chromatogram is the H-Lys-Gly-NH_2 templated library. Absorbance recorded at 315 nm.

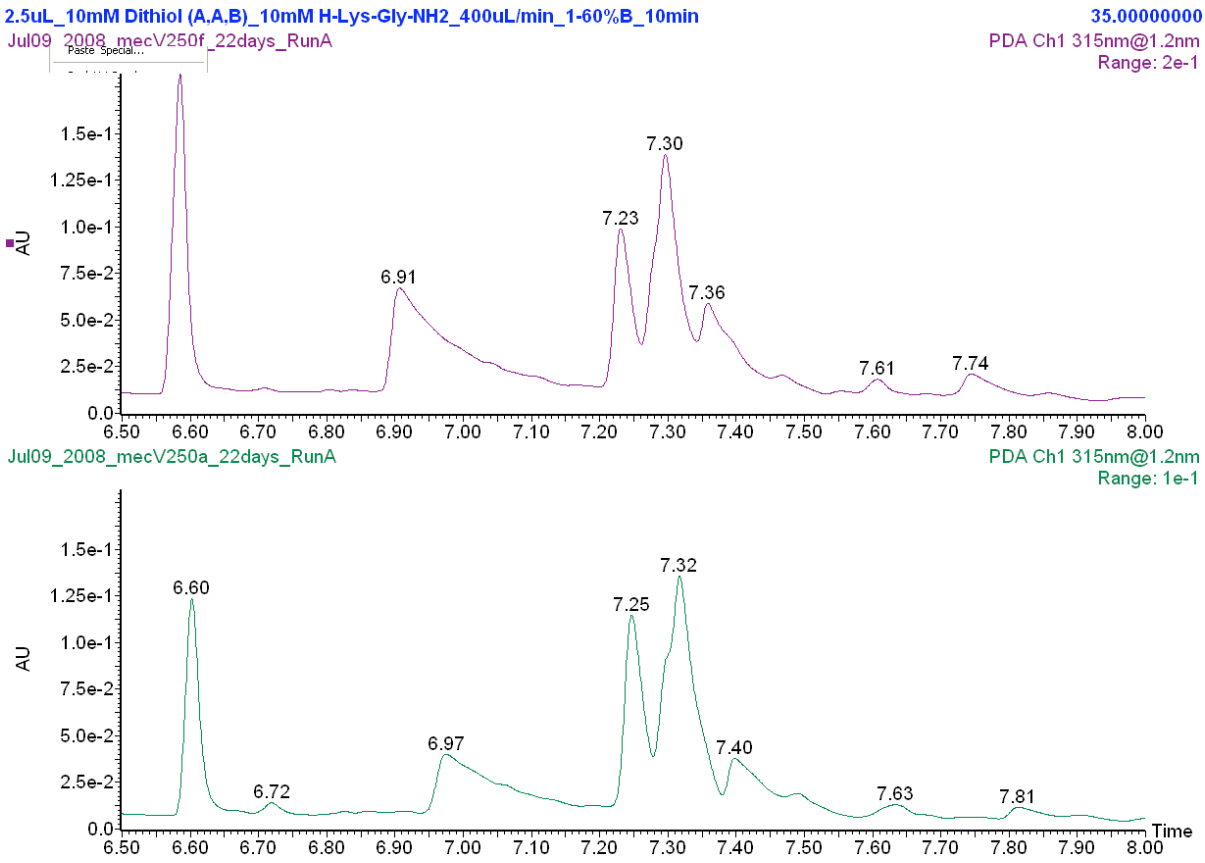

Figure 3.27: UPLC chromatogram for biased DCC library containing H-Lys(Me)-Gly-NH_2 (10 mM) and Dithiols A, A, B (3.3 mM each) at 30 °C. Bottom chromatogram is the control and the top chromatogram is the H-Lys(Me)-Gly-NH_2 templated library. Absorbance recorded at 315 nm.

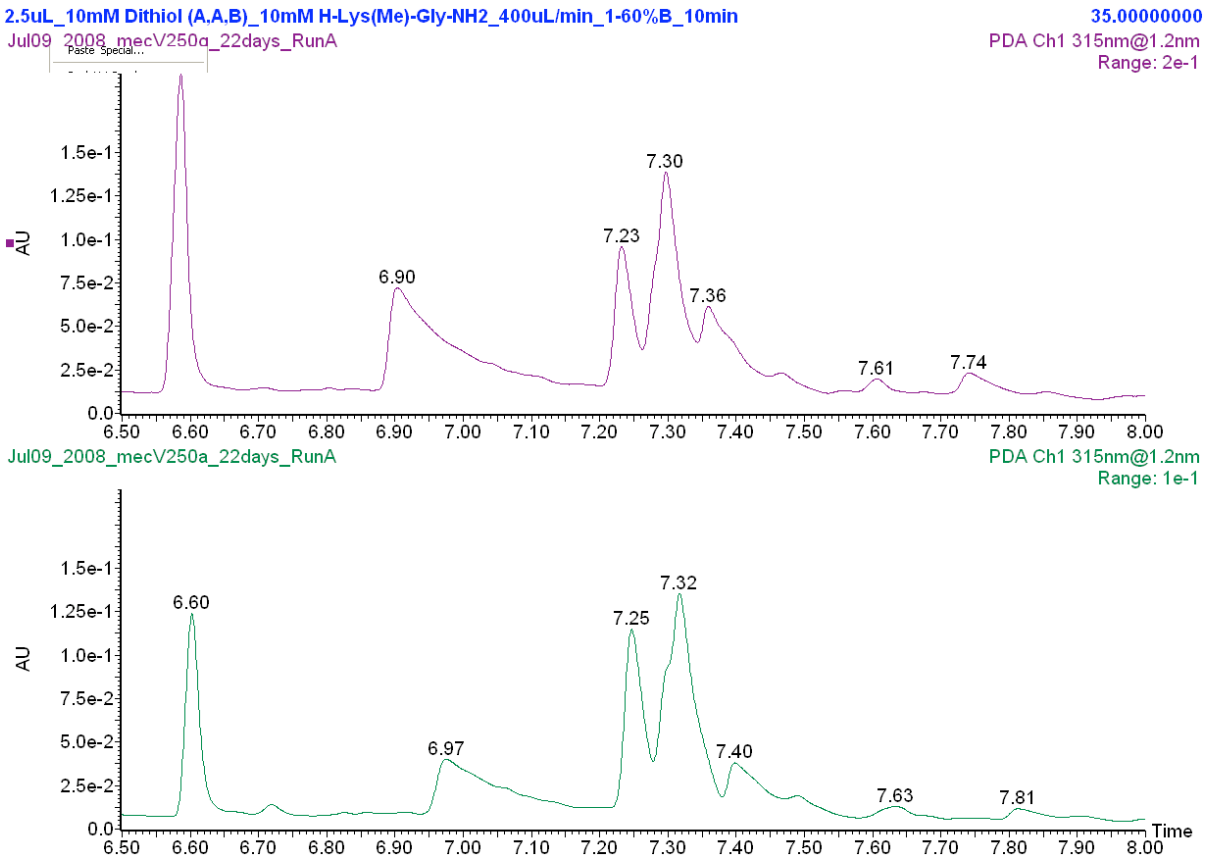

Figure 3.28: UPLC chromatogram for biased DCC library containing H-Lys(2Me)-Gly-NH_2 (10 mM) and Dithiols A, A, B (3.3 mM each) at 30 °C. Bottom chromatogram is the control and the top chromatogram is the H-Lys(2Me)-Gly-NH_2 templated library. Absorbance recorded at 315 nm.

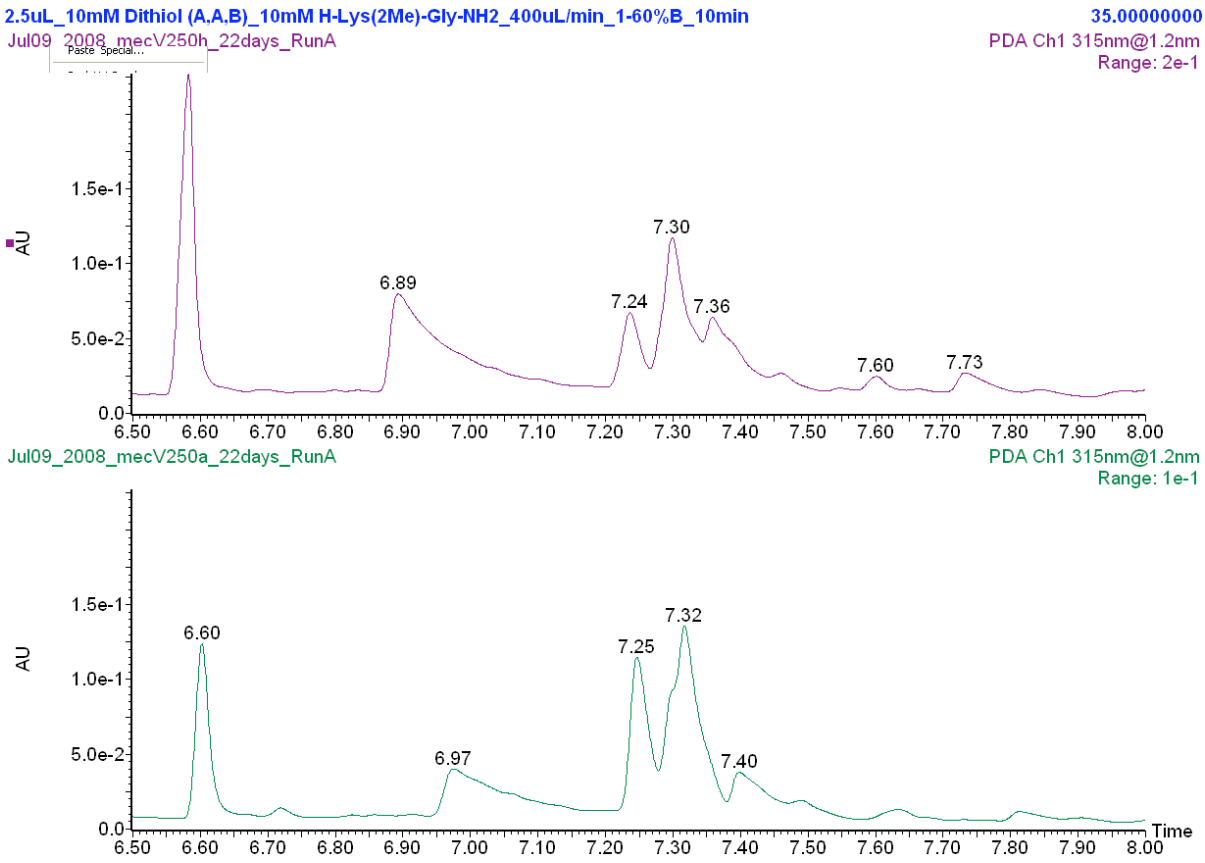

Figure 3.29: UPLC chromatogram for biased DCC library containing H-Lys(3Me)-Gly-NH_2 (10 mM) and Dithiols A, A, B (3.3 mM each) at 30 °C. Bottom chromatogram is the control and the top chromatogram is the H-Lys(3Me)-Gly-NH_2 templated library. Absorbance recorded at 315 nm.

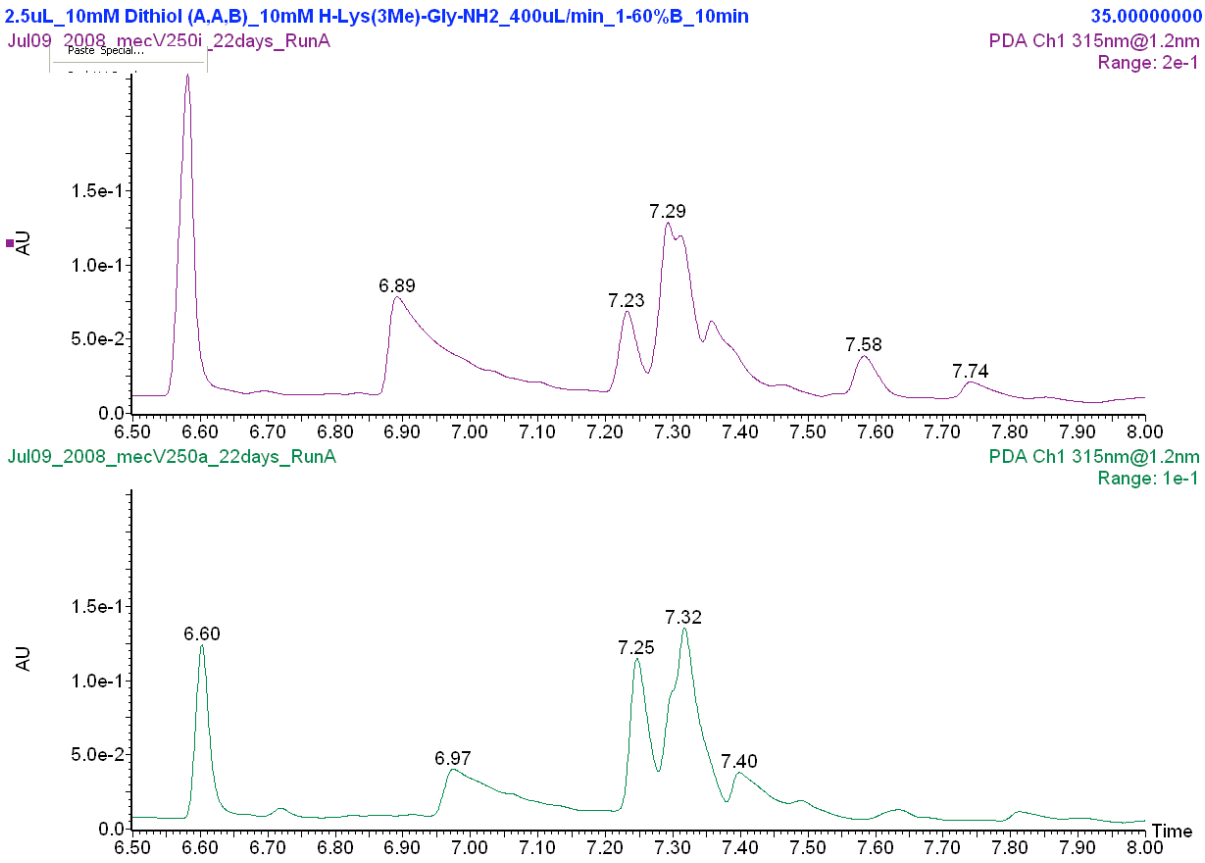

E. MS Analysis

Mass spectrometry was performed on a Micromass ZQ single quadrupole (Waters) using a standard electrospray ionization (ESI) source operated in negative ion mode. The desolvation gas rate was set to 700 L/hr at a temperature of 350 °C, the cone gas rate was set to 0 L/hr and the source temperature at 150 °C. The cone and desolvation gas flows were obtained from an in-house nitrogen source. The capillary voltage and the cone voltage were set at 700 V and 35 V, respectively. The extractor voltage and RF lens were set at 2 V and 0 V, respectively. Scan times were 0.8 s with a delay of 0.02 s. Data was collected in continuum mode from both *m/z* 300 to *m/z* 800 and *m/z* 800 to *m/z* 1300.

F. HPLC Purification

Disulfide receptors were purified by reversed phase HPLC, using a Waters Atlantis dC_{18} (5μm, 10 x 100mm) column and a gradient of 1-30% B in 1 minute, 30% B for 5 minutes and 30-70% B in 24 minutes. Solvent A was 5 mM NH_4OAc in water and solvent B was 5 mM NH_4OAc in acetonitrile. Once purified, the compounds were lyophilized to powder.

REFERENCES

Altmann, M.; Edery, I.; Trachsel, H.; Sonenberg, N. *J. Biol. Chem.* **1988**, *263*, 17229-17232.

Ball, L. J.; Jarchau, T.; Oschkinat, H.; Walter, U. *FEBS Lett.* **2002**, *513*, 45-52.

Ball, L. J.; Kühne, R.; Schneider-Mergener, J.; Oschkinat, H. *Angew. Chem. Int. Ed.* **2005**, *44*, 2852-2869.

Bhattacharyya, R.; Chakrabarti, P. *J. Mol. Biol.* **2003**, *331*, 925-940.

Bilgicer, B.; Xing, X.; Kumar, K. *J. Am. Chem. Soc.* **2001**, *123*, 11815-11816.

Boldt, P. *Chem. Ber.* **1967**, *100*, 1270-1280.

Brady, P. A.; Bonar-Law, R. P.; Rowan, S. J.; Suckling, C. J.; Sanders, J. K. M. *Chem. Commun.* **1996**, 319-320.

Butterfield, S. M.; Goodman, C. M.; Rotello, V. M.; Waters, M. L. *Angew. Chem. Int. Ed.* **2004**, *43*, 724-727.

Butterfield, S. M. Sweeney, M. M.; Waters, M. L. *J. Org. Chem.* **2005**, *70*, 1105-1114.

Butterfield, S. M.; Waters, M. L. *J. Am. Chem. Soc.* **2003**, *125*, 9580-9581.

Campoy, A. V.; Freire, E. *Biophys. Chemist.* **2005**, *115*, 115-124.

Cochran, A. G.; Skelton, N. J.; Starovasnik, M. A. *Proc. Nat. Acad. Sci., U.S.A.* **2001**, *98*, 5578-5583.

Corbett, P. T.; Leclaire, J.; Vial, L.; West, K. R.; Wietor, J.; Sanders, J. K. M.; Otto, S. *Chem. Rev.* **2006**, *106*, 3652-3711.

Corbett, P. T.; Sanders, J. K. M.; Otto, S. *Chem. Eur. J.* **2008**, *14*, 2153-2166.

Corbett, P. T.; Tong, L. H.; Sanders, J. K. M.; Otto, S. *J. Am. Chem. Soc.* **2005**, *127*, 8902-8903.

Cowan, P. M.; McGavin, S. *Nature* **1955**, *176*, 501-503.

CRC Handbook of Biochemistry and Molecular Biology, 3rd Edition, vol. 1: Nucleic Acids, CRC Press, **1975**.

Crowley, P. B.; Golovin, A. *Proteins* **2005**, *59*, 231-239.

Davies, J. E. D.; Ripmeeester, J. A. *Comprehensive Supramolecular Chemistry*; Vol. 8, Physical Methods in Supramolecular Chemisry; Pergamon Press: Oxford, UK, **1996**; p. 434.

Dougherty, D. A. *Science* **1996**, *271*, 163-168.

Edelhoch, H. *Biochemistry* **1967**, *6*, 1948-1954.

Field, L.; Engelhardt, P. R. *J. Org. Chem.* **1970**, *35*, 3647-3655.

Fisher, H. F.; Singh, N. *Methods Enzymol.* **1995**, *259*, 194-221.

Furuichi, Y.; LaFiandra, A.; Shatkin, A. J. *Nature* **1977**, *266*, 235-239.

Gallivan, J. P.; Dougherty, D. A. *Proc. Natl. Acad. Sci. USA* **1999**, *96*, 9459-9464.

Gingras, A. C.; Raught, B.; Sonenberg, N. *Annu. Rev. Biochem.* **1999**, *68*, 913-963.

Green, M. R.; Maniatis, T.; Melton, D. A. *Cell* **1983**, *32*, 681-694.

Hershey, J. W.; Miyamoto, S. *Translational Control*, Cold Spring Harbor Press, Cold Spring Harbor, NY, **2000**, pp. 637-654.

Hughes, R. M.; Wiggins, K. R.; Khorasanizadeh, S.; Waters, M. L. *Proc. Nat. Acad. Sci. U.S.A.* **2007**, *104*, 11184-11188.

Izaurralde, E.; Lewis, J.; Gamberi, C.; Jarmolowski, A.; McGuigan, C.; Mattaj, I. W. *Nature* **1995**, *376*, 709-712.

Izaurralde, E.; Mattaj, I. W. *Cell* **1995**, *81*, 153-159.

Jelesarov, I.; Bosshard, H. R. *J. Mol. Recognit.* **1999**, *12*, 3-18.

Kornberg, R. D.; Lorch, Y. *Cell* **1999**, *98*, 285-294.

Ladbury, J. E.; Chowdhry, B. Z. *Chem. Biol.* **1996**, *3*, 791-801.

Lewis, J. D.; Izaurralde, E.; Jarmolowski, A.; McGuigan, C.; Mattaj, I. W. *Genes Dev.* **1996**, *10*, 1683-1698.

Li, S. S. C. *Biochem. J.* **2005**, *390*, 641-653.

Lim, W. A.; Fox, R. O.; Richards, F. M. *Protein Sci.* **1994**, *3*, 1261-1266.

Ma, J. C.; Dougherty, D. A. *Chem. Rev.* **1997**, *97*, 1303-1324.

Marcotrigiano, J.; Gingras, A.-C.; Sonenberg, N.; Burley, S. K. *Cell* **1997**, *89*, 951-961.

Markovac, A.; LaMontague, M. P. *J. Med. Chem.* **1980**, *23*, 1198-1201.

Martin, C. Zhang, Y. *Nat. Rev. Mol. Cell Biol.* **2005**, *6*, 838-849.

Matsuo, H.; Li, H.; McGuire, A. M.; Fletcher, C. M.; Gingras, A.-C.; Sonenberg, N.; Wagner, G. *Nature Struct. Biol.* **1997**, *4*, 350-354.

Merrick, W. C.; Hershey, J. W. B. *In Translational Control*, Cold Spring Harbor Press, Cold Spring Harbor, NY, **1996**, pp. 31-69.

Morino, S.; Hazama, H.; Ozaki, M.; Teraoka, Y.; Shibata, S.; Doi, M.; Ueda, H.; Ishida, T.; Uesugi, S. *Eur. J. Biochem.* **1996**, *239*, 597-601.

Naghibi, H.; Tamura, A.; Sturtevant, J. M. *Proc. Natl. Acad. Sci. USA* **1995**, *92*, 5597-5599.

Niedzwiecka, A. *Personal Communication* **2005**.

Niedzwiecka, A.; Darzynkiewicz, E.; Stolarski, R. *Biochemistry* **2004**, *43*, 13305-13317.

Nishio, M. *Cryst. Eng. Commun.* **2004**, *6*, 130-158.

Nishio, M.; Umezawa, Y.; Hirota, M; Takeuchi, Y. *Tetrahedron* **1995**, *51*, 8665-8701.

Oakley, M. G.; Kim, P. S. *Biochemistry* **1998**, *37*, 12603-12610.

Otto, S.; Furlan, R. L. E.; Sanders, J. K. M. Curr. Opin. *Chem. Biol.* **2002**, *6*, 321-327.

Otto, S.; Furlan, R. L. E.; Sanders, J. K. M. *Drug Discov. Today* **2002**, *7*, 117-125.

Otto, S.; Furlan, R. L. E.; Sanders, J. K. M. *J. Am. Chem. Soc.* **2000**, *122*, 12063-12064.

Otto, S.; Furlan, R. L. E.; Sanders, J. K. M. *Science* **2002**, *297*, 590-593.

Parker, C. A. *Photoluminescence of Solutions*, Elsevier Publishing Company, Amsterdam, **1968**, p. 220-234.

Petti, M. A.; Shepodd, T. J.; Barrans, R. E.; Dougherty, D. A. *J. Am. Chem. Soc.* **1988**, *110*, 6825-6840.

Quiocho, F. A.; Hu, G.; Gershon, P. D. *Curr. Opin. Struct. Biol.* **2000**, *10*, 78-86.

Raught, B.; Gingras, A.-C. *Int. J. Biochem. Cell Biol.* **1999**, *31*, 43-57.

Schärer, O. D. *Angew. Chem. Int. Ed.* **2003**, *42*, 2946-2974.

Shuman, S. *Prog. Nucl. Acid Res. Mol. Biol.* **1995**, *50*, 101-129.

Staab, H. A.; Kirrstetter, G. H. *Liebigs. Ann. Chem.* **1979**, 886-898.

Svitkin, Y. V.; Ovchinnikov, L. P.; Dreyfuss, G.; Sonenberg, N. *EMBO J.* **1996**, *15*, 7147-7155.

Taverna, S. D.; Li, H.; Ruthenburg, A. J.; Allis, C. D.; Patel, D. J. *Nat. Struct. Mol. Biol.* **2007**, *14*, 1025-1040.

Thomas, K. M.; Naduthambi, D.; Zondlo, N. J. *J. Am. Chem. Soc.* **2006**, *128*, 2216-2217.

Ueda, H.; Iyo, H.; Doi, M.; Inoue, M.; Ishida, T.; Morioda, H.; Tanaka, T.; Hishikawa, S.; Uesugi, S. *FEBS Lett.* **1991**, *280*, 207-210.

Vazquez, M. E.; Rothman, D. M.; Imperiali, B. *Org. Biomol. Chem.* **2004**, *2*, 1965-1966.

Wang, Y.; Rando, R. R. *Chem. Biol.* **1995**, *2*, 281-290.

Williamson, M. P. *Biochem. J.* **1994**, *297*, 249-260.

Wiseman, T.; Williston, S.; Brandts, J. F.; Lin, L. N. *Anal. Biochem.* **1989**, *179*, 131-137.

Wiskur, S. L.; Ait-Haddou, H.; Lavigne, J. J.; Anslyn, E. V. *Acc. Chem. Res.* **2001**, *34*, 963-972.

Zhang, Y.; Reinberg, D. *Genes Dev.* **2001**, *15*, 2343-2360.